

https://dspace.org/

Development of a dynamic multivariate power system inertia model

Sibeko, Bonginkosi Johannes

2018

https://hdl.handle.net/10539/26476

Sibeko, Bonginkosi Johannes (2018) Development of a dynamic multivarate power system inertia model, University of the Witwatersrand, Johannesburg, https://hdl.handle.net/10539/26476

Downloaded from a DSpace repository. https://dspace.org/



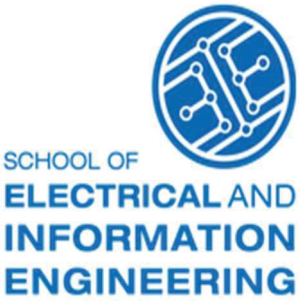

UNIVERSITY OF THE WITWATERSRAND
JOHANNESBURG, SOUTH AFRICA

Development of a dynamic multivariate power system inertia model

Mr. Bonginkosi Johannes Sibeko

A research project submitted to the Faculty of Engineering and the Built Environment, University of the Witwatersrand, in fulfilment of the requirements for the degree of Master of Science in Engineering

18 July 2018

Candidate's Declaration

I, Bonginkosi Johannes Sibeko, am registered for Master of Science in the School of Electrical and Information Engineering, I herewith submit this research report *"development of a dynamic multivariate power system inertia model"* for the fulfilment of the requirements for the degree of Master of Science in Engineering.

I hereby declare the following:

- I am aware that plagiarism (the use of someone else's work without their permission and/or without acknowledging the original source is wrong;
- I confirm that the work submitted herewith for assessment is my own unaided work except where I have explicitly indicated otherwise;
- This task has not been submitted before, either individually or jointly, for any course requirement, examination or degree at this or any other tertiary educational institution;
- I have followed the required conventions in referencing the thoughts and ideas of others;
- I understand that the University of the Witwatersrand may take disciplinary action against me if it can be shown that any part of this work is not my own unaided work or that I have failed to acknowledge the sources of the ideas or words in this research report.

Signature: _____

Date: _____

Abstract:

The power system inertia immediately following small and large system disturbances was investigated. By understanding factors affecting the system inertia and primary frequency response behaviour, an online inertia model was developed. Historical data was extracted from the Eskom Energy Management System (EMS) and Wide Area Monitoring System (WAMS). The developed model using Multivariate Analysis (MVA) includes measured and estimated data from Eskom generators, Renewable Energy Sources (RESs) and the interconnected Southern African Power Pool (SAPP). Inertia plus Fast Primary (Frequency) Response (FPR) (as determined by the load behaviour) and system inertia models were developed from June 2015-December 2016 and validated with past frequency disturbance events (June 2014-March 2017). From the comparison between the measured and model results for 355 actual disturbances, 225 disturbances resulted in errors within ±5% and 51 events resulted in errors between ±5% and ±10%. Eight disturbances caused errors greater than ±10%, which were largely from trips at particular large power stations and HVDC. During a large disturbance, the multivariate coefficients for Renewable Energy Sources, HVDC and interconnectors were very small for the pure inertia model (excluding the load frequency behaviour and the generator damping). In contrast, the spinning reserve provides significant contribution and is location based. The location of a disturbance affects the FPR behaviour and the system inertia but not the Rate of Change of Frequency (RoCoF) with reference to the central power station. The strong and weak areas with respect of the stiffness of the system (extent of frequency nadir for particular disturbances) were identified. This can contribute to future grid planning and real-time operations in managing the system inertia and primary frequency response. The model is expected to improve with time, as the accuracy of a statistical approach requires large amounts of data. The model can be used to determine and monitor the maximum level of RES in real-time.

Key words – Correlation, Frequency Stability, Inertia, Multivariate Analysis (MVA), Renewable Energy Sources (RES), System Operator (SO), Swing Equation, Situational Awareness (SA), Spinning reserve

Dedication

I dedicate this research project to my beloved country, South Africa.

Acknowledgements

I would like to thank the following people for all their effort, motivation, and support during this study:

- First, I would like to thank my late parents for their love and support. Without their encouragement, I would have never given myself the chance to continue my education - you are missed;
- To my supervisor Dr John Van Coller for his guidance and assistance throughout this research, and his encouraging words allowing me to complete these studies;
- To my colleagues of the Eskom System Operator, I thank them for their companionship and for providing a friendly working atmosphere. Special thanks to Gav Hurford for his continued support and mentorship from the day I joined System Operator until to-date. You are my role model.
- To my father in power system's operation and control, Riaan Viljoen. Thank you for believing in me and sharing your life skills and power system experience.
- To my best friend, Kgopotso Mathole, you have been there for me since early childhood in primary school grade one, through university and until today. No words can express my sincere gratitude towards your support, advise and unconditional love; Thanks also for introducing me to Multivariate Analysis.
- Lastly, to my wife Kefuoe and my three beautiful girls, Okuhle, Lethukwazi and Nokukhanya. Thank you for allowing me the time to complete my studies. I know I neglected you by putting my studies and career at Eskom first. I promise I will make up for the time lost.

Table of Contents

1. INTRODUCTION 1
   1.1 General Introduction 1
   1.2 Glossary 2
   1.3 Background 4
      1.3.1 Generation dispatch to meet the demand and evolving generation pattern 7
      1.3.2 Regulator 8
      1.3.3 Sustained lower economic growth 9
      1.3.4 Evolving customers and technologies 10
      1.3.5 System inertia and load balancing 13
   1.4 Problem statement 15
   1.5 Research Questions 16
   1.6 The research report structure 17
   1.7 Conclusion 18
2. POWER SYSTEM FREQUENCY STABILITY AND SYSTEM INERTIA 21
   2.1 Introduction 21
   2.2 Glossary 21
   2.3 Power system stability 22
   2.4 Frequency Staged Response following a generator loss 24
      2.4.1 Electromagnetic Energy Storage stage 25
      2.4.2 Inertial Response 25
      2.4.3 Secondary response 25
   2.5 Estimation of the system Inertia Constant, H 26
   2.6 Estimation of the system Inertia Constant using transients 27
      2.6.1 Swing Equation of a synchronous machine without Damping Torque 28
      2.6.2 Swing Equation of a synchronous machine with damping torque 31
      2.6.3 Swing Equation of a synchronous machine with damping torque plus FPR 32
   2.7 Offline system inertia calculation tools 34
   2.8 Real-time monitoring of system inertia 35
   2.9 Conclusion 37
3. MULTIVARIATE ANALYSIS 39
   3.1 Introduction 39
   3.2 First-order linear model 39
      3.2.1 Estimating the coefficients for a single independent variable 40

3.2.2 Sum of Squared Errors (SEE) 41
3.2.3 Standard Error of Estimate (SEE) 42
3.2.4 One-tail test 43
3.2.5 Coefficient of Determination ($R2$) 44
3.3 Multiple Regression 45
3.3.1 Multiple Regression Standard Error of Estimate 46
3.3.2 Testing the slope of a coefficient 46
3.3.3 F statistic test 46
3.3.4 Multicollinearity [29] 47
3.4 Assessing the model 47
3.5 Regression variables 48
3.6 Regression summary results table description 48
4. GATHERING, FILTERING AND MEASURING POWER SYSTEM DISTURBANCES DATA 51
4.1 Introduction 51
4.2 Glossary 51
4.3 Data accuracy factors affecting the system inertia 51
4.4 Frequency incident data collection and storage 52
4.5 Frequency disturbance by type in Eskom 53
4.5.1 Loss of a generator 53
4.5.2 Loss of large load 54
4.5.3 Loss of a transmission circuit 54
4.5.4 International incidents 54
4.5.5 Demand Side Management (DSM) and Instantaneous Demand Response (IDR) 54
4.6 Data sampling rate accuracy 56
4.7 Moving Average and Detrended Fluctuation Analysis (DFA) methods 57
5. MODEL DEVELOPMENT AND DEFINITION OF VARIABLES 61
5.1 Introduction 61
5.2 Model development plan 61
5.3 Inertia with FPR dependent variables 64
5.4 Independent variables 64
5.4.1 Sum of individual generator moments of inertia 65
5.4.2 SAPP simplified inertia contribution from tielines 66
5.4.3 Independent Power Producers 68

5.4.4 Stiffness of the system 68
6. THE ROCOF MODEL 73
6.1 Introduction 73
6.2 Disturbance location and frequency measurement points 73
6.3 Relationship between the RoCoF, system inertia and asynchronous generation sources 75
6.4 Measuring the Rate of Change of Frequency (RoCoF) from disturbances 76
6.5 The RoCoF model of independent and dependent variable 77
6.6 Cumulative system RoCoF factors versus the Coefficient of Determination 78
6.7 The Eskom system RoCoF model 79
6.8 Conclusion 80
7. THE SYSTEM INERTIA WITHOUT FPR MODEL DEVELOPMENT 81
7.1 Introduction 81
7.2 System inertia dependent variable 81
7.3 System inertia independent variables 82
7.4 Results for the system inertia using the MVA method 82
7.5 Conclusion 83
8. ESTIMATION OF THE INERTIA WITH FPR AND PREDICTION OF THE FREQUENCY NADIR FOLLOWING DISTURBANCES USING THE MVA METHOD 85
8.1 Introduction 85
8.2 Cumulative Inertia with FPR factors vs Coefficient of Determination of the Medupi model 85
8.3 Medupi Inertia with FPR model coefficients 88
8.3.1 Eskom AC system 88
8.3.2 International coefficients 90
8.3.3 RES coefficients 90
8.3.4 Model validation for Medupi normal incidences 92
8.3.5 Model validation for IDR events 93
8.4 Overall Inertia with FPR model and model validation 95
8.5 Inertia with FPR model validation for normal incidences 96
9. FACTORS AFFECTING ESKOM INERTIA WITH FPR 100
9.1 Introduction 100
9.2 Eskom generation and load centres 101
9.2.1 The Limpopo province 101

9.2.2 The KwaZulu-Natal province 102
9.2.3 The Gauteng province 102
9.2.4 The Mpumalanga province 102
9.2.5 The Western Cape province 103
9.2.6 The Eastern Cape 103
9.2.7 The Northern Cape province 103
9.2.8 The Free State province 104
9.2.9 The North West province 104
9.3 Fast Primary Response (FPR) model coefficients comparison between areas and power stations 105
9.3.1 Validation of selected power stations inertia with FPR models 106
9.3.2 AC power station Inertia with FPR model coefficients 106
9.3.3 Tie-line Inertia with FPR model coefficients 108
9.3.4 RES inertia with FPR model coefficients 108
9.4 Conclusion 108
9.5 Recommendation for future work 109
10.CONCLUSIONS 110
11.REFERENCES 116

Appendix A Inertia plus Fast Primary Response area and power stations model
Appendix B Inertia with FPR Model Validation Results - 2014-2017
Appendix C SAUPEC 2017 - Eskom Power System Inertia Model - A Dynamic Multi-Factor Approach to the Management of power system inertia
Appendix D Cigre International Symposium Paper, Paris 2018 - A Dynamic Multi-Variate Approach to the Management of Power System Inertia
Appendix E Comments and contribution from Eskom Industry Experts

List of Figures

Figure 1-1: The Transmission lines and generation in the Integrated SAPP network. 4
Figure 1-2: Long-term factors affecting the normal operations of the Eskom SO. 6
Figure 1-3: Change in average summer Eskom generation dispatch 2012-2016 vs. generation dispatch including operational reserves [EMS data downloaded by author]. ... 7
Figure 1-4: Total additional new capacity until 2030 [1], [3] (permission obtained for use of data). 9
Figure 1-5: Trends from Eskom SCADA data showing the changes in yearly load profiles between the years 2012 and 2016 [EMS data downloaded by author]. 10
Figure 1-6: Trends of the average winter load profiles from Eskom EMS data between the years 2012 and 2016 [EMS data downloaded by author]. 11
Figure 1-7: Trends of average summer load profiles from Eskom EMS data between the years 2012 and 2016 [EMS data downloaded by author]. 11
Figure 1-8: Profile of Residential Mass Rollout DSM between 2015-2022 adopted from [3] (permission obtained for use of data). 12
Figure 1-9: Modified block diagram showing the balancing of load and generation with the impact of the varying Inertia Constant (modification from [15]). 14
Figure 2-1: Block diagram showing the hierarchy of different power system stability classifications adapted from [3] and others..... 23
Figure 2-2: PMU data showing system primary response stages [PMU data downloaded by author]. 25
Figure 2-3: Flow of mechanical and electrical powers in a synchronous generator. 29
Figure 2-4: Estimation of Inertia Constant during the first 300 ms following a disturbance in the Eskom network [PMU data downloaded by author]. 30
Figure 3-1: Scatter diagram with the regression line. 40
Figure 3-2: Calculation of residuals [29]. 42
Figure 3-3: Partitioning the deviation for $i=n$ [29]. 45
Figure 4-1: Frequency incident data collection sources. 52
Figure 4-2: Filtering of frequency disturbances by type. 53
Figure 4-3: Frequency response following a large disturbance and frequency overshoot due to IDR [PMU data downloaded by author]. 55
Figure 4-4: UFLS response following multiple unit trips at Kendal power station – 06 June 2014 [PMU data downloaded by colleague]..... 55
Figure 4-5: Archived PMU frequency data with 100 ms sample rate [PMU data downloaded by author]. 56
Figure 4-6: RoCoF sampling rate measurements at Tutuka power station following a disturbance at Apollo-29 November 2013 [PMU data downloaded by a colleague]..... 57
Figure 4-7: Matimba and Kendal power station PMU measurements following a Medupi unit trip [PMU data downloaded by author] 58
Figure 5-1: Block diagram showing the balancing of load and generation with the impact of the varying Inertia Constant..... 62
Figure 5-2: MVA model development plan. 63
Figure 5-3: Model development showing known and unknown independent variables... 65
Figure 5-4: Simplified SAPP diagram. 66
Figure 5-5: BPC inertia simplified model with reference to the Eskom network. 67

Figure 5-6: Zesa simplified inertia model with reference to the Eskom network. 68
Figure 5-7: System equivalence for LFC analysis [6]. 70
Figure 5-8: Composite governor and load characteristic [6] 70
Figure 6-1: PMU data showing system primary response stages. 74
Figure 6-2: RoCoF as a function of system inertia. 75
Figure 6-3: Linear approximation of the RoCoF within the first 300 ms following a disturbance [PMU data downloaded by author]. 76
Figure 6-4: Cumulative RoCoF factors versus Coefficient of Determination (R^2)..... 78
Figure 8-1: Cumulative Inertia with FPR versus Coefficient of Determination of the Medupi PS model..... 86
Figure 8-2: Measured vs predicted frequency nadir %errors for all power station models excluding HVDC and particular power stations. 93
Figure 8-3: Overall system inertia with FPR correlation results..... 96
Figure 8-4: Summary of all power station model validations for 2017 disturbances. 99
Figure 9-1: RoCoF as a function of system inertia but now with FPR. 100
Figure 9-2: South Africa's existing and planned transmission grid, generation and RES. Adopted from [10] (permission obtained for use of data)..... 101

List of Tables

Table 2-1: Response following a generator loss 24
Table 3-1: Relationships among *standard error of estimate,* R^2 and *F statistic* 47
Table 3-2: Dependent (*y*) and independent (*x*) input variables used in the regression analysis tool 48
Table 3-3: Microsoft Excel Regression summary output 49
Table 5-1: Dependent (y) and Independent (x) input variables used in the regression analysis tool (similar table is used for the Inertia without FPR model and the Inertia with FPR model). 63
Table 5-2: Typical Inertia Constant (H) by generation type 66
Table 6-1: Relationship among frequency measurements in Central, Western Cape and Northern areas 74
Table 6-2: Detailed system RoCoF model 80
Table 7-1: Comparison of the Inertia Constant per Eskom area and independent variable coefficients (print in colour. Red=poor; yellow=average; green=good) 82
Table 8-1: Medupi inertia with FPR model 87
Table 8-2: Model validation following a Medupi unit trip (single contingency) 92
Table 8-3: Previous IDR events and model estimates of the Inertia with FPR 94
Table 8-4: Factors affecting Medupi Inertia with FPR during IDR events 94
Table 8-5: All Inertia with FPR model predictions vs measured values from Swing Equation 97
Table 9-1: Comparison of areas and power station Inertia with FPR models (print in colour. Red=poor; yellow=average; green=good) 106

List of Symbols

Symbols (power flow dynamics)

Active power change of generator *i*	ΔP_i	MW
Angular velocity	ω_m	((mech)rad/s)
Generator nominal apparent power	S_n	MVA
Inertial active power dispatch of generator *i*	$P_{i-dispatch}$	MW
Minimum instantaneous frequency	f_{nadir}	Hz
Modified active power of generator *i*	P_i	MW
Moment of inertia of a synchronous machine	J	$Kg.m^2$
Rated angular velocity	ω_{0m}	((mech)rad/s
Reference/nominal frequency	f_0	Hz
Rotational frequency of the synchronous machine	f_m	Hz
Time at the start of a disturbance	t_{start}	*s*
Time until the frequency reaches f_{nadir}	t_{nadir}	*s*
Total frequency deviation	Δf	*Hz*
Total mechanical power of the generators	P_m	*MW*
Total rated VA of the generators	S_B	MVA
Total system load of the grid	P_{load}	MW

SYMBOLS (Multivariate analysis)

Coefficient of Determination	R^2
Dependent variable	y
Error variable	ε
Fitted or calculated value of y	$\hat{y}$
Sample coefficient of correlation	r
Sample mean	$\bar{x}$
Sample slope coefficient	b_1
Sample y-intercept coefficient	b_0
Slope coefficient	β_1
Standard error of b_1	s_{b_1}
Standard error of estimate	s_ε
Std deviation of error variable	σ_ε

y-intercept coefficient	β_0

Abbreviation	**Description**
DEC	Data Energy Centre
DoE	South African Department of Energy
EMS	Energy Management System
EPRI	Electric Power Research Institute
ERCOT	Electric Reliability Council of Texas
GCSA	Grid Code of South Africa
GW	Gigawatt
HVDC	High Voltage Direct Current
Hz	Hertz
IDR	Instantaneous Demand Response
IPP	Independent Power Producer
IRP	Integrated Resource Plan
MCR	Maximum Continuous Rating
MW	Megawatt
NERSA	National Energy Regulator of South Africa
OCGT	Open Cycle Gas Turbine
PMU	Phasor Measurement Unit
PV	Photovoltaic
RES	Renewable Energy Source
RoCoF	Rate of Change of Frequency
RPM	Revolutions per minute
SAPP	Southern African Power Pool
SCADA	Supervisory Control and Data Acquisition
SNSP	System Non-Synchronous Penetration
SO	System Operator
SSA	Static Security Assessment
Tx	Transmission
UFLS	Under frequency load shedding

Southern African Power Pool (SAPP) Membership (with permission from SAPP)

Full Name of Utility	Status	Abbreviation	Country
Botswana Power Corporation	OP	BPC	Botswana
Electricidade de Mozambique	OP	EDM	Mozambique
Electricity Supply Corporation of Malawi	NP	ESCOM	Malawi
Rede Nacional de Transporte de Electricidade	NP	RNT	Angola
Eskom	OP	Eskom	South Africa
Hidroelectrica de Cahora Bassa	IPP	HCB	Mozambique
Lesotho Electricity Corporation	OP	LEC	Lesotho
Mozambique Transmission Company	ITC	MOTRACO	Mozambique
Nam Power	OP	Nam Power	Namibia
Societe Nationale d'Electricite	OP	SNEL	DRC
Swaziland Electricity Company	OP	SEC	Swaziland
Tanzania Electricity Supply Company Ltd	NP	TANESCO	Tanzania
ZESCO Limited	OP	ZESCO	Zambia
Copperbelt Energy Cooperation	ITC	CEC	Zambia
Lunsemfwa Hydro Power Company	IPP	LHPC	Zambia
Zimbabwe Electricity Supply Authority	OP	ZESA	Zimbabwe

IPP = Independent Power Producer

ITC = Independent Transmission Company

NP = Non-Operating Member

OP = Operating Member

1. INTRODUCTION

"You can't connect the dots looking forward - you can only connect them looking backwards. So you have to trust that the dots will somehow connect in your future. You have to trust in something: your gut, destiny, life, karma, whatever. Because believing that the dots will connect down the road will give you the confidence to follow your heart, even when it leads you off the well-worn path." - Steve Jobs, Stanford Commencement Address, 2000, US computer engineer & industrialist (1955 - 2011).

1.1 General Introduction

The slow economic growth and worldwide slump in the commodities markets have led to a reduction in customer demand while at the same time there has been an increase in asynchronous generation penetration. This has resulted in a power system with lower inertia supplying the same load levels experienced some years ago leading to concerns for the dynamic behaviour of the frequency. The growing concerns for system inertia require more sophisticated and affordable power system real-time tools to manage the challenges of a modern power system. Failure could likely lead to widespread blackouts with significant economic and social impact. As more zero-inertia generators are added to the Eskom power grid, the traditional synchronous generators, which provide inertia to the system, are starting to be displaced, put into cold reserve or two shifted and see early retirement.

This chapter begins with a glossary of terms followed by background, which provides an overview of the Eskom network. Challenges regarding historical, present and future power system inertia are then presented. The problem statement introduces the framework for the work done in the past that comprises the focus of this research. A guide of different chapters is then presented.

1.2 Glossary

1. *Base load plant* refers to power plants that are able to produce power at a constant, or near constant, rate, i.e. power plants with high capacity factors [1].
2. *Capacity Reserve* refers to the installed power plant that is in excess of that required to carry peak load.
3. *Curtailed Active Power* refers to the amount of active power that the Renewable Power Plant (RPP) is permitted to generate by the SO, Network Service Provider or their agent subject to network or system constraints [1], [2].
4. *Demand Side Management (DSM)* refers to interventions to reduce energy consumption [1].
5. *Deemed Energy* means that energy output that would otherwise be available to the buyer but due to a system event or compensation event, as determined in accordance with Schedule 6 (Deemed Energy Payment) of the Power Purchase Agreement (PPA), was not supplied [1], [2].
6. *Distributed Generation* is defined as the installation and operation of electric power generation units connected directly to the distribution network or connected to the network on the customer side of the meter [1], [3].
7. *Frequency nadir* refers to the minimum instantaneous frequency following a loss of a generator [4]. In this work, *frequency nadir* refers to the minimum frequency reached after a disturbance prior to slow primary response and secondary response.
8. *Independent Power Producer (IPP)* means any undertaking by any person or entity, in which the government of South Africa does not hold a controlling ownership interest (whether direct or indirect), of new generation capacity at a generation facility following a determination made by the Minister in terms of Section 34(1) of the Act [1].
9. *Instantaneous reserve* is the generating capacity available to operate automatically in the event of a sudden trip of a large generating plant or the HVDC link.

10. *Integrated Resource Plan 2010* refers to the co-ordinated schedule for generation expansion and demand-side intervention programmes, taking into consideration multiple criteria to meet electricity demand [1].
11. *NERSA* means the National Energy Regulator of South Africa established in terms of the National Energy Regulator Act, (Act No. 4 of 2004), or its legal successor [5].
12. *Regulation reserve* refers to the amount of operating reserve that is quick to respond to Automatic Generation Control.
13. *Reliability* is the degree to which the performance of the elements of the power system results in power being delivered to consumers within accepted standards and in the amount desired. The degree of reliability may be measured by the frequency, duration and magnitude of adverse effects on consumer service [6], [7].
14. *Security* refers to the degree of risk in a power system's ability to survive imminent disturbances (contingencies) without interruption of customer service. It relates to robustness of the system to imminent disturbances and, hence, depends on the system operating condition as well as the contingent probability of disturbances [4].
15. *Spinning reserve* is the on-line reserve capacity that is synchronised to the grid and ready to meet demand within 10 minutes of a dispatch instruction by the SO. Spinning reserve is needed to maintain system frequency stability during emergency operating conditions and unforeseen load swings [5], [6].
16. *South African Grid Code (SAGC)* consists of the following documents: Preamble, Governance Code, Network Code, System Operation Code, Metering Code, Tariff Code and Information Exchange Code as approved by NERSA and updated from time to time by the Secretariat.
17. *Stiffness* of the system refers to the composite frequency response characteristic of the system The stiffness of the system depends highly on load damping, spinning reserve and governor droop (steady state) [6].
18. *System Operator is t*he legal entity licensed to be responsible for short-term reliability of the Integrated Power System (IPS), which is in charge of

controlling and operating the Transmission system and dispatching generation (or balancing the supply and demand) in real-time [2], [5].

19. *Two shifting* is starting up and shutting down a plant to meet load demand during periods of high and low demand.

1.3 Background

The interconnected part of the Southern African Power Pool (SAPP) is made up of Botswana, Mozambique, South Africa, Lesotho, Namibia, Democratic Republic of Congo, Swaziland, Zambia and Zimbabwe [8]. The Eskom transmission network is synchronously connected to the neighbouring Southern African Development Community (SADC) utilities shown in Figure 1-1.

The Cahora Bassa Hydro Power Station in Mozambique dispatches power through parallel AC and DC interconnections and is controlled by the Grid Master Power Controller (GMPC) [9]. The DC power flows directly to the Apollo converter station in South Africa. The AC power is delivered to Zimbabwe and Botswana that are interconnected with the South African AC grid via a single 400 kV transmission interconnector (colloquially called tie-line).

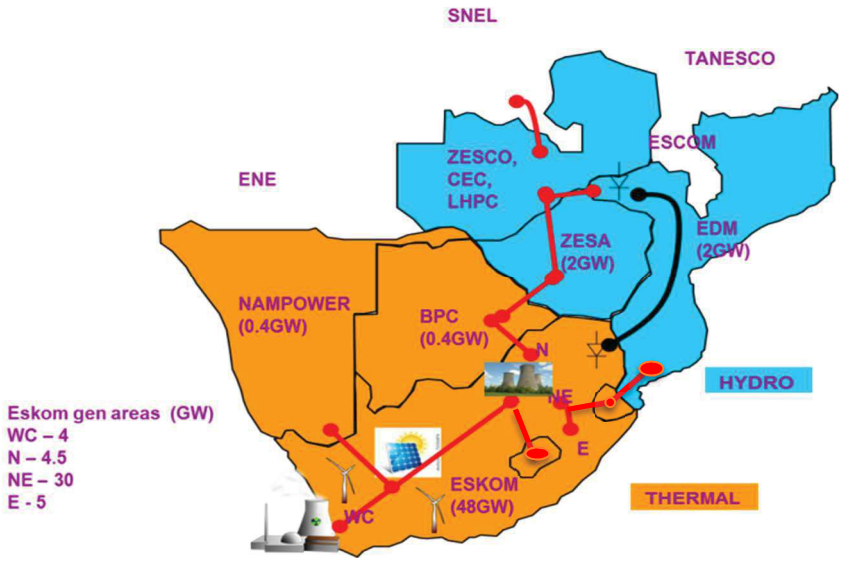

Figure 1-1: The Transmission lines and generation in the Integrated SAPP network.

Approximately 90% of SAPP electricity generation is in South Africa. The long single 400 kV AC circuit outside the Eskom network and asynchronous HVDC interconnectors are relatively weak compared to the Eskom grid. Therefore, Eskom must rely on the actions of generators and additional demand services within the Eskom network to maintain the Eskom system reliability, security and stability.

Base load plants are mostly coal-fired in the Mpumalanga (North Eastern) and Lephalale (Northern) parts of the country which amounts to approximately 77% of the total installed generation capacity [10]. A nuclear power station is located in the Western Cape (Southwestern) part of South Africa. The peaking plants consist of hydro pump storage, which are in the Western Cape and East grid (KwaZulu Natal). Other peaking plants include conventional hydro power stations and Open Cycle Gas Turbines (OCGTs) in the Western Cape. OCGTs are currently non-economical to dispatch, as there is excess generation on the grid.

The large number of Renewable Energy Sources (RESs) in the Northern Cape, Western Cape and Eastern Cape parts of South Africa are mostly embedded in distribution networks (132 kV and lower). Approximately 95% of RESs are connected in the distribution network and the remaining 5% are connected directly to the transmission network. The large number of RESs are connected far from load centres and are electrically connected to the Interconnected Power System (IPS) via high impedance distribution lines. Therefore, from the Eskom IPS perspective, RESs provides only active power (MW) to the power system and contribute either very little or no power system inertia.

As the concerns towards power system security, stability and safety continue, the regulators and SOs around the world want to see the more advanced applications deployed in power system control rooms to address system operational matters at near real-time. South Africa's SO would like to know how the system will respond to load or generator disturbances at near real-time.

It was shown in [4], [11] the traditional assumption that grid inertia is sufficiently high with only small variations over time is not valid for power systems with high RES shares. This has implications for frequency dynamics and power system stability and operation. Frequency dynamics are faster in power systems with low rotational inertia, making frequency control difficult.

In a real-time operational environment, it is important to make available information to the SO about the global security margins so that preventive and/or corrective actions may be decided with sufficient time to avoid dangerous operational conditions. The information in this work focuses on the system inertia, Fast Primary Response (FPR) and the Rate of Change of Frequency (RoCoF) following single contingencies.

The way in which energy is produced, distributed and consumed in the Eskom network is changing significantly. Figure 1-2 shows some of the factors that triggered the concerns of the Eskom network. These are and will in future be impacted by the regulator, evolving customers and technologies, evolving generation patterns, and sustainable economic growth, system inertia and load balancing.

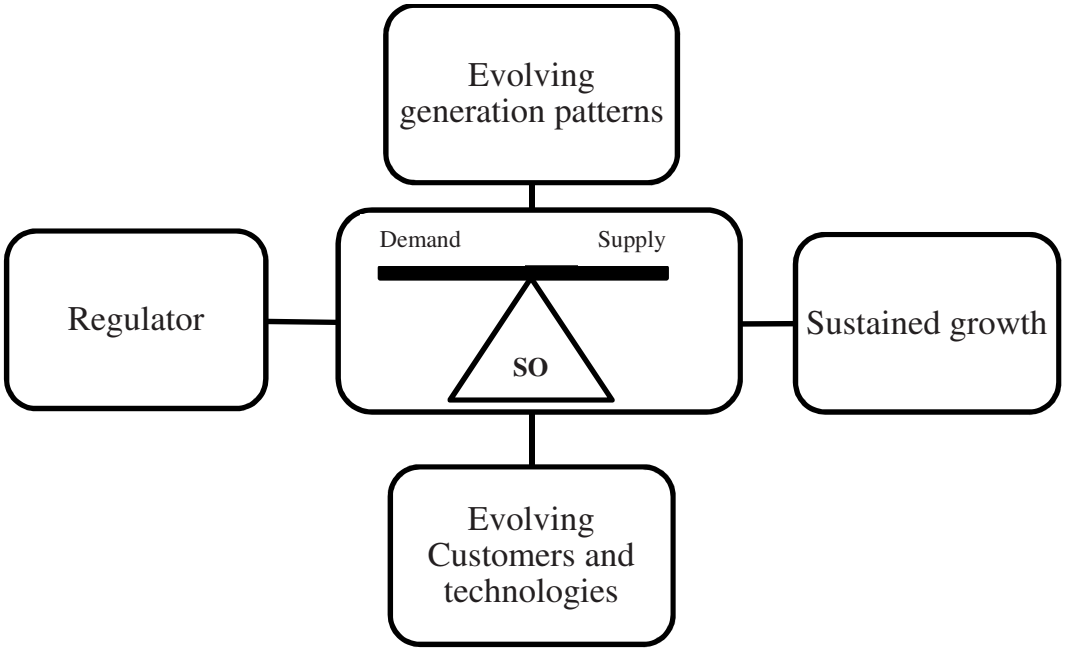

Figure 1-2: Long-term factors affecting the normal operations of the Eskom SO.

Although these factors are outside real-time operations, they are expected to affect the traditional way of operating the power system. Amidst all of these changing network conditions, the System Operator (SO) in South Africa is mandated to control the operation of and be responsible for the short-term reliability of the IPS as defined in the South African Grid Code [5].

1.3.1 Generation dispatch to meet the demand and evolving generation pattern

The conventional method of managing system security, stability and reliability of the Eskom grid is using Capacity Reserves, Base Load plants and Peaking Plants. The SO dispatches generators based on meeting the evening peak demand with an allowance of at least 2000 MW of operating reserve a day-ahead and 1000 MW on the day as required by the South African Grid Code [5]. Figure 1-3 shows the comparison between 2012 and 2016 winter generation dispatch.

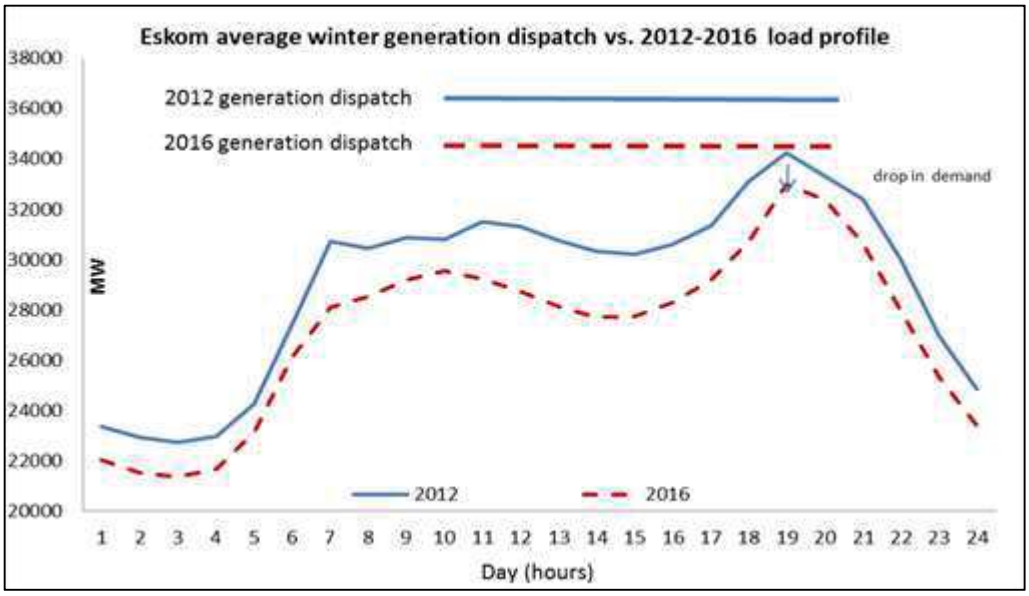

Figure 1-3: Change in average summer Eskom generation dispatch 2012-2016 vs. generation dispatch including operational reserves [EMS data downloaded by author].

From Figure 1-3, the drop of 2000 MW of the Eskom average generation dispatch translates to less synchronised generation on the grid. It is apparent that the load has decreased by approximately 2000 MW and the implications of that is that the

system inertia provided by synchronous generators was less in 2016 compared to in 2012.

1.3.2 Regulator

South Africa is ranked among the world's top 12 largest carbon dioxide (CO_2) emitters, largely due to dependence on coal for electricity generation and an energy-intensive industrial and mining sector [12]. In the December 2009 Copenhagen climate change negotiations, South Africa committed to add its own share to the global greenhouse gas emissions reduction and voluntarily announced that it would act to reduce domestic emissions by 34 per cent by 2020 and 42 per cent by 2025 [12]. This was on the condition that it receives adequate financial, technological and other support from the international community to establish those goals [12]. Fortunately, South Africa had largely untapped abundance of renewable energy sources, especially solar and wind energy [12].

In recent years, large-scale deployment of RES, mostly in the form of wind turbines, concentrated solar power (CSP) and PV units has led to substantial generation shares of variable RES. The National Development Plan (NDP) of South Africa has a long-term vision of 5 million Solar Water Heaters (SWHs), 8.4 GW of wind turbines, 1 GW of CSP and 8.4 GW Solar PV by 2030 [1], [13]. Currently, wind IPPs are delivering approximately 1809 MW (including 110 MW Eskom owned wind generation) followed by 1474 MW of solar PV, 35 MW of biomass, 91 MW of Hydro and lastly 300 MW of CSP. Figure 1-4 shows the planned new generation capacity mix for 2030.

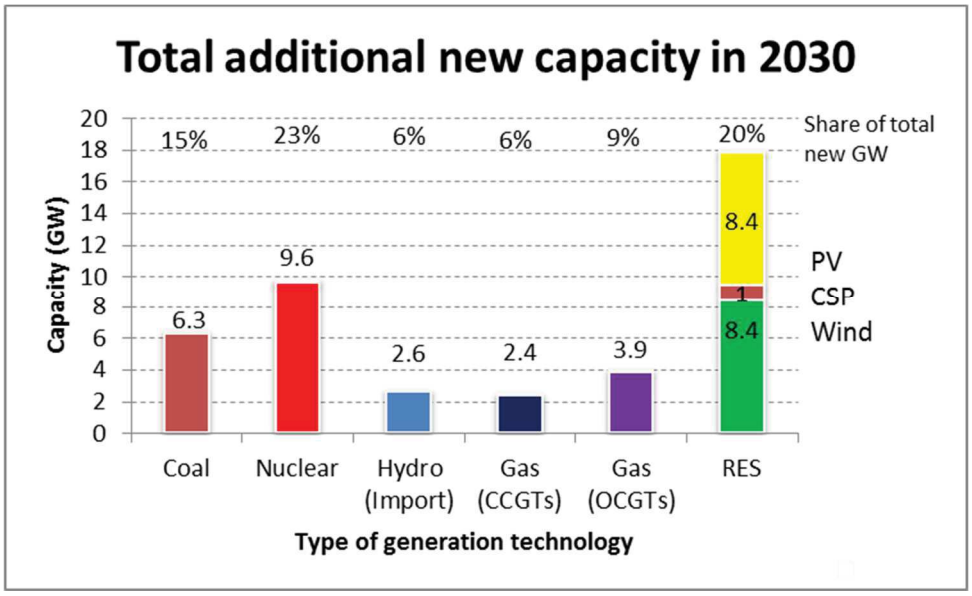

Figure 1-4: Total additional new capacity until 2030 [1], [3] (permission obtained for use of data).

Most of the current Eskom generators are ageing and will soon be decommissioned [1], [3]. These plants will be replaced by the new capacity as shown in Figure 1-4. The Renewable Power Plants (RPPs) are not dispatchable and, if curtailed by the SO due to excess capacity, unserved energy payments must be made [1], [2]. Curtailment and/or delta mode production have serious economic consequences (lost energy production) [1], [3]. As more potential energy sources are discovered in other parts of South Africa, a mix of generation technologies and primary fuels is a priority for the Department of Energy (DOE).

1.3.3 Sustained lower economic growth

Following the response to the effects of the global financial crises, countrywide load-shedding and sustained lower economic growth in 2007/8, Eskom sales only recovered between 2010 and 2012 to the levels experienced in 2007, but have been in decline since [12]. The South African economy moved into recession with the reported decrease of 0,7% in GDP during the first quarter of 2017, following a 0,3% contraction in the fourth quarter of 2016 [14].

According to the Department of Energy and National Development Plan of South Africa [2] [4], the forecasted peak demand will grow from 38.9 GW to 67.8 GW (assuming average growth of 2.8% per annum) by 2030. Contrary to the assumed

average growth, Figure 1-5 illustrates a downward trend from Eskom generation sent-out over the past 5 years. This was due to various reasons including a negative economic growth, electricity price increase, IPPs and Demand Side Management (DSM) initiatives (Capacity Constraints).

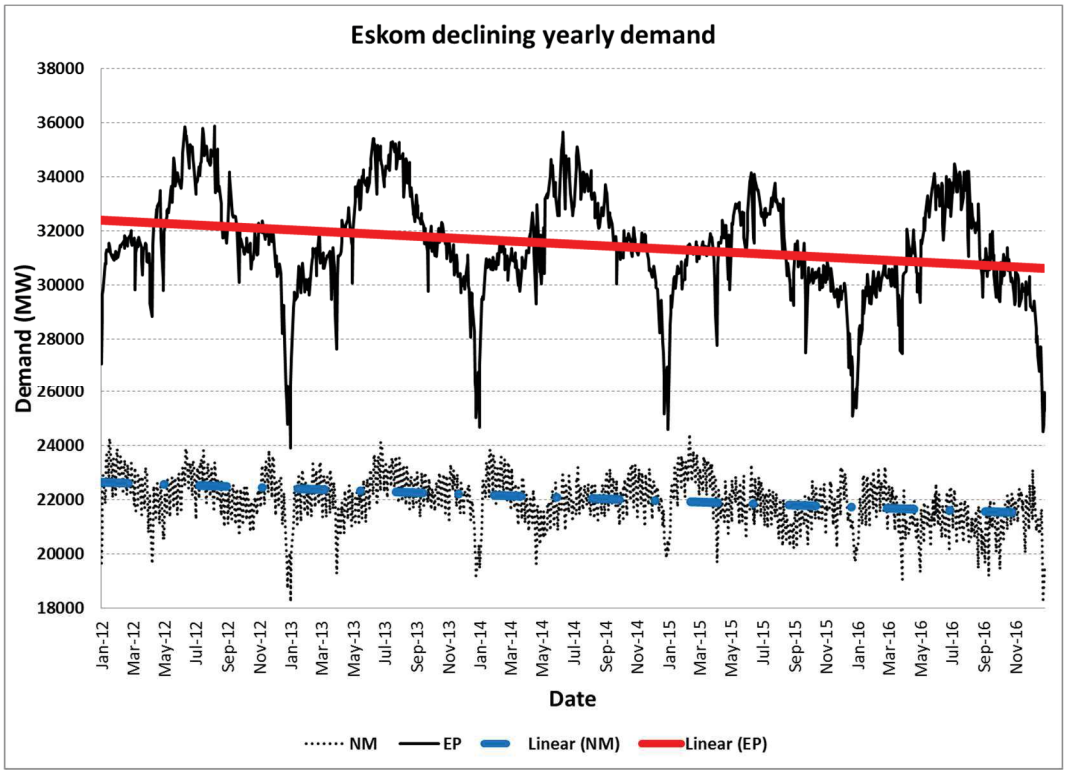

Figure 1-5: Trends from Eskom SCADA data showing the changes in yearly load profiles between the years 2012 and 2016 [EMS data downloaded by author].

As more zero-inertia generators i.e. asynchronous generators, are added to the Eskom power grid, the traditional synchronous generators, which provide inertia to the system, are starting to be displaced, put into cold reserve or two shifted and see early retirement. The slow economic growth with high asynchronous penetration also translates to less synchronous generation dispatch by the SO. This could negatively affect system inertia.

1.3.4 Evolving customers and technologies

The introduction of renewable energy adds new challenges to managing the supply and demand on the power system. The bulk of the Eskom generation fleet

is thermal mid-merit and base load plant. The demand profiles shown in Figure 1-6 and Figure 1-7 are currently not aligned with the PV production profiles.

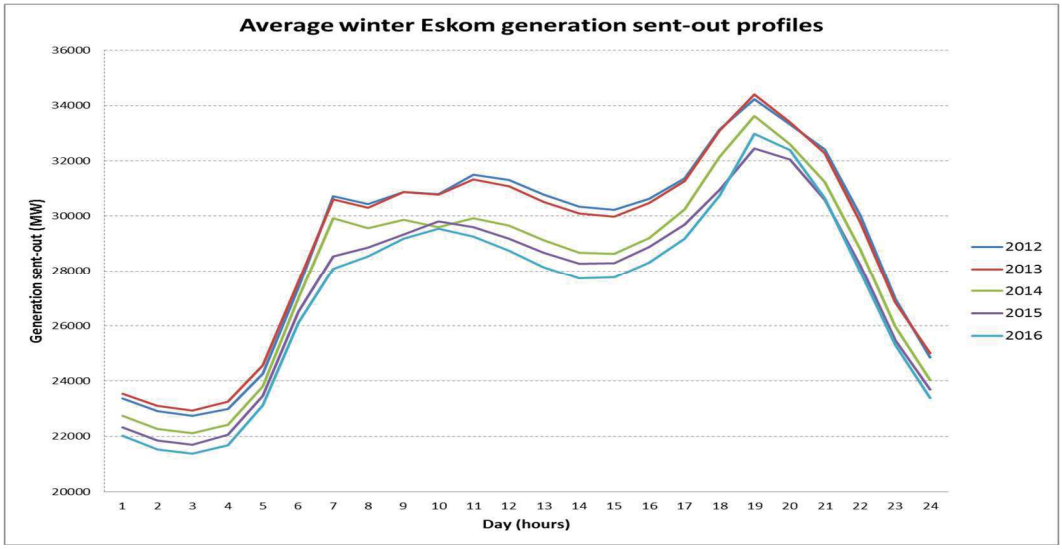

Figure 1-6: Trends of the average winter load profiles from Eskom EMS data between the years 2012 and 2016 [EMS data downloaded by author].

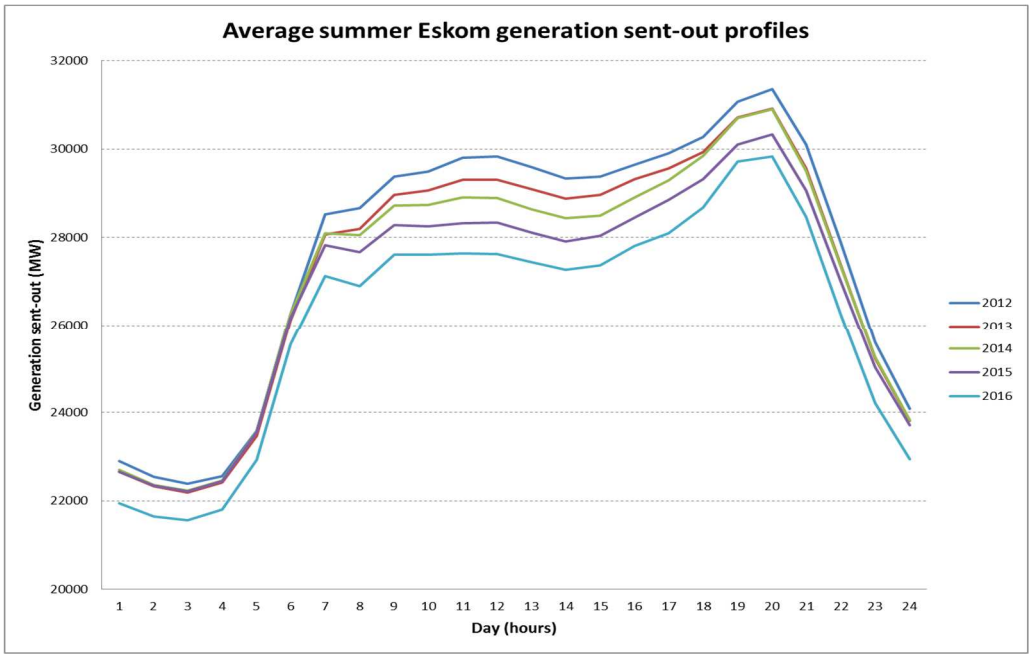

Figure 1-7: Trends of average summer load profiles from Eskom EMS data between the years 2012 and 2016 [EMS data downloaded by author].

This kind of load profile is very challenging to manage when there is inflexible excess generation. The Eskom power station fleet is largely base-load coal. Most of these plants do not have the ability to temporally shut down or reduce output beyond a narrow operating output once synchronised on the grid. By design, base load generators do not have the ability to ramp up quickly when demand increases. The plants need time to synchronise or increase production to support the ramping-up of generators preparing for evening peak. Some of these plants in the Eskom network are needed for fault levels, voltage support and network stability.

During the period of shortage of generation in the Eskom network between the years 2007 and 2014, the drive to replace the traditional light bulbs with fluorescent type light bulbs was initiated to save energy [3]. The Integrated Demand Management Plan rolled out the residential lighting LED program that commenced in 2015/2016 and continued in 2016/2017 reaching cumulative savings of 466 MW shown in Figure 1-8 [3].

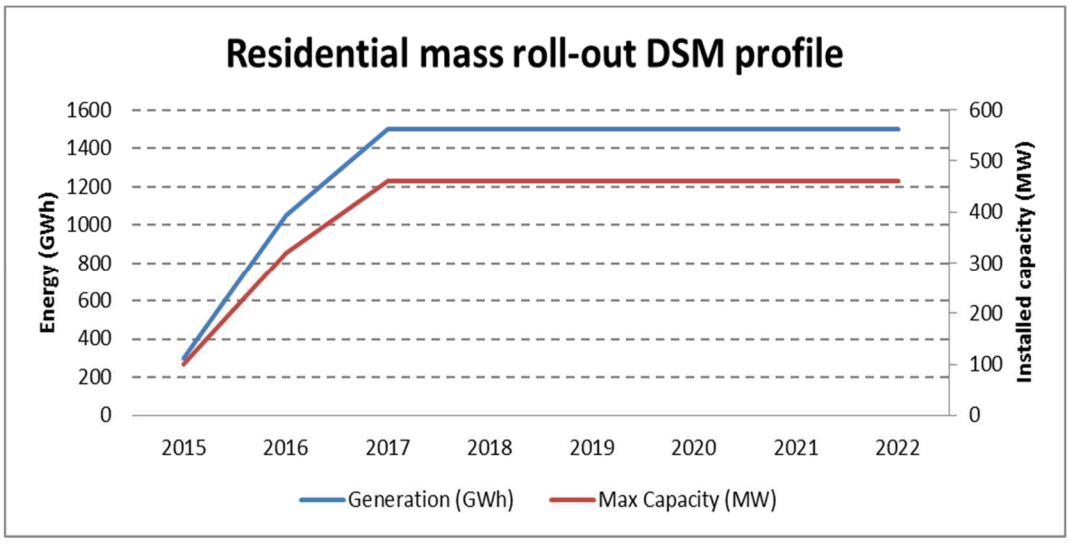

Figure 1-8: Profile of Residential Mass Rollout DSM between 2015-2022 adopted from [3] (permission obtained for use of data).

This effort saw significant success in active power saving from the demand side. On the one hand there was energy saving which saved costs to Eskom. On the other hand, the system inertia was compromised because the saved energy

displaced the equivalent of a large synchronous generator unit. Therefore, the system inertia was indirectly reduced.

1.3.5 System inertia and load balancing

During a frequency disturbance, the generation/load power balance is lost. The system frequency will change at the rate initially determined by the total system inertia [15]. This kinetic energy, which is stored in the synchronously rotating masses of the power system, is often called inertial, stored, or rotational energy [7]. Asynchronous generators, mostly in the form of HVDC, wind turbines and PV units, use power converters as an interface to the grid, and are therefore synchronously decoupled from the traditional AC power system [11], [15]–[18].

In Figure 1-9, the outer loop shows the connection and balancing of load and generation. The load, interconnectors, PV and wind generation are categorised as self-dispatch or non-dispatchable by the SO. The synchronous generators and HVDC are categorised as dispatchable by the SO. The strength of the AC power system is mainly determined by the system inertia, which is mainly provided by connected synchronous generators and the stiffness of the system [6], [17], [19] shown in the inner loop of Figure 1-9. The large reduction in supply/load can trigger protection systems that may result in system separation, loss of load/generation, blackout and customer outages. Severe system upsets generally result in large excursions of frequency, power flows, voltage and other system variables thereby invoking the actions of processes, controls and protections that are not modelled in conventional transient stability or voltage stability studies [6],[7].

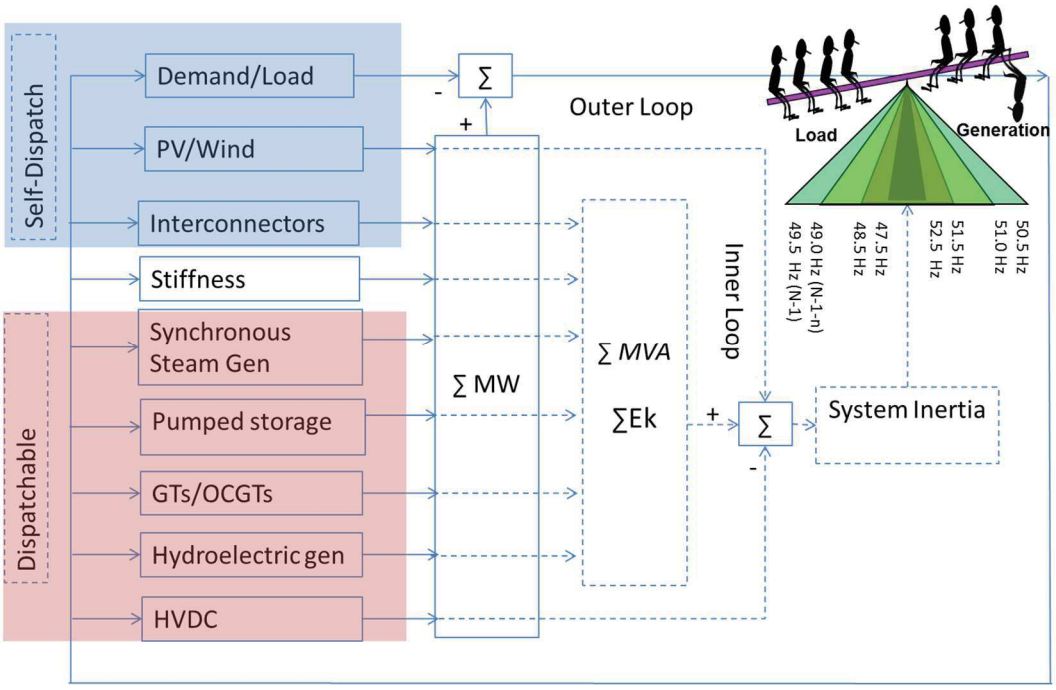

Figure 1-9: Modified block diagram showing the balancing of load and generation with the impact of the varying Inertia Constant (modification from [15]).

As stated in the Grid Code of South Africa [2], [5] the SO shall dispatch generation and demand-side resources on the IPS subject to the constraints of safety of personnel and equipment, IPS security, reliability, resource availability, legislation and the environment [5].

The GCSA requires the SO to keep the frequency above 49.5 Hz following all credible single contingency losses. The largest loss is currently the loss of a Koeberg unit at full load, i.e. 930 MW. It is also a requirement on the SO to keep the frequency above 49.0 Hz after credible multiple contingencies.

With the current integration of the new large Medupi and Kusile power stations, the units that are relatively similar sizes (720 MW) to the Koeberg units, the probability of violating the Grid Code is therefore increasing. This could be due to the following:

1. During commissioning, testing and the initial operation of Kusile and Medupi, reliability is low while problems are sorted out.

2. Medupi, Kusile and other base load power stations are coal-fired and load following. Koeberg is a nuclear unit that does not load follow and is fairly reliable
3. There are older base-load coal-fired units than the newer mid-merit and peaking units, so it expected that the base-load would have more trips due to ageing.

1.4 Problem statement

Sustaining grid security is a fundamental requirement for power grids. Failure could likely lead to widespread blackouts with significant economic and social impact. The growing security and stability needs recently experienced by the Eskom demand require more sophisticated and affordable power system real-time tools. The present and future challenges include the changing patterns in consumer electricity usage, increased and ongoing uptake of residential and commercial rooftop solar PV, withdrawal of traditional generating sources, demand stagnation, oversupply and integration of Renewable Energy Sources (RESs).

The South African Grid Code (SAGC) [2], [5] was written prior to the installation of significant amounts of renewable generation and hence the code does not cover the system inertia requirements. The SAGC does, however, define the limits of acceptable frequency response and it is therefore important to understand what level of non-synchronous generators can be tolerated before the Grid Code requirements are violated.

Eskom uses a number of different offline simulation tools that have the ability to calculate the inertia and the Inertial Response of the power system. However, these are of limited use in the operational environment due to the number of possible network configurations encountered and the lack of accuracy for certain critical component models. The theoretical approach has largely been investigated in the past for Static Security Assessment (SSA) tools, but less for the dynamic

security tools. Hence, an interesting investigation is how to revise the South African power system's defence plan.

While there is nothing that the SO can do to prevent natural disasters or severe large frequency events, advanced analytics in conjunction with the ability to deal with large amounts of data, can help to predict or forecast the near future power system inertia to enable better preparation and faster and more effective disaster response. By analysing a combination of historical data points combined with power system equations and applying them to new data, before, during and after system disturbances occur, the SO can do more in forecasting and managing the system inertia and primary frequency response.

1.5 Research Questions

The focus of this research is on the behaviour of the power system frequency immediately following a disturbance in the Eskom network.
A model can be developed using Multivariate Analysis (MVA) to estimate the power system inertia in real-time and predict the frequency nadir following a large disturbance. Frequency dynamics can be predicted if factors affecting power system inertia can be investigated and understood.

This research was guided by a desire to address the following research questions:

- By reducing the contribution of conventional synchronous generators to accommodate (asynchronous) renewable generation, what would be the resultant impact on system inertia and frequency stability?
- How can online inertia model tools be utilised in the Eskom National Control Centre to improve the power system operation?
- Is the assumption that while doing frequency stability analysis the (aggregated) Inertia Constant, H, is constant for all Swing Equations of a multi-area system? What is the impact of disturbance location in the accuracy of H?
- Are the primary frequency control schemes installed in South Africa's power transmission system adequately calibrated for mitigating fault events before a critical frequency drop can occur?

- Can the use of under frequency load shedding schemes be linked to the online variable system inertia to shed the required load at the time of an incident?
- In what way does transient location, spinning reserve, instantaneous reserve, load types and renewables affect the inertial and primary response of the power system?

1.6 The research report structure

The research scope (development of a dynamic multivariate power system inertia model) includes ten chapters, which are organised in the following manner:

Chapter 2 presents background theory into power system stability analysis and factors affecting system inertia. The purpose in this chapter is to survey previous studies conducted on calculating, measuring or estimating the power system inertia, simulation methods and available online models.

Chapter 3 is an introduction to Multivariate Analysis (MVA), which involves observation and analysis of more than one statistical outcome variable at a time. This chapter builds on the model development that will follow in Chapter 5.

Chapter 4 gives background of how data was gathered and describes on what type of data the calculation shall be performed so that the results are reliable.

Chapter 5 introduces the model development and background to the factors that are expected to affect system inertia, RoCoF and FPR in Eskom.

In Chapter 6, the disturbance location and frequency measurement points in the Eskom network are investigated by measuring the Rate of Change of Frequency (RoCoF) from previous disturbances. MVA is used to develop the RoCoF model and determine the factors affecting the system RoCoF. This lays a foundation for developing a model using normal incidences to determine the best reference centre inertia and frequency.

Chapter 7 evaluates the impact of disturbance location and the factors affecting the system inertia during the first 300 ms following the disturbances in the network and develops a simplified system inertia model without FPR.

In Chapter 8, estimation of the Inertia Constant and the prediction of the frequency nadir following disturbances using the MVA method are performed and validated with the past and recent incidences. The Inertia with FPR models are developed.

Chapter 9 focuses on the short-term frequency stability and understanding the relationship between system inertia and FPR of the Eskom power system including but not limited to RES, location of disturbance, stiffness of the system and the interconnected part of the Southern African Power Pool (SAPP). It begins by providing a background into the Eskom network, generation, load centres and typical known challenges. The strong and weak areas with respect of the inertia and stiffness of the system are identified using the MVA.

Chapter 10 presents the conclusion to the research.

1.7 Conclusion

In this chapter, a brief picture of the SAPP network and some challenges faced by Eskom such as declining network strength were provided. The decline of the Eskom average generation dispatch from 2012 to 2016 could translate to less synchronised generation on the grid. This is attributed to sustained lower economic growth, increased penetration of RES, evolving customers and technologies. The strength of the AC power system is mainly determined by the system inertia, which is mainly provided by connected synchronous generators and the stiffness of the system.

The Grid Code of South Africa clearly requires the SO to operate the power system within frequency limits. The only gap is that the Code does not directly specify the minimum required system inertia and the maximum RoCoF following a disturbance. The SAGC was written prior to the renewable generation being

installed and that is why the Grid Code is silent on inertia. It is however, covered in the frequency response rules and now it becomes important to understand what level of non-synchronous generators can be tolerated before we violate the Grid Code requirements. The Grid Code of South Africa requires that a minimum of 10% of instantaneous response from the installed capacity be maintained across the entire system. The code does not specify the minimum spinning and instantaneous reserves per area. The following chapter surveys previous studies conducted on calculating, measuring or estimating the power system inertia.

2. POWER SYSTEM FREQUENCY STABILITY AND SYSTEM INERTIA

2.1 Introduction

In the seven-year period spent working at the generation and load balancing dispatch desk in the Eskom National Control Centre, strange system behaviour during certain system disturbances was observed. The frequency responds differently for similar disturbances but different times and different network configurations.

The purpose of this chapter is to survey previous studies conducted on calculating, measuring or estimating the power system inertia, simulation methods and available online models. This chapter begins with a glossary of terms followed by background theory into power system frequency stability analysis. The different stages of generator and frequency response following a disturbance are discussed. The two methods (Inertia Constant and Swing Equation) of estimating the power system aggregated Inertia Constant (H) are discussed in detail. The real-time power system inertia monitoring methods used by other utilities are discussed. The methods are compared and the gaps are then identified.

2.2 Glossary

1. *Transient stability/large-disturbance rotor angle stability*: is concerned with the ability of the power system to maintain synchronism when subjected to a severe disturbance, such as a short circuit. The resulting system response involves large excursions of generator rotor angles and it is influenced by the nonlinear power-angle relationship. Transient stability depends on both the initial operating state of the system and the severity of the disturbance. Instability is usually in the form of aperiodic angular separation due to insufficient Synchronising Torque, manifesting as first swing instability. In large power systems, transient instability may not always occur [6], [7].
2. *Large-disturbance voltage stability*: refers to the power system's ability to maintain steady voltages following large disturbances such as system faults,

loss of generation or circuit contingencies. This ability is determined by the system and load characteristics, protection and the interactions of both continuous and discrete controls [2], [5].

2.3 Power system stability

Power system stability is the ability of an electric power system, for a given initial operating condition, to regain a state of operating equilibrium after being subjected to a physical disturbance, with most system variables bounded so that practically the entire system remains intact [6], [7]. Power System Stability is classified into three categories, Voltage Stability, Rotor Angle Stability and Frequency Stability shown in Figure 2-1 [7].

1) Voltage stability - the ability of a power system to maintain steady acceptable voltages at all buses in the system under normal operating conditions and after being subjected to a disturbance [7]. It depends on the ability to maintain/restore equilibrium between load demand and load supply from the power system. Instability that may result occurs in the form of a progressive fall or rise of voltages of some buses. Voltage stability is threatened when a disturbance increases the reactive power demand beyond the sustainable capacity of the available reactive power resources [2], [5].
2) Frequency stability refers to the ability of a power system to maintain steady frequency following a severe system disturbance resulting in a significant imbalance between generation and load [7].
3) Rotor angle stability: refers to the ability of synchronous generators of an IPS to remain in synchronism after being subjected to a disturbance [7]. It depends on the ability to maintain/restore equilibrium between electromagnetic torque and mechanical torque of each synchronous generator in the system. Instability that may result occurs in the form of increasing angular swings of some generators leading to their loss of synchronism with other generators [2], [5].

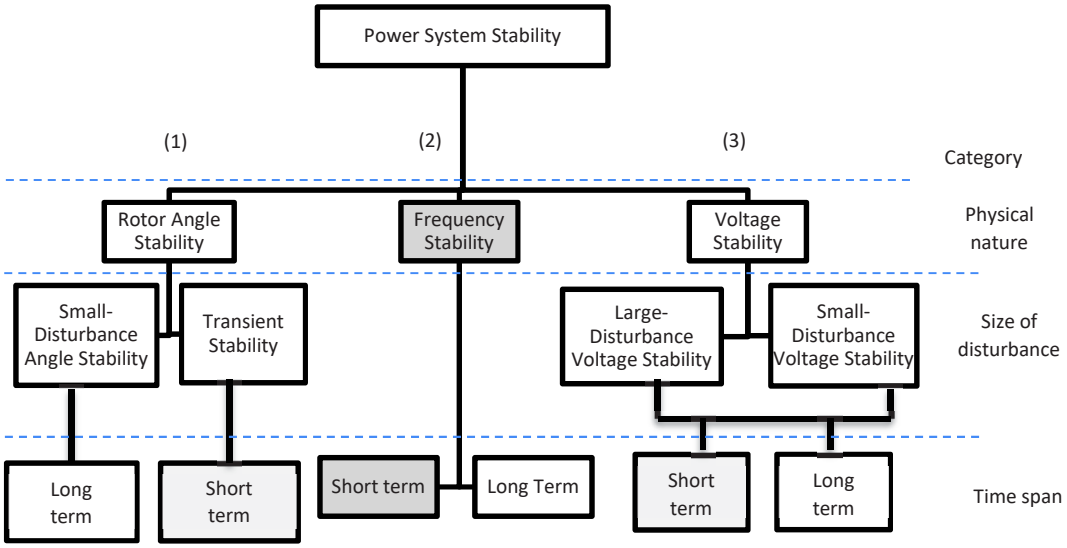

Figure 2-1: Block diagram showing the hierarchy of different power system stability classifications adapted from [3] and others.

During frequency excursions following a disturbance, the characteristic times of the processes and devices that are activated will range from [6], [20]:

- *fractions of a second* corresponding to the response of devices such as under-frequency load shedding and generator controls and protections,
- *several minutes* corresponding to the response of devices, such as prime mover systems and load voltage regulators.

In Figure 2-1, frequency stability may be a short-term phenomenon or a long-term phenomenon. Short-term frequency instability can result from a network with insufficient synchronous generation and insufficient under frequency load shedding such that the frequency decays rapidly causing blackout of the grid within a few seconds [4]. The Inertial Response of the system is closely related to the short-term frequency stability. In isolated systems like the Eskom network, frequency stability could be of concern for any large disturbance caused by significant loss of load or generation.

2.4 Frequency Staged Response following a generator loss

Frequency response following a generator loss can be classified into two categories based on the response time, namely primary and secondary response as shown in Table 2-1 [4], [6], [21].

Table 2-1: Response following a generator loss

	Primary response			Secondary response	
Stage	Electromagnetic Energy Storage	Inertial	Governor Response	AGC	SO controller involvement
Approximate reaction time	Very Fast		Slow	Slow	Very Slow
	< 1/3 s	> 1/3 s <12 s	> 2 s < 20 s	> 20 s	2-10 minutes

From Figure 2-2, the purpose of the primary response is to arrest the frequency following a disturbance (in the inertial stage). The secondary response is required to restore the frequency back to within normal operating limits (long term). The Primary Response category comprises Electromagnetic Energy Storage (EES), Inertial and governor stages [21]. Figure 2-2 shows the three stages of the primary response during a loss of a large generator in the Northern parts of the Eskom network. The measurements were taken from Phasor Measurement Units (PMUs) at Western Cape (Koeberg), Northern Province (Matimba) and Mpumalanga (Kendal).

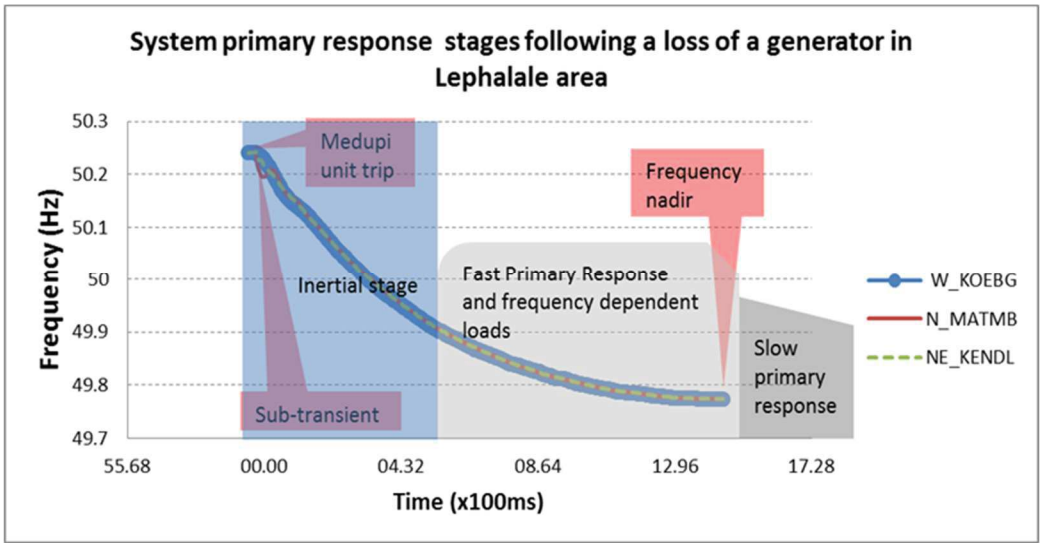

Figure 2-2: PMU data showing system primary response stages [PMU data downloaded by author].

2.4.1 Electromagnetic Energy Storage stage

The EES stage responds immediately following a loss of a generator. The generators that are electrically closest to the point of disturbance respond first and with the most active power [21]. When a load is suddenly applied to a generator, its internal impedance reduces sharply and then returns to normal in a few seconds. This drop in impedance enables the generator to supply more active power for a short duration. Similar generator responses were also observed from the KZN and Western Cape areas. This response happens within 100 ms following the disturbance in the Eskom network as illustrated in Figure 2-2.

2.4.2 Inertial Response

Inertial Response is defined as the power delivered by the rotating mass of machines synchronously connected to the bulk power system, including both load and generation [4]. The total inertia of all on-line synchronised generators determines the transient response of the entire generation system [4].

2.4.3 Secondary response

The secondary response is executed by the Automatic Generation Controller (AGC) often referred to as the Load Frequency Controller. The AGC system deploys regulating reserves to restore the frequency closer to the nominal

frequency. Generally the AGC can take anywhere from seconds to minutes [6]. The governor is normally co-ordinated with AGC after the initial response from the governors, AGC should deploy regulating reserves so that frequency is recovered back to 50 Hz [4], [6], [21]. The secondary response (AGC) is not covered in this work, since the response time is excessively slow compared to the primary response, where the interest of this work lies.

The aim of the following subsection is to understand the behaviour of the Inertia Constant, H, and the Rate of Change of Frequency (RoCoF) immediately following a disturbance in a power system.

2.5 Estimation of the system Inertia Constant, H

From the previous work on the system inertia, it was discovered that there are many different ways of calculating, measuring or estimating the power system inertia. The Inertia Constant estimation can be grouped into two general categories, (1) Inertia Constant Method and (2) Swing Equation Method.

The Inertia Constant Method takes advantage of precise models of a specific generation technology and uses parameter estimation techniques to find the value of the Inertia Constant for a specific generation unit as was used by [15], [17], [22], [23]. The basic application of this method consists of estimating the Inertia Constant of each generator in the system and then taking the sum of these estimates. In [24], a model for each power plant to simulate the response of its generating power to the frequency change was developed. All power plants including the once-through boiler and the drum boiler and the combustion turbine in the power system were modelled and the validity of each model was tested with measured data. In [25], an Inertia Constant estimation was demonstrated in a single bus simulation environment.

The Inertia Constant H in Equation 2.1 describes the normalised inertia of an individual generator, measured in seconds. It is the ratio between the Kinetic Energy (E_{kin}) in joules at rated speed and rated apparent power (S_{base}) in VA [6].

The Inertia Constant can be interpreted as the time that energy stored in the rotating parts of a generator is able to supply a load equal to the rated apparent power of the turbine-generator [2].

$$H = \frac{E_{kin}}{S_{base}} = \frac{1}{2}\frac{J\omega_{0m}^2}{S_{base}} \tag{2. 1}$$

Where:

J is the Moment of inertia ($kg.m^2$),

ω_{0m} is the normalised angular velocity (mechanical) (rad/s),

S_{base} is the apparent power (VA base).

The sum of the Inertia Constants and the rated apparent powers of individual generators can then be used to calculate the Inertia Constant of the entire IPS as given by Equation 2.2 [6].

$$H_{sys} = \sum_{i=1}^{n} \frac{S_{i,base} H_i}{S_{n,base}} \tag{2. 2}$$

Where:

$S_{i,base}$ is the rated apparent power of generator i (VA),

H_i is the Inertia Constant of generator i (s),

$S_{n,base}$ is the sum of the rated apparent powers of all the generators (VA).

The Inertia Constant Method is considered difficult for large power systems [4], [19]. For the IPS, information on the response of power plants of neighbouring countries may not be easily obtainable.

2.6 Estimation of the system Inertia Constant using transients

This section contains a derivation and a discussion of the Swing Equation, which is the mathematical relation describing how the rotor of a synchronous machine will move (swing) when there is an unbalance between mechanical power fed into the machine and the electrical power extracted from it [5].

The analysis of frequency measurements from a single location during a known disturbance to the system is classified as Inertia Constant Estimation using the Swing Equation method as was used by [19], [25]–[27].

2.6.1 Swing Equation of a synchronous machine without Damping Torque

The unbalance between the torques acting on the rotor and the net torque causing acceleration is given by Equation 2.3 [6].

$$T_a = T_m - T_e \tag{2. 3}$$

Where:

T_a is the accelerating torque (Nm)

T_m is the mechanical input torque (Nm)

T_e is the electromagnetic output torque (Nm)

The Swing Equation governs the motion of the machine rotor in the presence of an accelerating torque and isgiven by Equation 2.4 [6].

$$J \frac{d\omega_m}{dt} = T_a \tag{2. 4}$$

Where:

J is the combined moment of inertia of the generator and turbine $[kg.m^2]$

ω_m is the angular velocity of the rotor ((mech)rad/s)

By rearranging Equation 2.1, the moment of inertia *J* in terms of H is given by

$$J = \frac{2HS_{base}}{\omega_{0m}^2} \tag{2. 5}$$

Substituting 2.5 into Equation 2.4 gives

$$\frac{2H}{\omega_{0m}^2} S_{base} \frac{d\omega_m}{dt} = T_a \tag{2. 6}$$

Rearranging Equation 2.6 gives

$$2H\frac{d}{dt}\left(\frac{\omega_m}{\omega_{0m}}\right)=2H\frac{d}{dt}\left(\overline{\omega_m}\right)=\frac{T_a}{T_{base}}=\overline{T_a} \tag{2. 7}$$

Where:

$$\begin{aligned} &T_{base}=S_{base}/\omega_{0m} \text{ is the base torque (Nm)} \\ &\bar{\omega}_m=\omega_m/\omega_{0m} \text{ is the per unit speed ((mech)rad/s)} \\ &\bar{T}_a=T_a/T_{base} \text{ is the per unit acceleration torque ((mech)rad/s)} \end{aligned} \tag{2. 8}$$

The equation of motion in per unit form is given by Equation 2.9

$$2H\frac{d\bar{\omega}_r}{dt}=\bar{T}_a \tag{2. 9}$$

In this work, it is convenient to represent the swing equation in terms of change in active power and electrical frequency. Figure 2-3 shows the relationship between the torque, speed and flow of mechanical and electrical power in a synchronous machine [6]. The machine windage, friction and iron-loss torque are ignored.

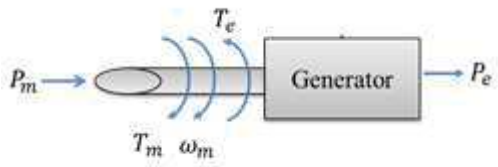

Figure 2-3: Flow of mechanical and electrical powers in a synchronous generator.

Equation 2.9 can be converted into its more convenient power form by assuming the rotor speed to remain constant at the synchronous speed (ω_{0m}) [6].

$$2H\frac{d}{dt}\left(\overline{\omega_m}\right)=\overline{P_a} \tag{2. 10}$$

Where:

$$\bar{P}_a=\bar{T}_a\,\omega_{0m}$$

$\bar{P}_a$ is the fractional power change (pu)

The Inertia Constant of the power system can also be estimated using the Swing Equation and post-disturbance frequency measurement data from a single location during a known disturbance [8]–[10]. This method was considered valid for a highly meshed grid by [11], in which all units can be assumed to be connected to the same grid bus, representing the centre of inertia of the given grid.

The Swing Equation Method derived in this section can be used to calculate H (pure inertia or RoCoF) and uses the data for the first 300 ms following a loss of a generator in the Interconnected Power System (IPS) as shown in Figure 2-4.

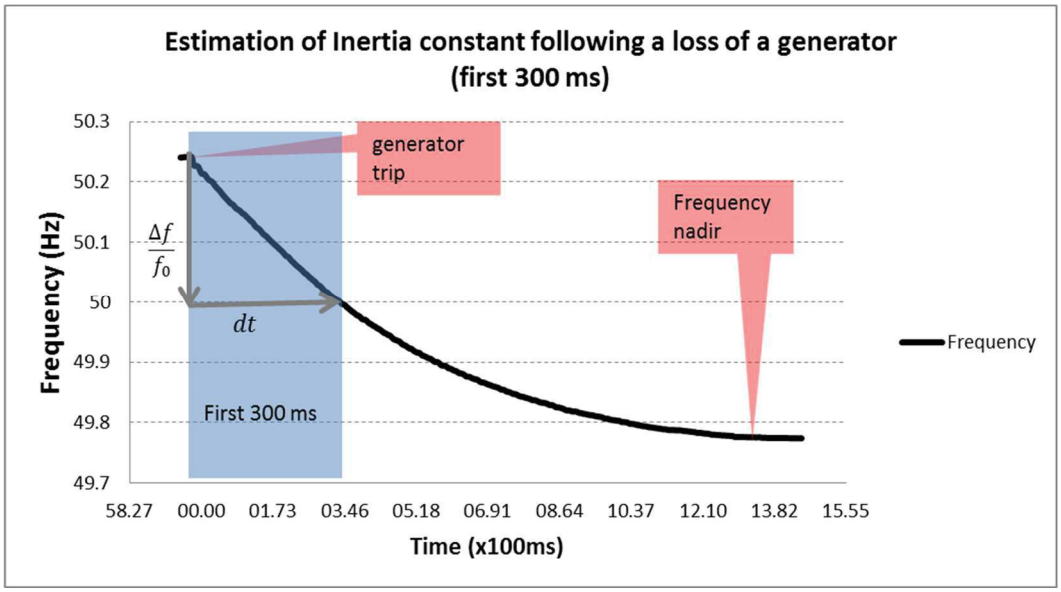

Figure 2-4: Estimation of Inertia Constant during the first 300 ms following a disturbance in the Eskom network [PMU data downloaded by author].

The behaviour of the system frequency following a loss of a generator is approximately represented using Equation 2.11 [6].

$$\frac{df}{dt} = \frac{\Delta P}{2H} f_{start} \tag{2. 11}$$

Where:

df / dt: is the Rate of Change of Frequency (RoCoF) (Hz/s)

$\Delta P = (P_{start} - P_{300ms})/P_{start}$ is the fractional power change (pu)

P_{start} is the Generation/Load prior to Generator/Load loss (MW)

P_{300ms} is the Generation/Load after Generation/Load loss (MW)

f_{start} is the Frequency at the start of the disturbance (Hz)

H is the Inertia Constant on system base (s)

The Swing Equation Method used to calculate H (pure Inertia Constant and RoCoF) uses the data for the first 300 ms. In contrast, when data is used up to the frequency nadir, this gives information on the inertia with Fast Primary Response (FPR).

2.6.2 Swing Equation of a synchronous machine with damping torque

The behaviour of the frequency deviation following a loss of a large generator is approximately represented using Equation 2.10 [21]–[23]. The equation uses the average system frequency and does not consider inter-machine oscillations due to synchronising power and transmission performance. According to [6], [21], the assumption of lossless machine and ignoring the torque of damper windings leads to pessimistic results in transient stability analysis damping helps to stabilise the system. Damping must be considered in a dynamic stability study.

In Equation 2.8,

$$\overline{\omega_m} = \frac{\omega_m}{\omega_{0m}} = \frac{\omega_r / p_f}{\omega_0 / p_f} = \frac{\omega_r}{\omega_0} \qquad (2.\ 12)$$

Where:

ω_r is the angular velocity of the rotor in ((elec)(rad/s)

ω_0 is the nominal value of ω_r((elec)rad/s))

p_f is the number of field pole pairs of the synchronous machine

The angular position of the rotor with respect to a synchronous rotating reference is given by [5]

$$\delta = \omega_r t - \omega_0 t + \delta_0 \tag{2. 13}$$

Where:

δ is the angular position of the rotor in ((elec) radians)

δ_0 is the value of δ at t=0 ((elec) radians)

Taking the first and the second derivative gives

$$\frac{d^2\delta}{dt^2} = \frac{d\omega_r}{dt} = \frac{d(\Delta\omega_r)}{dt} \tag{2. 14}$$

Substituting Equation 2.12 in Equation 2.14 results in

$$\frac{d^2\delta}{dt^2} = \omega_0 \frac{d\bar{\omega}_r}{dt} = \omega_0 \frac{d(\Delta\omega_r)}{dt} \tag{2. 15}$$

By substituting Equation 2.15 in Equation 2.9 gives

$$\frac{2H}{\omega_0}\frac{d^2\delta}{dt^2} = \bar{T}_a \tag{2. 16}$$

The complete Swing Equation can be represented by adding the Damping Torque, which is proportional to the speed deviation. It follows that the Swing Equation is a non-linear second-order differential equation given by Equation 2.17.

$$\frac{2H}{\omega_0}\frac{d^2\delta}{dt^2} = \bar{T}_a - K_D\Delta\bar{\omega}_r \tag{2. 17}$$

Where:

K_D is the damping coefficient of a synchronous machine

2.6.3 Swing Equation of a synchronous machine with damping torque plus FPR

A procedure different from the Inertia Constant Method for estimating the Inertia Constant of a power system and total on-line capacity of spinning-reserve

generators, using the measured transients of the frequency, is first presented in [19]. This estimates the dynamic behaviour of the system frequency for loss of generation or load. The Coefficient of Determination between the Inertia Constant and the power/frequency characteristic was calculated and yielded positive results [19]. However, the standard deviation of the coefficient was so big that the authors gave up the statistical evaluation. The study in this literature was done in the mid 1990s where the measurement sample rates were lower when compared to the latest PMU data which samples at a much faster rate. A polynomial approximation with respect to time was fitted to the waveform of the transients when estimating the Inertia Constant. The small number of frequency disturbances was a reason for the large standard deviation. The gap in this work is that the authors attempted to validate the model by only considering the standard error. According to [29], the value of the standard error, s_ε, is judged by comparing it to the values of the dependent variable. However, because there is no predefined upper limit on s_ε, it is often too difficult to assess the model in this way. In general, the standard error of estimate cannot be used as an absolute measure of the model's validity. This method may be applicable to Eskom given the available number of generator disturbances.

In [26], a similar approach to [19] was followed by Western Electricity Coordinating Council (WECC) to estimate system inertia using observed frequency transients. The difference was that WECC did not consider the stiffness of the system in their calculations. The advantage of the WECC study was that they had a large number of generator trips. The data collected by WECC was taken at ten samples per second. The rate was higher than in [19]. From 388 events, WECC successfully validated 167 events. For the remaining events 221 events had insufficient data to compute an Inertia Constant correctly at the time. Errors were reported to be due to data accuracy and the search algorithm which was not able to obtain a frequency profile. In addition, the study excluded events that did not result in a frequency below 59.95 Hz (60 Hz network). When the Inertia Constant was compared to system load, a linear fit was obtained and the standard error of 4.15 was achieved. It was also suggested that the other factors other than system load, such as seasonal variation and generator dispatch

scheduling, might contribute to variation of the Inertia Constant. The effects of measurement, disturbance locations, asynchronous generation and system damping were not studied.

In [30], inertia estimation of the Great Britain (GB) power system using synchro-phasor measurements was developed. This method proposed to first detect a suitable event for analysis and then filter the measured transients to obtain a reliable estimate of inertia for a given region of the GB network. Large frequency deviations because of instantaneous in-feed losses are a rare occurrence on the GB system.

2.7 Offline system inertia calculation tools

The common simulation packages used in Eskom to estimate system inertia are DiGSILENT and Power System Simulation for Engineers (PSSE) offline simulation tools. These tools are stand-alone and offered by different service providers. They are presently not synchronised with the operational online tool, Energy Management System (EMS).

In the DiGSILENT model, power balance is established by all generators and the contribution of each is according to the inertia and it is proportional to the acceleration time constant [31]. This relationship is described in Equation 2.18:

$$P_i = P_{i-dispatch} + \Delta P_i \tag{2. 18}$$

Where:

P_i is the modified active power of generator i (MW),

$P_{i-dispatch}$ is the inertial active power dispatch of generator i (MW),

ΔP_i is the active power change of generator i (MW).

The theoretical approach has largely been investigated in the past in Eskom - for the static security tools, but less for the dynamic security tools. The offline studies are inaccurate and unrealistic in the Eskom operational environment because the network scenarios change rapidly and an extensive set of simulations are required to achieve close to realistic results. The simulation package is good for long term

planning and in determining the steady state power system inertia hard limits. However, the offline simulation software is difficult to rely on, since:

- Equivalent models/networks are used to simplify the large distribution networks.
- Not all the critical parameters are known, i.e. Inertia Constant (H). The users often use the manufacturer specification data, which could gradually change as generators are refurbished, upgraded or degraded with time [32].
- The load modelling can be very difficult due to the lack of data, from its stochastic nature in time and its geographically distributed nature [17].
- International tielines are over-simplified given the unavailability of neighbouring data.
- The tool assumes that the contribution of each individual generator towards the total additional power required is proportional to its Inertia Constant, i.e. the generator acceleration time constants must be known. In Eskom not all the generators are capable of providing instantaneous reserves due to various reasons, including ageing/deterioration and design capability.
- The Inertia Constant is a parameter of rotating electrical machinery often required from suppliers by customers as guaranteed data. It is commonly used by power system analysts who use it as input data for simulation programs [32].

2.8 Real-time monitoring of system inertia

The system inertia of the Nordic power system was calculated in [17] using the Inertia Constant Method. Efforts were made to analyse the historical frequency disturbances and to estimate the consequences of reduced inertia on the frequency disturbances. The model that was developed used only the relation between power imbalance and kinetic energy. Other factors affecting system inertia were not considered due to unavailability of data and information from neighbouring countries. Although this method provided good results for certain areas of the network, it did not fully give a clear insight to the overall power system inertia, given that the system inertia varies depending on the dependent variables.

EIRGRID has developed a real-time tool, namely System Non-Synchronous Penetration (SNSP) [33]. SNSP is a single, easily computed, parameter, which gives an indication of the ability of the system to maintain adequate frequency response to events on the grid. SNSP is given by Equation 2.19.

$$SNSP = \frac{RES_{generation} + imports}{System_demand - exports} \quad (2.19)$$

The following requirements have been identified for the Irish system:

- Inertia of ±22,600 MW.s (MJ)
- Maximum RoCoF of 0.5 Hz/s

These requirements translate to a maximum SNSP of 60%. In order for Ireland to meet increasing European Union targets of reducing the CO_2 emissions, it is envisaged that SNSP will have to increase to at least 75%, at which levels EIRGRID envisages problems relating to frequency control.

The Inertial Frequency Response Estimator Tool (IFRET) was developed by [4] 137 historical frequency disturbance events in the ERCOT interconnection were used as an input to back-cast the Inertial Response. Inertial Response was correlated with system load, total on-line conventional generation capacity, spinning reserves and ratio of wind generation to total generation. The estimated Inertial Responses for the historical frequency disturbances were compared to the actual recorded data and the average error for estimated Inertial Response was 5.92% with 3.5% standard deviation of error. The Coefficient of Correlation (R) between system load and Inertial Response was found to be closer to one, which implied that the relationship between loss of active power and change in frequency was highly correlated and varied linearly with system inertia.

This work demonstrated that previous frequency events could be used through correlating the Inertial Response with system load, total on-line conventional generation capacity, spinning reserves and ratio of wind generation to total

generation. However, the impact of disturbance location and stiffness of the system was not covered. The model was validated using only the Coefficient of Determination and the Standard Deviation of Error. Other statistical model validations were not demonstrated.

2.9 Conclusion

There is a lot of literature available, which presents the system inertia and primary frequency response for utilities worldwide. However, the power system networks differ in size and characteristics. The Eskom network, compared to other interconnected utilities, is viewed as an "Isolated Grid" since the tielines connected to the neighbouring utilities are too weak (with respect to primary response) to assist in case of large disturbances. The load pattern, generation location and dispatch patterns are also different.

In this chapter, two methods of estimating the Inertia Constant were discussed. The Inertia Constant Method requires knowledge of the frequency, mechanical power and electrical power of every generator synchronised on the system and it is applicable to a meshed network. Post-disturbance analysis of frequency measurements from a single location during a known disturbance in the system is classified as inertia estimation using the Swing Equation Method. None of the methods reviewed in this chapter are perfectly suitable for the Eskom network to meet the South African Grid Code (SAGC) requirements.

3. MULTIVARIATE ANALYSIS

3.1 Introduction

Regression Analysis is used to predict the value of one variable based on another variable. The technique involves developing a mathematical equation that describes the relationship between the variable to be forecast, which is called the dependent variable and the independent variables [29].

The techniques applicable to this work are Analysis of Variance (ANOVA) and Multivariate Analysis of Variance (MANOVA). MVA examines the relationship between several categorical independent variables and two or more metric dependent variables [29].

This chapter is a build up to Chapters 5 to Chapter 9, which cover the model development for the Rate of Change of Frequency (RoCoF) and Inertia with Fast Primary Response (FPR) for the Eskom power system. The chapter starts with the basics of determining regression lines. The chapter ends with a discussion of the four important indicators of a good or poor model.

3.2 First-order linear model

In the first order linear model or the simple linear regression model, the relationship between *x* and *y* is given by Equation 3.1 [29].

$$y = \beta_0 + \beta_1 x + \varepsilon \tag{3.1}$$

Where:

y is the dependent variable

β_0 is the value of *y* where the true line intercepts the y axis (x=0)

$\beta_1$is the slope of the true line

x is the independent variable

ε is an error variable

Regression analysis assumes that the two variables, *x* and *y* are linearly related and correlated. Figure 3-1 shows the scatter diagram with the regression line.

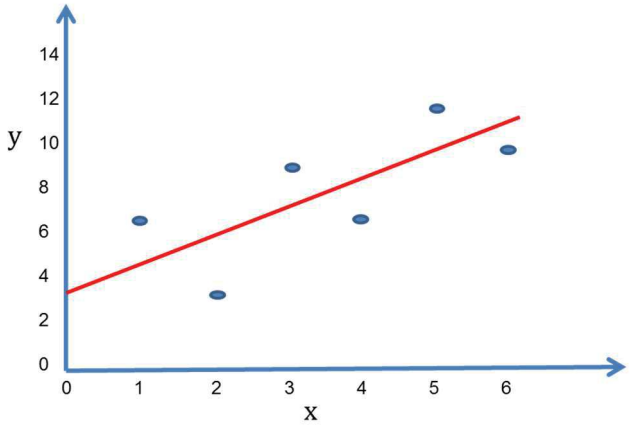

Figure 3-1: Scatter diagram with the regression line.

3.2.1 Estimating the coefficients for a single independent variable

The least squares or regression line method aims to produce a straight line that minimises the sum of the squared differences between the sample values of y and the line. Equation 3.2 represents the regression line [29].

$$\hat{y} = b_0 + b_1 x \tag{3.2}$$

Where:

$\hat{y}$ is the value of y obtained from the regression line,

b_0 is the regression line intersection with the *y*-axis (x=0),

b_1 is the slope of the regression line.

The coefficients b_0 and b_1 are derived so that the sum of the squared deviations $\sum_{i=1}^{n}(y_i - \hat{y}_i)^2$ is minimised.

Where:

y_i is the *i*th sample of y

$\hat{y}_i$ is the *i*th value of y obtained from the regression line

The least squares coefficients; b_1 and b_0 are given by Equation 3.3 and 3.4 respectively [29].

$$b_1 = \frac{s_{xy}}{s_x^2} \tag{3.3}$$

$$b_0 = \bar{y} - b_1\bar{x} \tag{3.4}$$

Where:

$$s_{xy} = \frac{\sum_{i=1}^{n}(x_i - \bar{x})(y_i - \bar{y})}{n-1}$$

$$s_x^2 = \frac{\sum_{i=1}^{n}(x_i - \bar{x})^2}{n-1}$$

$$\bar{x} = \frac{\sum_{i=1}^{n} x_i}{n}$$

$$\bar{y} = \frac{\sum_{i=1}^{n} y_i}{n}$$

The least squares method produces the best straight line. However, there may in fact be no relationship or perhaps a nonlinear relationship between the two variables [29]. To evaluate the model, two statistics and one test model procedure were used. All these methods are based on the sum of squared errors.

3.2.2 Sum of Squared Errors (SEE)

The deviations between the actual data points and the line are called residuals and are given by Equation 3.5 [29]. The residuals are observations of the error variable shown in Figure 3-2.

$$\varepsilon_i = y_i - \hat{y}_i \tag{3.5}$$

Where

y_i is the *i*'th sample of *y*,

$\hat{y}_i$ is the *i*'th sample of y obtained from the regression line.

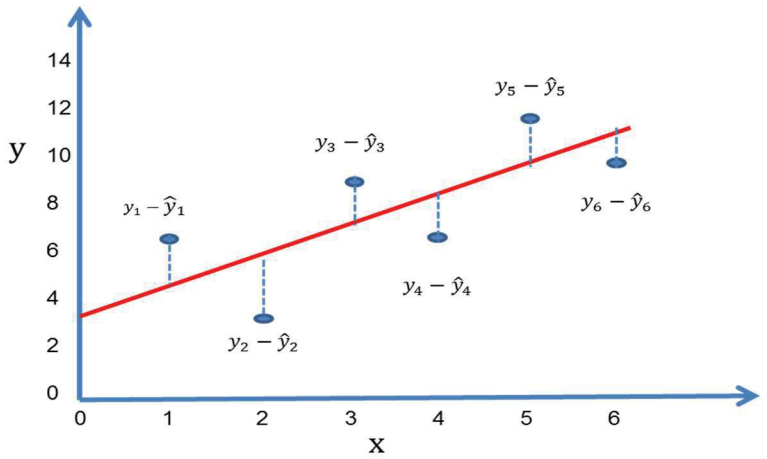

Figure 3-2: Calculation of residuals [29].

The Sum of Squared Errors (SSE) is given by Equation 3.6 [29]

$$SSE = \sum \left(y_i - \hat{y}_i \right)^2 = (n-1)\left(s_y^2 - \frac{s_{xy}^2}{s_x^2} \right) \tag{3.6}$$

Where s_y^2 is the sample variance of the dependent variable.

Note that the $\hat{y}_i$ is computed by substituting x_i into the formula of the regression line [29]. The residuals are the differences between the observed values of y_i and the fitted or predicted values of $\hat{y}_i$.

3.2.3 Standard Error of Estimate (SEE)

The Standard Error of Estimate, also called the Standard Error of Regression Slope, measures the average distance that the observed values deviate from the regression line [29]. It is the measure of the accuracy of prediction. The smaller the value of s_ε, the closer are the values to the regression line.

The standard deviation of the error variable, σ_ε, measures the suitability of using a linear model. According to [29], the σ_ε is a population parameter and is unknown. However, the σ_ε can be estimated from the data that is based on the outcome of the Standard Error of Estimate (*SSE*). The unbiased estimator of the variance of the error variable σ_ε^2 is given by Equation 3.7 [29].

$$\sigma_\varepsilon^2 = \frac{SSE}{\mathrm{n}-2} \tag{3.7}$$

The square root of σ_ε^2 is called the Standard Error of Estimate (*SEE*) given by Equation 3.8 [29].

$$SEE = s_\varepsilon = \sqrt{\frac{SSE}{n-2}} \tag{3.8}$$

The value of s_ε is judged by comparing it to the values of the dependent variable *y* or more specifically the sample mean $\bar{y}$ [29]. However, because there is no predefined upper limit on s_ε, it is often too difficult to assess the model in this way. In general, the Standard Error of Estimate, *SEE,* cannot be used as an absolute measure of the model's validity [29].

3.2.4 One-tail test

The sampling distribution of the *t-statistic* or the test statistic for β_1 (the true slope) is expressed by Equation 3.9 [29]. The Confidence Interval Estimator of β_1 is given by Equation 3.10 [29].

$$t = (b_1 - \beta_1)/s_{b_1} \quad v = n - 2 \tag{3.9}$$

$$b_1 \pm t_{\alpha/2} s_{b_1} \quad v = n - 2 \tag{3.10}$$

Where *v* is the number of degree of freedom.

In order to test for positive or negative linear relationships, a one-tail test is conducted. This method starts with a null hypothesis, which indicates that there is

no linear relationship, meaning that the slope is zero. The hypothesis is specified by [29]:

$$H_0: \beta_1 = 0$$
$$H_1: \beta_1 < 0$$

The case of *P-value* would be the two-tail *P-value* divided by two. If the hypothesis is true, it does not necessarily mean no relationship exists. If the alternative hypothesis is true, it may be that the linear relationship exists or that a nonlinear relationship exists [29].

3.2.5 Coefficient of Determination (R^2)

The Coefficient of Determination is the key output of regression analysis. It measures the proportion of the variance in the dependent variable that is predictable from the independent variable [29]. The test of Slope coefficient; β_1 addresses only the question of whether there is enough evidence to infer that a linear relationship exists [29]. In many cases, however, it is useful to measure the strength of that linear relationship, particularly in this work where several different models require comparison. The statistic that performs such a function is called the Coefficient of Determination, defined in Equation 3.11 [29].

$$R^2 = \frac{s_{xy}^2}{s_x^2 s_y^2} \tag{3.11}$$

SSE measures the amount of variation in *y* that remains unexplained. By incorporating this analysis into the definition of R^2, R^2 can therefore by expressed by Equation 3.12.

$$R^2 = 1 - \frac{SSE}{\sum(y_i - \bar{y})^2} = \frac{\sum(y_i - \bar{y})^2 - SSE}{\sum(y_i - \bar{y})^2} = \frac{\text{Explained variation}}{\text{Variation in y}} \tag{3.17}$$

It follows that R^2 measures the proportion of the variation in *y* that is explained by the variation in *x* shown in Figure 3-3.

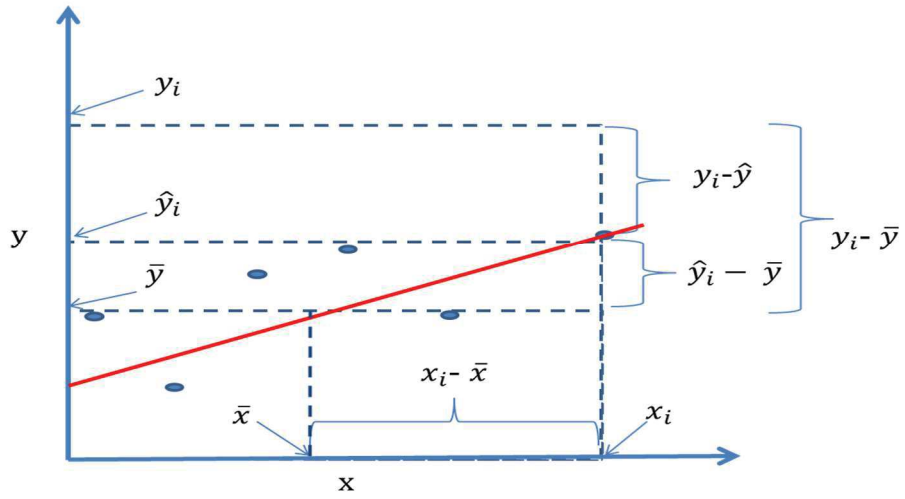

Figure 3-3: Partitioning the deviation for *i=n* [29].

3.3 Multiple Regression

Multivariate Analysis (MVA) is based on the statistical principle of multivariate statistics, which involves observation and analysis of more than one statistical variable outcome at a time [29]. This section assumes that *k* independent variables are potentially related to the dependent variable. It follows that the model can be represented by Equation 3.13 [29].

$$y = \beta_0 + \beta_1 x_1 + \beta_2 x_2 + \cdots + \beta_k x_k + \varepsilon \tag{3.13}$$

Where:

y is the dependent variable

$x_1 x_2 \ldots x_k$ are the independent variables

$\beta_1 \beta_2 \ldots \beta_k$ are the true coefficients

ε is the error variable

The sample regression equation is expressed similar to the simple regression given by Equation 3.14.

$$\hat{y} = b_2 + b_2 x_1 + b_2 x_2 + \cdots + b_k x_k \tag{3.14}$$

3.3.1 Multiple Regression Standard Error of Estimate

In multiple regression, the Standard Error of Estimate, s_ε, is given by Equation 3.15.

$$s_\varepsilon = \sqrt{\frac{SSE}{n-k-1}} \tag{3.15}$$

Where:

n is the sample size
k is the number of independent variables in the model

3.3.2 Testing the slope of a coefficient

One or two tail tests of β_1 can be conducted. In most cases, a two-tail test method is used to determine whether there is sufficient evidence to infer that a linear relationship exists [29]. If the alternative hypothesis is true, it may be that a linear relationship exists or that a nonlinear relationship exists but that the relationship can be approximated by a straight line. The estimated standard error of b_1 is given by Equation 3.16 [29].

$$s_{b_1} = \frac{s_\varepsilon}{\sqrt{(n-1)s_x^2}} \tag{3.16}$$

Where:

s_ε is the standard error of estimate,

s_x^2 is the variance of the samples of the independent variable.

3.3.3 F statistic test

An *F* statistic is a value in a regression analysis that determines if the means between two populations are significantly different. The *F-test* indicates if a group of variables are jointly significant [29]. A large value of *F* indicates that most of the variation in *y* is explained by the regression equation and that the model is valid. A small value of *F* indicates that most of the variation in *y* is unexplained.

The *F statistic* is the ratio between the MSR and MSE shown in Equation 3.17. A large value of F indicates that most of the variation in *y* is explained by the regression equation and that the model is valid.

$$F = \frac{MSR}{MSE} \tag{3.17}$$

Where:

$$MSR = \frac{SSR}{dfR} = \frac{SSR}{1}$$

Where dfR = a number referred to as its degrees of freedom, which is always 1.

$$MSE = \frac{SSE}{dfE} = \frac{SSE}{n-2} \tag{3.18}$$

Where dfE = a number referred to as its degrees of freedom, which is n-2.

The *significance of F* indicates that most of the studied variables are jointly significant.

3.3.4 Multicollinearity [29]

Multicollinearity is a condition wherein the independent variables are highly correlated. Multicollinearity distorts the *t-tests* of the coefficients of the independent variables. There are two consequences of multicollinearity. First, because the variability of the coefficient is larger, the sample coefficient may be far from the actual population parameter, including the possibility that the statistic and the parameter may have opposite signs. Secondly when the coefficients are tested, the t statistics will be small, which leads to the inference that there is no linear relationship between the affected independent variable. The multicollinearity does not affect the *F* test of the analysis of variance [29].

3.4 Assessing the model

The assessment of the model can be summarised in Table 3-1 [29]. The model is perfect if SSE and $\mathbf{s_\varepsilon}$ are zero, $\boldsymbol{R^2}$ is one and the *F statistic* is infinite. The model is poor if SSE and $\mathbf{s_\varepsilon}$ are large, $\mathbf{R^2}$ is zero and the *F statistic* is small.

Table 3-1**:** Relationships among *standard error of estimate,* R^2 and *F statistic*

SSE	$\mathbf{s_\varepsilon}$	$\boldsymbol{R^2}$	***F statistic***	**Assessment of Model**
0	0	1	∞	**Perfect**
Small	Small	Close to 1	Large	**Good**
Large	Large	Close to 0	Small	**Poor**

3.5 Regression variables

MVA requires sets of inputs of *y range* (dependent variable) and *x range* (independent variables) as shown in Table 3-2.

Table 3-2: Dependent (*y*) and independent (*x*) input variables used in the regression analysis tool

Observations	Input y range	Input x range					
1	y_1	x_{11}	x_{12}	x_{13}	x_{14}	...	x_{1n}
2	y_2	x_{21}	x_{22}	x_{23}	x_{24}	...	x_{2n}
3	y_3	x_{31}	x_{32}	x_{33}	x_{34}	...	x_{3n}
⋮	⋮	⋮	⋮	⋮	⋮		⋮
n	y_n	x_{n1}	x_{n2}	x_{n3}	x_{n4}	...	x_{nn}

3.6 Regression summary results table description

Table 3-3 shows the standard regression results output in Microsoft Excel. This format was used throughout this work in the following chapters to present the results.

This work focuses on the Coefficient of Determination (R^2) and the Standard Error of Estimate, which are reported on the second and fourth lines of the Regression Statistics, respectively. The number of observations is shown on the fifth line of Table 3-3.

The results of the analysis of variance are reported in an analysis of variance (ANOVA) table. The ANOVA contains three rows, “Regression”, “Residual” and “Total”. The sum of squares (“SS”) column gives the SSR, SSE and SS Total. This work focuses on the value of SSE indicated in row 3 of Table 3-3. The *F statistic* is given in column five and the *significance of F* is given by the *P-value* in column six, row seven.

Table 3-3: Microsoft Excel Regression summary output

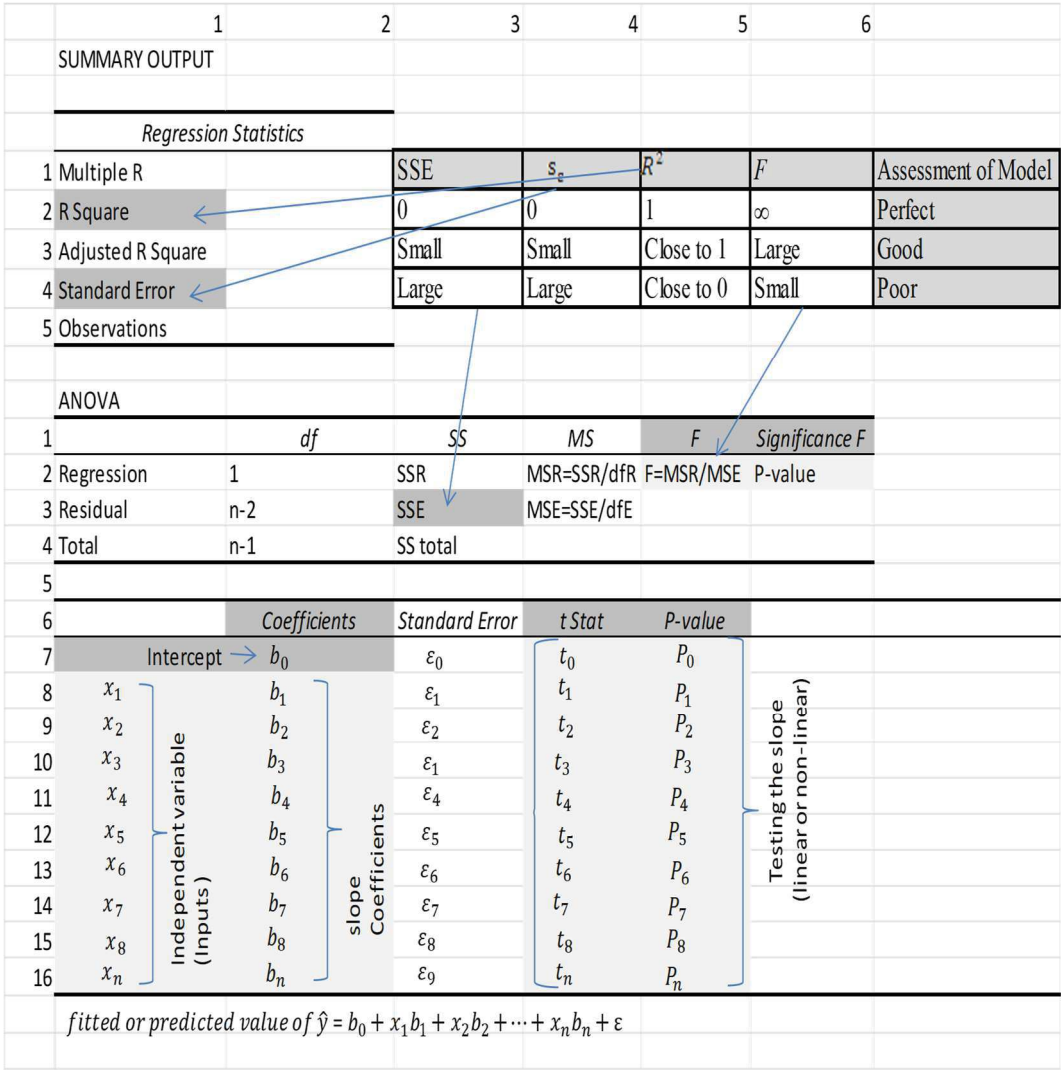

The values of SSE, s_ε, R^2 and F statistics were discussed in this chapter and are used in the following chapters as a basis of the model development and validation.

4. GATHERING, FILTERING AND MEASURING POWER SYSTEM DISTURBANCES DATA

4.1 Introduction

This chapter gives background on the data collection that was used for this work. Attempts to calculate the inertia of a system from frequency measurements in the past have resulted in widely varying results. The inertia estimates were very sensitive to the frequency data used and to the calculation method. The aim of this work was to define how and with what type of data the calculation shall be performed so that the results are accurate and realistic.

4.2 Glossary

1. **Frequency nadir** refers to the minimum instantaneous frequency following a loss of a generator [4]. In this work, the frequency nadir refers to the minimum frequency reached after a disturbance prior to slow primary and secondary responses.

2. Instantaneous Reserve from **Demand Response** (IDR) is consumer load contracted to respond to a drop in frequency [34].

3. The **moving average** for a time period is the arithmetic mean of the values in that time period [29].

4.3 Data accuracy factors affecting the system inertia

The ability to estimate the inertia of the system through the Inertia Constant Method and Swing Equation Method is dependent on the accuracy of the measured data. In [17], [30] the data accuracy factors affecting system inertia were summarised as follows:

- Precise data on the size of the generator loss;
- Online plant inertias (for estimate of the residual contribution);
- Identification of event start time;
- Accuracy of frequency measurement;

- Method of system inertia calculation;
- Location of measurement point relative to the generator loss.

The PMU extracts the magnitude, phase angle, frequency and Rate of Change of Frequency (RoCoF) from the signals appearing at its input terminals. These signals may be corrupted by harmonics, noise and changes in state caused by system loads and control and protective actions [35].

4.4 Frequency incident data collection and storage

The Eskom SO stores real-time data on Data Energy Centre (DEC) servers. The data ranges from one second to hourly data. The data remains on the servers for a certain period and is then archived. This data includes and is not limited to the generator sent-out, spinning reserves, installed capacity, Area Control Error (ACE), Automatic Generator Control (AGC) status, frequency, generation load losses, instantaneous reserves, time error and 1 to 15-minute system snap shots of the state of the transmission network. Figure 4-1 shows the data sources.

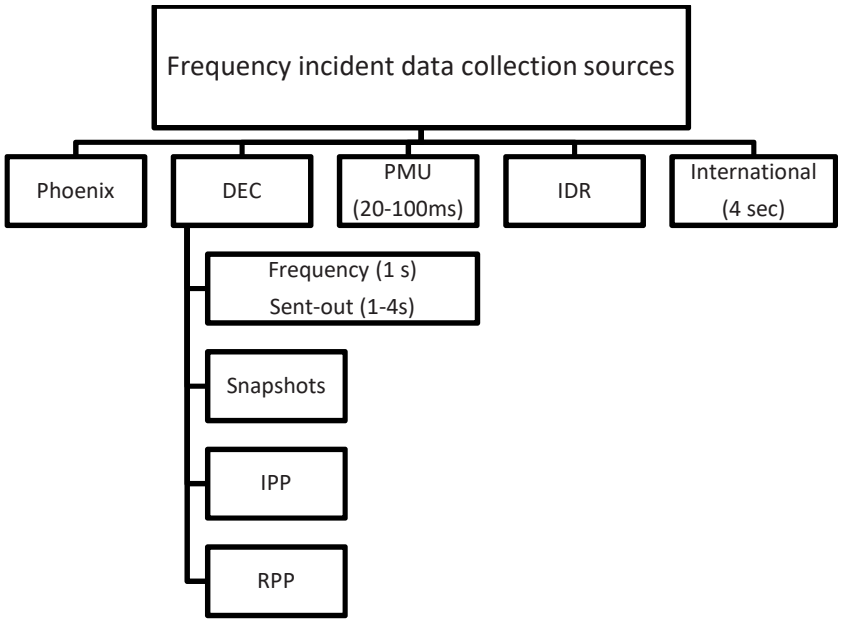

Figure 4-1: Frequency incident data collection sources.

This section describes the process used to collect the data. Frequency incident data for the period of June 2014-March 2017 was collected from the Eskom EMS/DEC

and Wide Area Monitoring System (WAMS). The method of extracting data, storing and calculation of required data was developed and partly automated. The data is correlated with system snapshots at the time of incidents, which comprises Eskom generator sent-outs, generation load losses, spinning reserve, renewable generation output, tie-line flows, IPP outputs and IDR data.

This data was analysed in the next chapters where the power system Inertia Constant is calculated for different system conditions. Microsoft Excel was used to collect and store the recovered frequency incidents in a database and to perform MVA calculations.

4.5 Frequency disturbance by type in Eskom

Frequency instability in the Eskom network can be caused by the loss of generation, load or transmission equipment resulting in either loss of generation or load or both. Figure 4-2 shows the typical examples of different disturbance types that may result in frequency disturbances in the Eskom network. Transmission equipment refers to various components such as transformers, transmission lines, Static Var Compensators (SVC), shunt reactors and capacitors.

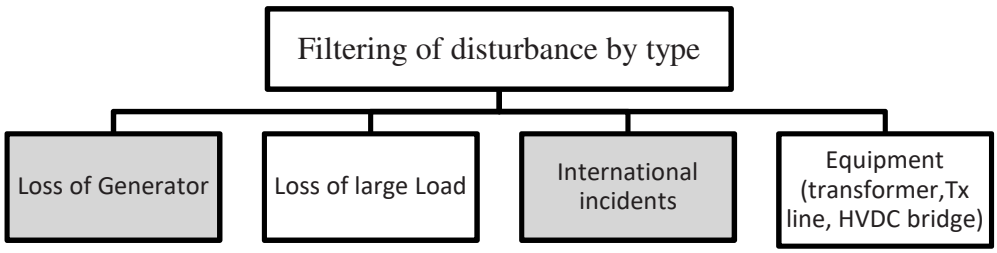

Figure 4-2: Filtering of frequency disturbances by type.

4.5.1 Loss of a generator

This research is focused on studying the Eskom system inertia using historical frequency disturbances. There are a number of available generation incidences - approximately 2000 events in the past three years that made it possible to continue with this study.

4.5.2 Loss of large load

The loss of large loads such as smelters is not covered in this research due to confidentiality clauses signed between Eskom and customers. However, the data is available and will be studied in future, as high frequencies caused by loss of large loads can be of great concern.

4.5.3 Loss of a transmission circuit

The loss of a transmission circuit is not covered in this work due to the small number that lead to frequency disturbances. However, loss of the Cahora Bassa (HVDC) infeed is covered since these events are considered as a credible multiple unit trip by the Grid Code of South Africa.

4.5.4 International incidents

The loss of cross-border generators is not covered in this research since relevant data was difficult to gather.

4.5.5 Demand Side Management (DSM) and Instantaneous Demand Response (IDR)

The purpose of the Instantaneous Reserve is to arrest the frequency at an acceptable limit following a contingency, for example a generator trip. If available, it responds to a frequency incident within 10 seconds and is sustained for at least 10 minutes [34]. A frequency lower than 49.65 Hz (with a certain time delay), will trigger the first load block of the Instantaneous Demand Response (IDR). A frequency lower than 49.60 Hz, will trigger of the second load block. Figure 4-3 shows the successful IDR response following a loss of a large unit. Furthermore, the response resulted in a frequency overshoot, which was above the nominal frequency of 50 Hz.

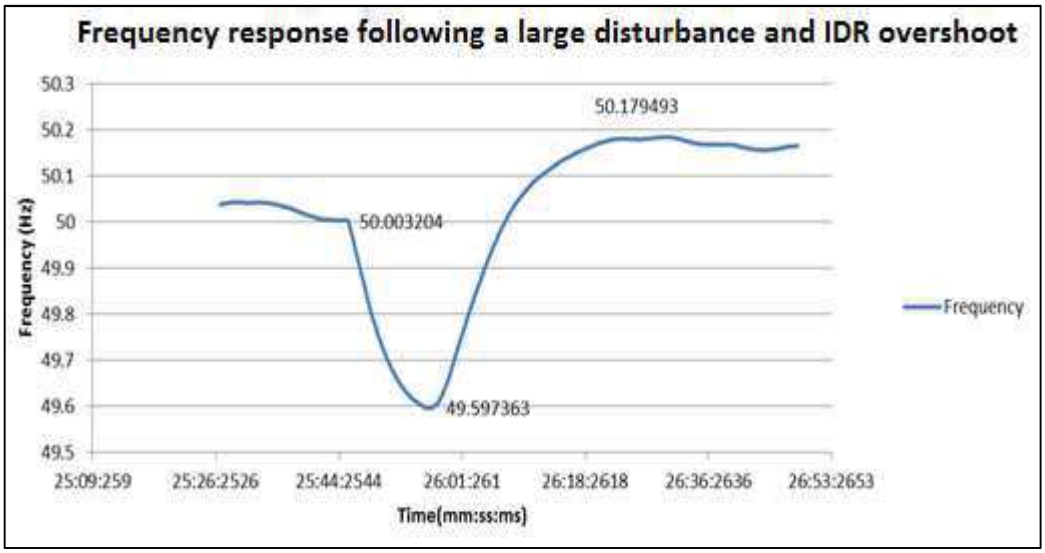

Figure 4-3: Frequency response following a large disturbance and frequency overshoot due to IDR [PMU data downloaded by author].

The Under Frequency Load Shedding (UFLS) scheme is also consumer load mandated to respond to a drop in frequency. UFLS is designed to trip blocks of load from the system in a period faster than any human controller can respond. A frequency lower than 49.20 Hz, will trigger approximately 3.3% of peak load. Figure 4-4 shows the UFLS response following a multiple unit trip.

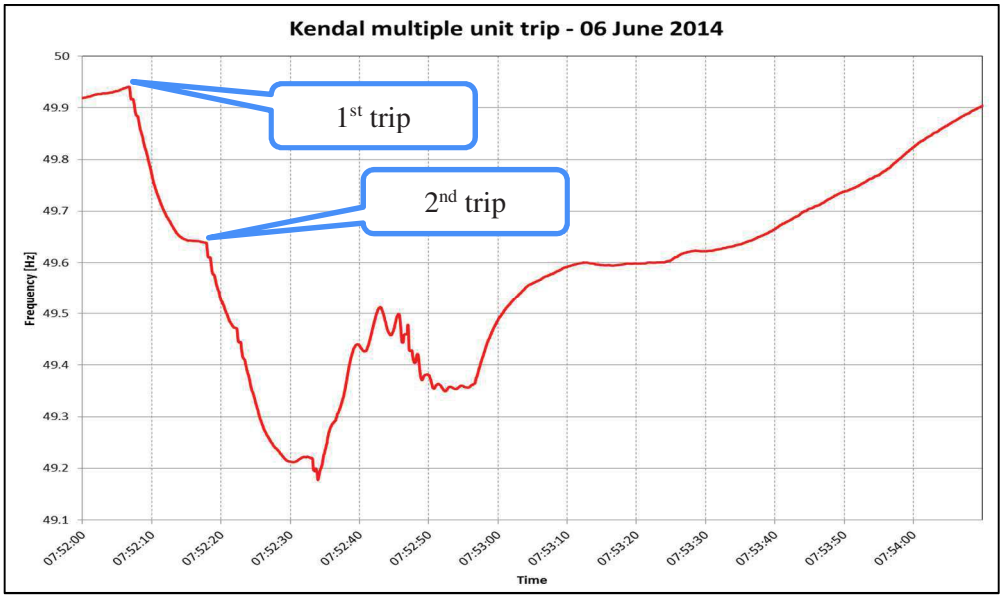

Figure 4-4: UFLS response following multiple unit trips at Kendal power station – 06 June 2014 [PMU data downloaded by colleague].

Calculating or measuring the RoCoF resulting from multiple unit trip incidents was beyond the scope of this work as the frequency nadir was not fixed per trip

(e.g. the breakers do not normally open at the same time). Therefore, future work will look into how the model adapts for multiple unit trips.

4.6 Data sampling rate accuracy

Figure 4-6 shows the RoCoF measurements taken at Tutuka power station. The current SCADA sampling rate is one second and the PMU data-sampling rate is 20 ms and averaged to 100 ms after 6 months when archived. An example of an archived frequency incident data is shown in Figure 4-5.

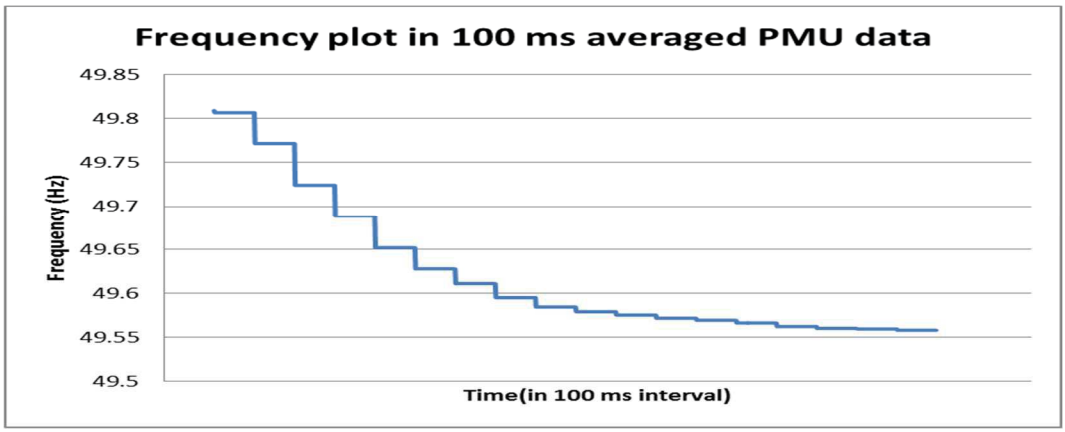

Figure 4-5: Archived PMU frequency data with 100 ms sample rate [PMU data downloaded by author].

The output data of the Rate of Change of Frequency (RoCoF) from PMUs was not easy to use in the studies. It can be observed from Figure 4-6that the higher the sampling rate the more accurate the RoCoF. The method of averaging or filtering of PMU noise is discussed in the next section.

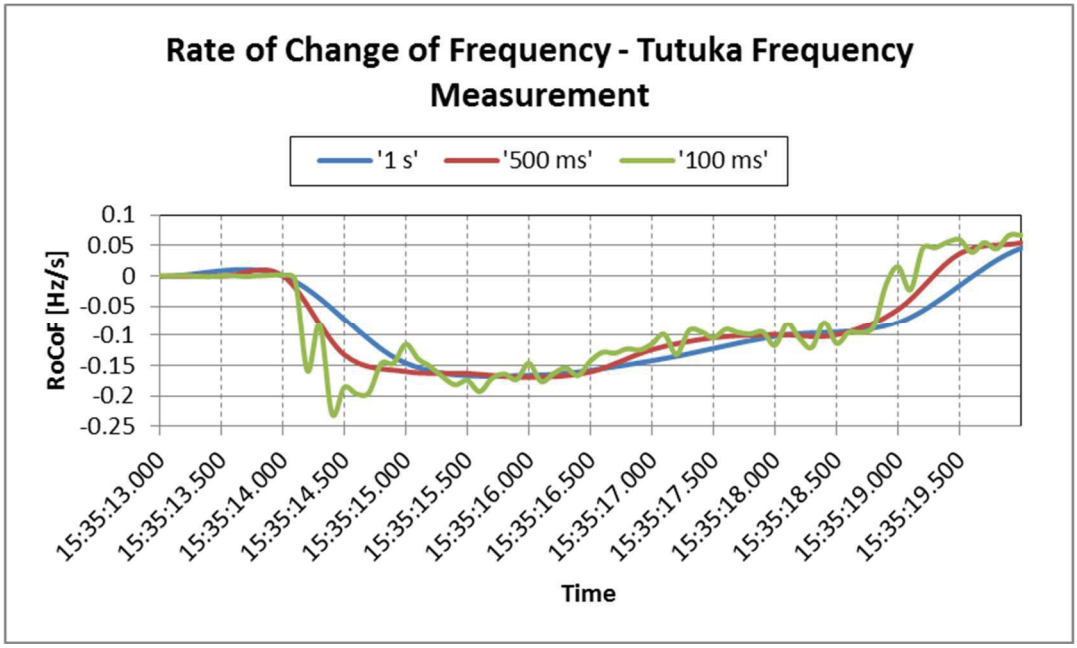

Figure 4-6: RoCoF sampling rate measurements at Tutuka power station following a disturbance at Apollo-29 November 2013 [PMU data downloaded by a colleague].

4.7 Moving Average and Detrended Fluctuation Analysis (DFA) methods

Electromechanical oscillation is an inherent property of an AC transmission system and cannot be eliminated. The change in electromagnetic torque of a synchronous generator following a disturbance is divided into two components; synchronising torque component (in phase with rotor angle deviation) and damping Torque component (in phase with the speed deviation) [7], [20]. Figure **4-7** shows the actual PMU frequency measurements from two power stations following a unit trip at Medupi power station.

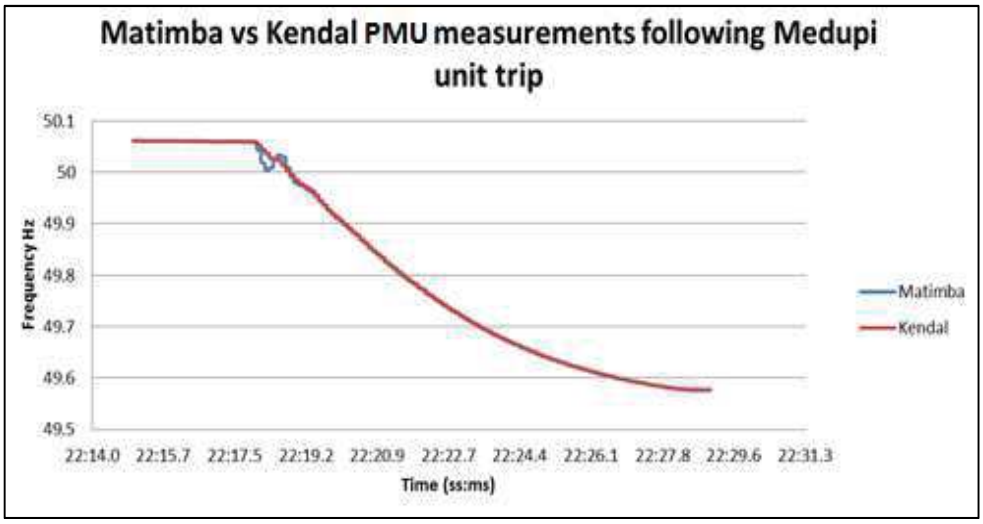

Figure 4-7: Matimba and Kendal power station PMU measurements following a Medupi unit trip [PMU data downloaded by author]

The Electromagnetic Torque Oscillation Stage can be observed from the Matimba power station PMU a few ms following the disturbance. The moving average methods were used to filter out the Electromagnetic Torque Oscillations and noise from the PMU data.

The Detrended Fluctuation Analysis (DFA) algorithm is used to remove extrinsic fluctuations present in a signal in order to allow the analysis of the background variability [36]. The first step to implementing the DFA algorithm is to remove any DC offset by using Equation 4.1.

$$y(k) = \sum_{i=1}^{k} \left[x(i) - \bar{x} \right] \tag{4.1}$$

Where:

$y(k)$ is the running sum of the samples from the first sample up to the k'th sample where the average value of all the samples has been subtracted out from each sample value.

$x(i)$ is the i'th sample of the actual signal

$\bar{x}$ is the average value of all the samples in the actual signal

The running sum of the samples y(k) is then divided into segments of width *n* samples. A least-squares first-order linear (straight-line) approximation of the running sum is calculated for each segment. The individual segment running sum of the samples, $y_n(k)$, can be considered a (straight-line) approximation of the running sum of the actual samples $y_n(k)$.

The next step is to de-trend the running sum of the actual samples, y(k), by removing the segment (straight line) running sum of the samples.

$$y'(k) = y(k) - y_n(k) \tag{4.2}$$

$y'(k)$ is now the de-trended running sum of the actual samples. A root-mean-square fluctuation of $y'(k)$ is then calculated by using Equation 5.3

$$F(n) = \sqrt{\frac{1}{n}\sum_{k=1}^{n}\left[y(k) - y_n(k)\right]^2} \tag{4.3}$$

This process of de-trending followed by the fluctuation calculation is repeated over a range of different segment width, *n*, and a graph of log[$F(n)$] versus log(*n*) is plotted. The least-square straight-line fit to the above graph is defined as having a slope α.

Where:

α < 0.5 indicates negative correlation

α ≈ 0.5 indicates white noise (no correlation)

α > indicates positive correlation

For the PMU frequency disturbance data extracted from WAMS, the five-period moving average was used to average the frequency data before and after a disturbance. The starting frequency and the corresponding time were obtained. Similarly, the moving average method was used to determine the minimum frequency or frequency nadir following a disturbance.

5. MODEL DEVELOPMENT AND DEFINITION OF VARIABLES

5.1 Introduction

This chapter presents the model development methodology. It introduces the background to the different stages of the frequency response following a disturbance and factors affecting system inertia in Eskom. In chapter two, the estimating the system inertia calculation and estimates methods from the literature were presented. The MVA concepts developed in chapter three are used in this chapter. In [4], [6], [17], [27], the factors affecting system primary response were summarised as follows:

- Kinetic energy and inertia of individual generators and motor;
- Stiffness of the system;
- Generation dispatch;
- Transient or fault location;
- Load types;
- Renewable energy sources;
- Distributed or Centre of Frequency;
- Size of loss;
- Method of the Inertia Constant and primary response calculation.

5.2 Model development plan

In Figure 5-1, the outer loop shows the connection and balancing of load and generation. The load, interconnectors, PV and wind generation are categorised as self-dispatch or non-dispatchable by the SO. The synchronous generators and Apollo HVDC are categorised as dispatchable by the SO. The strength of the AC power system is mainly determined by the system inertia, which is mainly provided by connected synchronous generators and the stiffness of the system [6], [17], [19] shown in the inner loop of Figure 5-1.

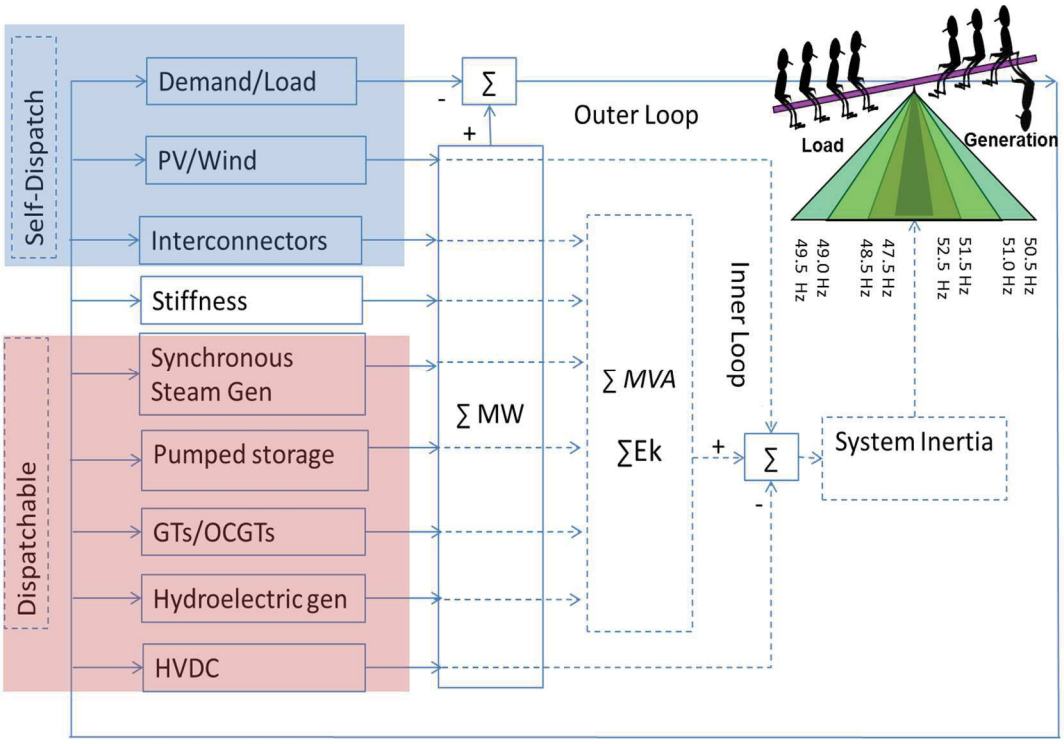

Figure 5-1: Block diagram showing the balancing of load and generation with the impact of the varying Inertia Constant.

The model was developed by equating the Swing Equation Method and the Inertia Constant Method from historic power system frequency disturbance data. Multivariate Analysis was used to determine the behaviour, contribution and relationship between the independent and dependant parameters. The multiple regression models will be determined in the following chapter and used to design the RoCoF, the inertia without Fast Primary Response (FPR) and inertia with FPR online models. The MVA development plan is shown in Figure 5-2.

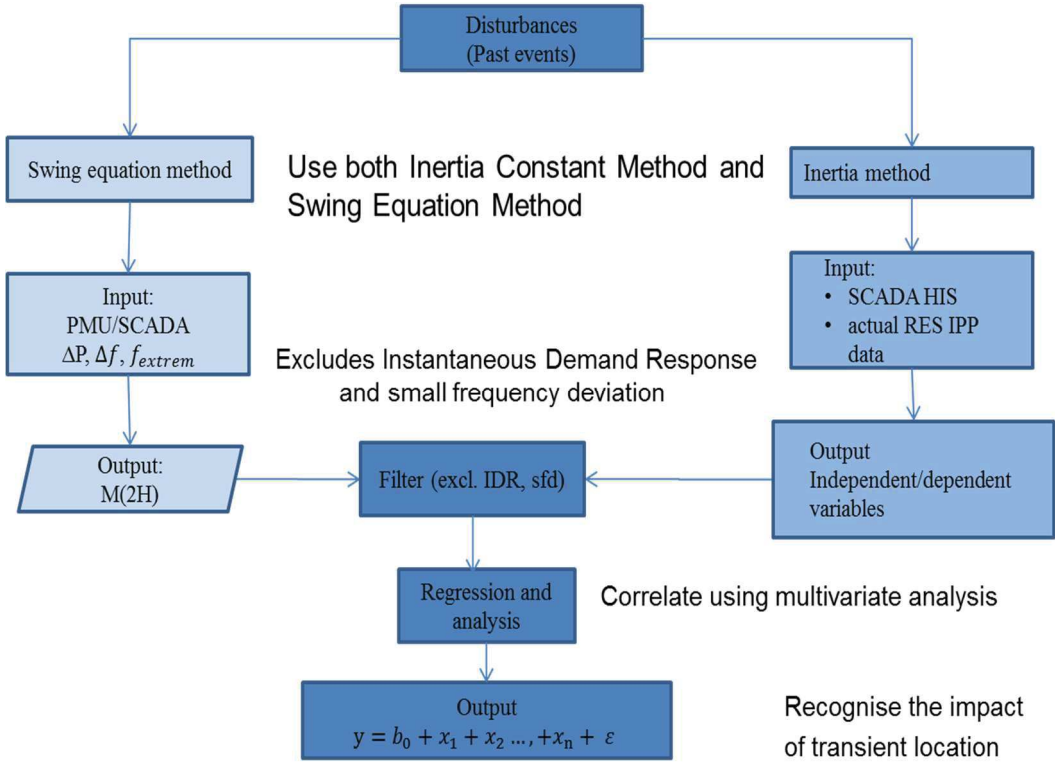

Figure 5-2: MVA model development plan.

MVA requires a certain minimum set of data (observations) for the regression to solve and produce accurate results. The approximately 2000 frequency disturbances in the past three years made it possible to perform this study. MVA involves observation and analysis of more than one statistical outcome variable at a time [29]. MVA requires sets of inputs of *y range* (dependent variable) and *x range* (independent variables) as shown in Table 5-1.

Table 5-1: Dependent (y) and Independent (x) input variables used in the regression analysis tool (similar table is used for the Inertia without FPR model and the Inertia with FPR model).

Observations	Input y range	Input x range					
1	y_1	x_{11}	x_{12}	x_{13}	x_{14}	...	x_{1n}
2	y_2	x_{21}	x_{22}	x_{23}	x_{24}	...	x_{2n}
3	y_3	x_{31}	x_{32}	x_{33}	x_{34}	...	x_{3n}
⋮	⋮	⋮	⋮	⋮	⋮		⋮
n	y_n	x_{n1}	x_{n2}	x_{n3}	x_{n4}	...	x_{nn}

The *Coefficient of Determination* (R^2) measures the proportion of the variation in *y* that is explained by the variation in the independent variable *x*. The Sum of Squared Error (SSE) measures the amount of variation in *y* that remains unexplained and the Sum of Squared Residuals (SSR) measures the amount of variation in *y* that is explained by the variation in the independent variable.

5.3 Inertia with FPR dependent variables

The Inertia with FPR dependent variable is derived by rearranging Equation 2.13 to calculate the Inertia Constant using the power change ΔP (sourced from EMS SCADA data) and frequency at the start time of the disturbance (sourced from Eskom PMU data). The Inertia Constant (H) is defined as the Inertia with FPR dependent variable (y_n) given by Equation 5.1.

$$H + FPR = \frac{\left(\frac{(P_{start} - P_{nadir})}{P_{start}} (t_{start} - t_{nadir}) \right)}{2\left(\frac{f_{start} - f_{nadir}}{f_{start}} \right)} \quad (5.1)$$

Where:

$H+FPR$ is the Inertia Constant with FPR (s)
P_{start} is the system generation prior to loss of generation (MW)
P_{nadir}: is the system generation at the frequency nadir (MW)
f_{start} is the frequency at the start of a disturbance (Hz)
f_{nadir} is the nadir frequency (Hz)
$t_{start}$is the time at the start of a disturbance (s)
t_{nadir} is the time at frequency nadir (s)

5.4 Independent variables

The factors that are expected to contribute to Inertial Response of the Eskom power system are summarised in Figure 5-3. Known variables can be defined as variables that can be measured directly from PMU and SCADA/EMS data without manipulation. Unknown variables can be defined as variables that are

approximated by solving an equation or developing a simplified model from measured SCADA/EMS data.

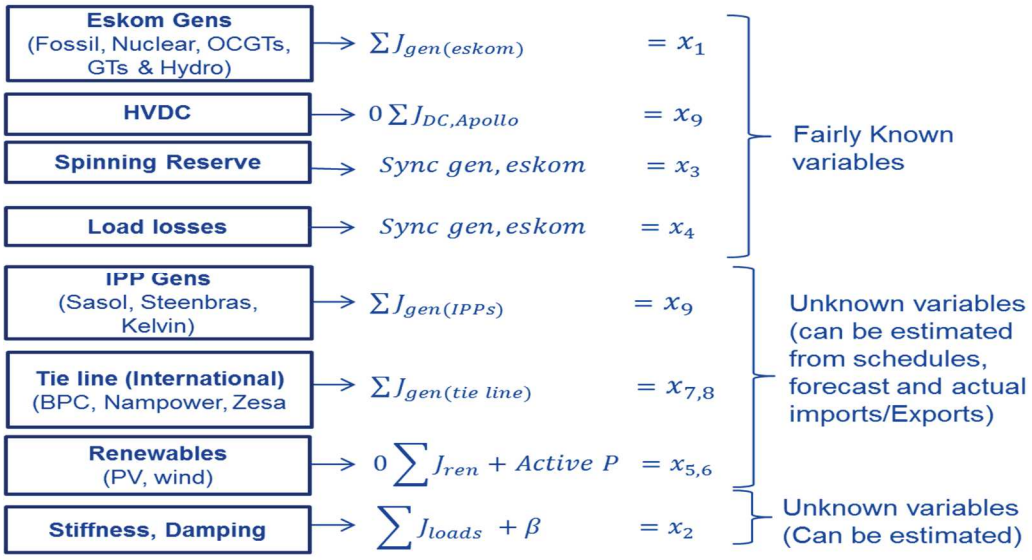

Figure 5-3: Model development showing known and unknown independent variables.

5.4.1 Sum of individual generator moments of inertia

The Inertia Constant of individual generators is measured in seconds. The model will use actual frequency measurement at the start of the disturbance (before any FPR has any effect). The first dependent variable is derived from Equation 2.1.

$$H = \frac{1}{2} \frac{J \omega_{0m}}{S_{base}} \tag{5. 2}$$

Where:

J is the moment of inertia ($kg.m^2$)
ω_{0m} is the synchronous speed (rad (mech)/s)
S_{base} :is the apparent power rating of the generator (VA)

Since the system frequency is highly variable, it is convenient to express the second dependent variable as the sum of all the synchronous masses and moments of inertia in Equation 5.3 by rearranging Equation 2.2.

$$x_1 = J_{eskom,gens} = \sum_{i}^{n} \frac{2HS_{base}}{\omega_{0m}^2} \tag{5. 3}$$

Not all the Inertia Constant s in Eskom are known. The unknown Inertia Constant are estimated from Table 5-2 [6] [13].

Table 5-2: Typical Inertia Constant (H) by generation type

Generation type	H(s)
Turbine generator (1800 rpm)	6-9
Turbine generator (3000 rpm) condensing	4-7
Turbine generator (3000 rpm) non-condensing	3-4
Water wheel generator (>200rpm)	2-4
Water wheel generator (<200rpm)	2-3
Synchronous Condenser (Large)	1.25
Synchronous Condenser(small)	1.00

It must also be noted that hydro pump storage has different modes of operation, generation, pumping, Synchronous Condenser (SCO) and standstill modes. The Inertia Constant for these modes was taken into consideration during frequency disturbance studies.

5.4.2 SAPP simplified inertia contribution from tielines

Due to the relatively small size and unavailability of data in other utilities, only BPC, ZESA and Songo were considered. Figure 5-4 shows a simplified SAPP diagram.

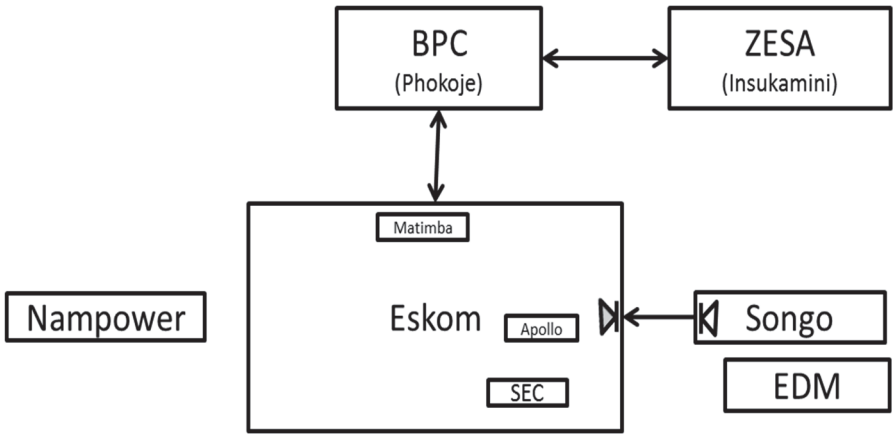

Figure 5-4: Simplified SAPP diagram.

A simplified model to estimate the inertia contribution by BPC is shown in Figure **5-5**. The y-axis is the moment of inertia contribution from the BPC network. The x-axis is the power flow difference between the Matimba-Phokoje and Phokoje-Insukamini 400 kV lines.

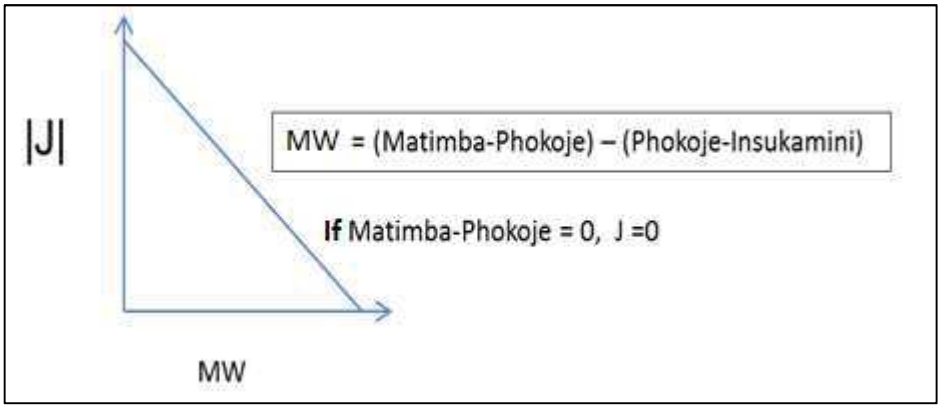

Figure 5-5: BPC inertia simplified model with reference to the Eskom network.

The BPC simplified model shows that the higher the power difference between the Matimba-Phokoje 400 kV and Insukamini-Phokoje 400 kV lines, the fewer units are committed by BPC. If the Matimba-Phokoje 400 kV line is out of service, then the moment of inertia contribution from BPC and Zesa is zero since both utilities would be disconnected from the Eskom network. These conditions are valid for normal system conditions in BPC.

A simplified model for estimating the inertia contribution by Zesa is shown in Figure 5-6. The y-axis is the moment of inertia contribution from the Zesa network and the x-axis is the power import from Zesa via the Insukamini-Phokoje 400 kV line.

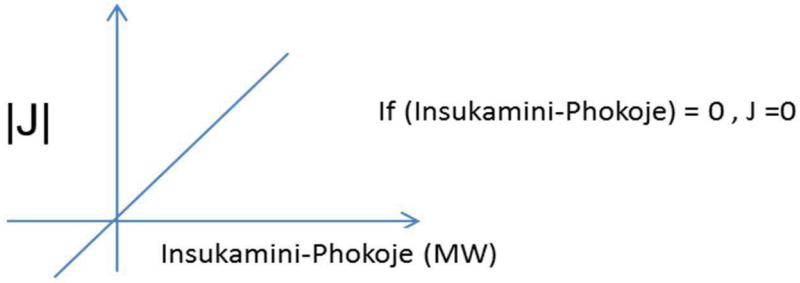

Figure 5-6: Zesa simplified inertia model with reference to the Eskom network.

The higher the power import through the Insukamini-Phokoje 400 kV line, the higher the inertia contribution from Zesa. If the Insukamini-Phokoje 400 kV line is out of service then the moment of inertia contribution to Eskom from Zesa is zero.

5.4.3 Independent Power Producers

The inertia contributions from synchronous Independent Power Producers (IPPs), (e.g. Sasol, Kelvin) were estimated from the known dispatch schedules and actual power flows. These IPPs were lumped with Eskom's sum of individual generator moments of inertia.

5.4.4 Stiffness of the system

Load modelling is very difficult due to the lack of data, its stochastic nature in time and its geographical distributed nature [23]. Load behaviour immediately after the onset of the disturbance was studied in [17] looking at every combination of simulation case and fault. The change in load is dependent on the operational scenario, power imbalance and location of the disturbance. The main finding was that immediately following a disturbance the change in system load is mainly caused by voltage dependent loads.

The stiffness of the system depends highly on load damping, spinning reserve and governor droop (steady state) [6]. Motor loads are dependent on the power system frequency. If the frequency declines, the connected motor load will decline [6]. Most of the residential loads in South Africa are voltage dependent. If the voltage declines, the connected load magnitude will also decline depending on the

reactive power reserves provided by the local synchronous generators and Var Compensators i.e. Static Var Compensators (SVCs). The load damping in the Eskom network changes with time and is dependent on the area. Eskom adopted the NERC standards, which states that when frequency drops 1%, the motors slow down, and the active power consumption drops by 3%. The non-motor (resistive) load generally remains constant when the frequency drops. The net of these is the general rule of thumb that a 1% change in frequency causes a 2% change in load [21]. This rule of thumb was used as a starting point for the model development.

The analysis of the Load Frequency Characteristics (LFC) is described as the collective performance of all generators in the system [6]. The inter-machine oscillations and transmission system performance are normally ignored. For a system with *n* generators and a composite load-damping constant of D, the steady-state frequency deviation following a load change ΔP_L is given by Equation 5.4 [6].

$$\Delta f_{ss} = \frac{-\Delta P_L}{\left(1/R_1 + 1/R_2 + \ldots + 1/R_n\right) + D} \qquad (5.4)$$

$$= \frac{-\Delta P_L}{\left(1/R_{eq}\right) + D} \qquad \ldots.(5.5)$$

Where:

$$\frac{1}{R_{eq}} = \frac{1}{\frac{regulation\,\%}{100} P_{start}(MW) \frac{1}{generation contributing\ to regulation (MW)}} = \frac{\Delta P_G}{\Delta f_{ss}} \qquad (5.6)$$

The composite frequency response characteristic of the system, β, is sometimes referred to as the stiffness of the system and is expressed by Equation 5.7 [6].

$$\beta = \frac{\Delta P_L}{\Delta f_{ss}} = \frac{1}{R_{eq}} + D \qquad (5.7)$$

The composite regulating characteristic of the system is equal to $1/\beta$ [6] The coherent response of all generators to changes in system load is assumed and represented by an equivalent generator. Figure 5-7 shows the system equivalence for LFC analysis [6].

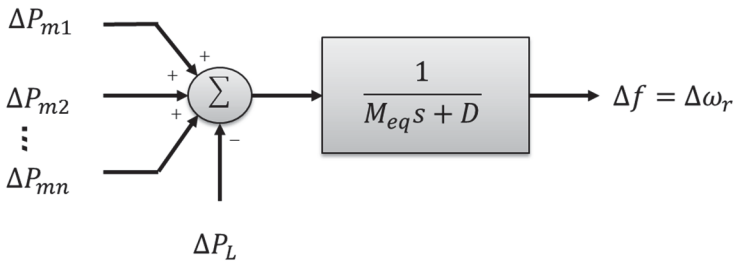

Figure 5-7: System equivalence for LFC analysis [6].

The equivalent generator has an Inertia Constant, H_{eq}, equal to the sum of the Inertia Constant s of all generating units and is driven by the combined mechanical outputs of the individual turbines [6]. Similarly, the effects of system loads are lumped into a single damping constant D. The speed of the equivalent generator represents the system frequency $2\pi\Delta f = \Delta\omega_r$. [6] Thus, it follows that the composite power/frequency characteristics of a power system depends on the combined effects of the droops of all generator speed governors [6]. It also depends on the frequency characteristics of all the loads in the system.

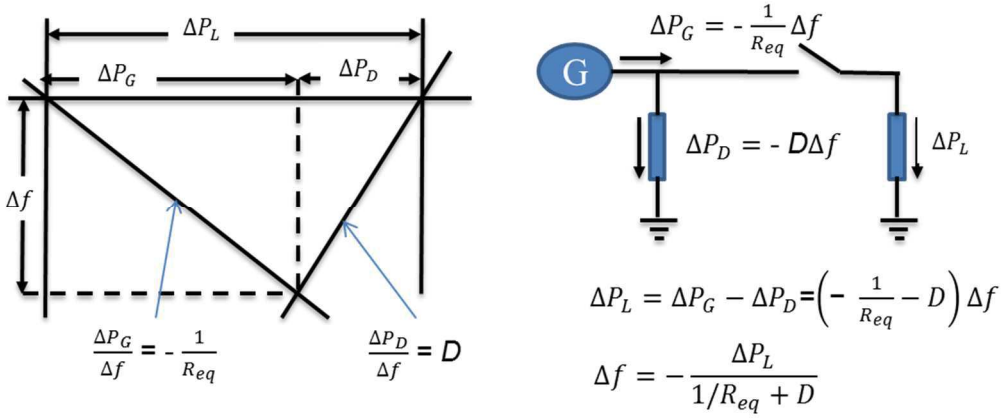

Figure 5-8: Composite governor and load characteristic [6]

An increase of system load by ΔP_L (at nominal frequency) results in a total generation increase of ΔP_G due to governor action and a total system load reduction of ΔP_D due to its frequency characteristic [6].

The units which were committed for instantaneous reserves, were used to calculate the spinning reserves per generator at the times of the actual frequency disturbances. In the time scale considered, governors do not have time to respond so that the damping present is due to the load response (FPR).

6. THE ROCOF MODEL

6.1 Introduction

The aim of this chapter is to study the system RoCoF following small and large disturbances. This chapter proposes a possible way of estimating the maximum instantaneous system RoCoF. The model estimates the RoCoF from the change in power (worst possible contingency or multiple unit trip), f_{start}, online sum of moments of inertia (*J*), RES, generation load losses and spinning reserve from past disturbances and finds a relation between these factors. These can be used in conjunction with under frequency trip settings and response times to evaluate online whether the limits would be violated.

6.2 Disturbance location and frequency measurement points

The frequency is not the same throughout the whole IPS. During a disturbance a measurement location in the system plays a role due to a propagation of the frequency wave [17]. However, it has been shown in [27] that the placement of a PMU with respect to a system event can greatly affect the post-fault frequency measurement and any corresponding analysis of that event. In addition, the standard for synchrophasor measurements (IEEE C37.118.1-2011) leaves both the method of frequency measurement and the device performance under transient conditions unspecified [27], [35], meaning that under such conditions devices from different manufactures could produce different results.

Figure 6-1 shows the three stages of the primary response during a loss of a large generator in the Northern part of the Eskom network. The measurements were taken from Phasor Measurement Units (PMUs) at Western Cape (Koeberg), Northern (Matimba) and Mpumalanga (Kendal) power stations.

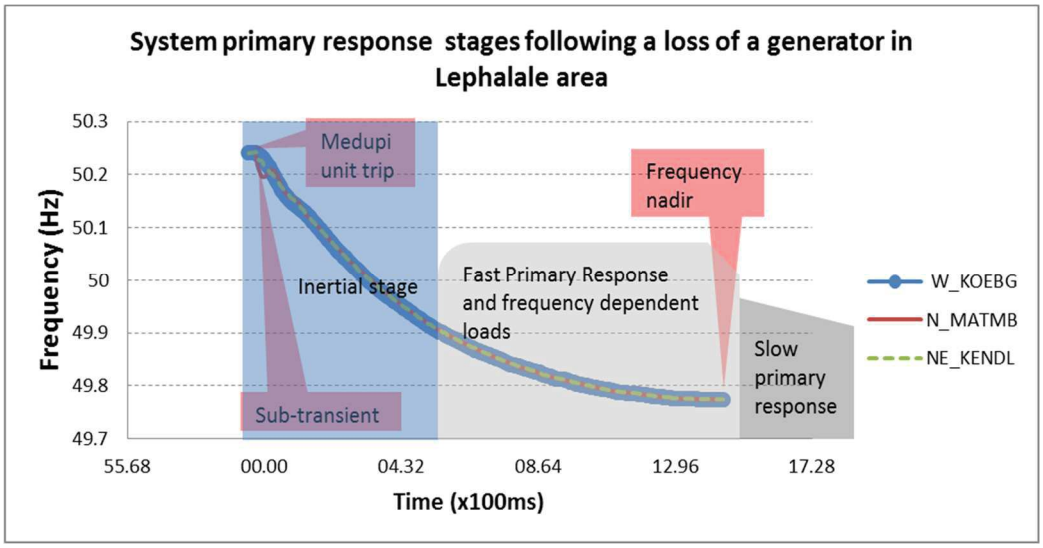

Figure 6-1: PMU data showing system primary response stages.

The centre of system frequency/inertia and impact of disturbance location were studied using the past frequency disturbances which were randomly selected across the Eskom areas. The sub-transient behaviour of generators i.e. within 20 ms following a disturbance were largely identified in the disturbances in the Northern (Matimaba), Western Cape (Koeberg) and Eastern (Kendal) areas as opposed/compared to the power stations in the Mpumalanga area. Table 6-1 shows a summary of regression results following a single generator disturbance in the central area.

Table 6-1: Relationship among frequency measurements in Central, Western Cape and Northern areas

SUMMARY OUTPUT					
Regression Statistics					
Multiple R	0.9999				
R Square	0.9999				
Adjusted R Square	0.9999				
Standard Error	0.0014				
Observations	750				
ANOVA					
	df	*SS*	*MS*	*F*	*Significance F*
Regression	2	14.59	7.29	3714393.36	0
Residual	747	0.0015	1.9639E-06		
Total	749	14.5907			
	Coefficients	*Standard Error*	*t Stat*	*P-value*	
Intercept	-0.0497	0.0184	-2.6997	0.00710	
W_KOEBG_01_400	0.6437	0.0098	65.5676	0	
N_MATMB_01_400	0.3573	0.0098	36.2777	6.0E-167	

In Table 6-1, R^2 is equal to 0.999 and the standard error is equal to 0.0014. This indicates that 99.99% of the variation in the frequency deviation in the Central part of the Eskom network during a disturbance is explained by the variation in frequency deviation reading at Koeberg (approx. 1500km away from Kendal) and Matimba (approx. 500km from Kendal). There is overwhelming evidence to infer that a linear relationship exists between all three locations following a single generator disturbance since the values of the test statistics are large (t = 65.56 for Koeberg and 36.27 for Matimba) and with *P-value* of zero for both power stations. Therefore, a linear relationship exists between the PMUs in the Eskom regions, which provides confidence in the dependency of measurements points based on locations.

6.3 Relationship between the RoCoF, system inertia and asynchronous generation sources

It was shown in [15] that the maximum Rate of Change of Frequency (RoCoF) following a loss of generation is independent of the asynchronous generation sources. Because of differing inertia, the RoCoF will increase when asynchronous generation displaces conventional generation. Figure 6-2 illustrates the relationship between RoCoF for high (3), medium (2) and low (1) system inertia.

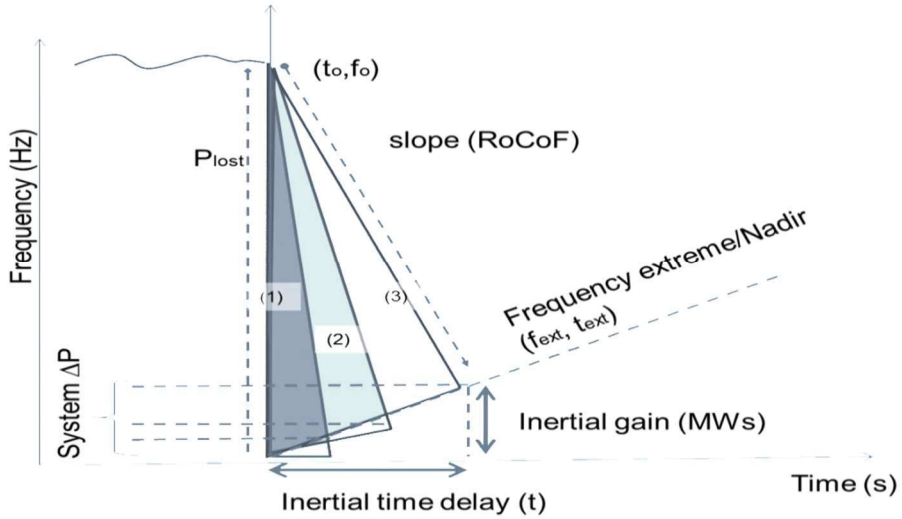

Figure 6-2: RoCoF as a function of system inertia.

The characteristic times of the Inertial Response will be of the order of fractions of a second [5], [24]. In this short time-frame, it is impossible for the slow primary response and the secondary response to react. Therefore, this period requires adequate stored energy provided mainly by synchronous generator inertia to reduce the RoCoF [19],[23], [27].

6.4 Measuring the Rate of Change of Frequency (RoCoF) from disturbances

This section evaluates the impact of disturbance location and the factors affecting the system inertia during the first 300 ms. The moving average [29] and Detrended Fluctuation Analysis (DFA) [36] methods were used to filter out the Electromagnetic Torque Oscillations and PMU measurement noise following large disturbances. Figure 6-3 shows the linear approximation for the first 300 ms following a disturbance.

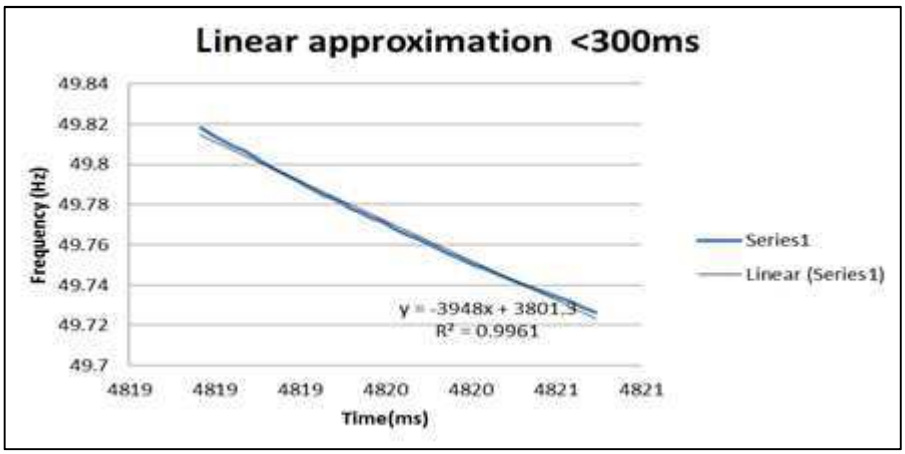

Figure 6-3: Linear approximation of the RoCoF within the first 300 ms following a disturbance [PMU data downloaded by author].

The RoCoF is calculated directly from the slope of the frequency change. The start and end times together with the corresponding frequency were recorded. A linear approximation was used to calculate the Coefficient of Determination (R^2). The data that contained correlations below 99% were adjusting the moving average period.

6.5 The RoCoF model of independent and dependent variable

The System RoCoF derived from section 6.3 is defined as the dependent variable (y_n)

The first independent variable x_1 is f_{start}.

The second independent variable x_2 is the sum of all the synchronous moments of inertia (generators) in term of H given by Equation 2.2.

The third independent variable x_3 is the stiffness of the system given by Equation 5.8

The fourth independent variable is the drop in power (ΔP) x_4

The fifth independent variable x_5 is the system load, which is equivalent to generation sent-out.

The sixth independent variable was chosen to be the total spinning reserve (x_6) on its own and is the unloaded generation which is synchronised and ready to be used (with or without governor action).

The seventh independent variable is the generation load losses (x_7) and was chosen to be the units that are synchronised on the grid but unable to output Maximum Continuous Rating (MCR) (limited ability to provide spinning reserves).

The simplified models to estimate the contribution from two international interconnectors, Botswana Power Corporation (BPC) load (x_8) and Zimbabwe Electricity Supply Authority (ZESA) load (x_9) were developed from the line flows and interconnector schedules.

Power generated at the Cahora Bassa hydro power station in Mozambique and which is imported into the Eskom network via long HVDC lines was measured at the injection substation, Apollo. HVDC (x_{10}) is asynchronous, thus it does not contribute to the Inertia Constant.

The Renewable Energy Sources (RES) are wind (x_{11}) (may or may not contribute to the moment of inertia depending on the technology) and PhotoVoltaic (PV) (x_{12}) (does not contribute to the moment of inertia).

6.6 Cumulative system RoCoF factors versus the Coefficient of Determination

The study was performed to determine the contribution of every factor that is expected to influence the RoCoF such as System Inertia Constant (H), the drop in power (ΔP), Spinning reserve, the generation load losses, the HVDC and the renewables (Wind and PV). Figure 6-4 shows the cumulative RoCoF factors measured against the Coefficient of Determination (R^2).

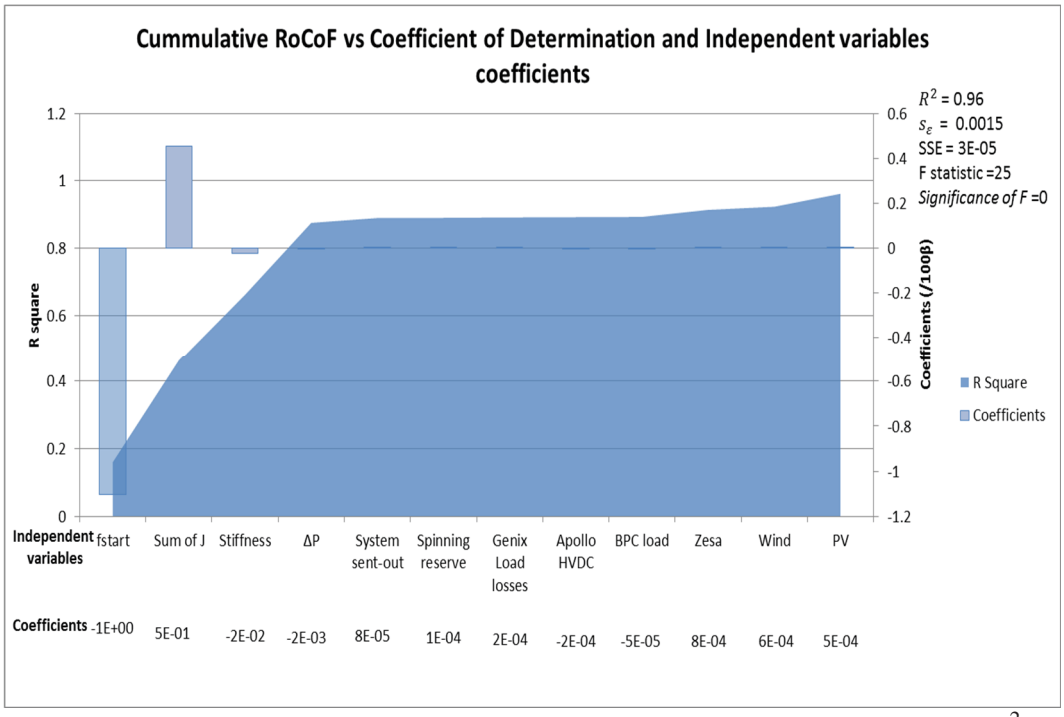

Figure 6-4: Cumulative RoCoF factors versus Coefficient of Determination (R^2).

The system RoCoF with reference to Kendal power station resulted in an R^2 of 0.96, standard error of 0.0015, *F statistic* of 25, SSE close to zero and *significance of F* close to zero.

The main contributing factors of the RoCoF were starting frequency, sum of moments of inertia, drop in ΔP (lost generation) and system stiffness.

The moment of inertia makes a large contribution to the RoCoF. The stiffness of the system also makes a large contribution to the RoCoF. The amount of generator drop in ΔP (lost generation) makes a larger contribution. The amount of the sum of generation online (system sent-out) makes a smaller contribution.

The spinning reserve, BPC load, Apollo HVDC, wind and PV do not contribute to the RoCoF, but are considered multicollinearity factors. During large disturbances, the coefficients of RES, spinning reserve, HVDC and load losses are very small and distort the *t-test* of the coefficients of the RoCoF. Example would be during low load and/or excess generation capacity conditions when the SO is forced to take synchronous generation off the grid, which affects the system inertia.

6.7 The Eskom system RoCoF model

From the previous section, 96% of the variation in the frequency deviation in any part of the Eskom network during the incidences could be explained by the variation in frequency deviation reading at Kendal power station. It follows that Kendal power station can be used as a reference centre of frequency for any disturbance in the network. Table 6-2 shows a detailed summary of results and validation of the system RoCoF model.

Table 6-2: Detailed system RoCoF model

SUMMARY OUTPUT						
Regression Statistics						
Multiple R	0.9806					
R Square	0.9617					
Adjusted R Square	0.9233					
Standard Error	0.0015					
Observations	25					
ANOVA						
	df	*SS*	*MS*	*F*	*Significance F*	
Regression	12	0.00067	5.58E-05	25.08	0.00	
Residual	12	3E-05	2.22E-06			
Total	24	0.00070				
	Coefficients	*Standard Error*	*t Stat*	*P-value*	*Lower 95%*	*Upper 95%*
Intercept	0.4914	0.3973	1.237	0.240	-0.3742	1.3570
f0(pmu) (x_1)	-0.0110	0.0081	-1.366	0.197	-0.0286	0.0066
System total J (x_2)	0.0045	0.0035	1.283	0.224	-0.0032	0.0122
Stiffness (x_3)	-0.0002	0.0047	-0.051	0.960	-0.0106	0.0101
Unit tripped from (x_4)	-2E-05	6E-06	-3.922	0.002	-4E-05	-1E-05
System sent-out (x_5)	8E-07	3E-07	2.797	0.016	2E-07	2E-06
Spinning reserve (x_6)	1E-06	4E-07	2.529	0.026	1E-07	2E-06
Genix Load losses (x_7)	2E-06	1E-06	1.652	0.124	-6E-07	5E-06
Apollo DC (x_8)	-2E-06	1E-06	-1.698	0.115	-5E-06	7E-07
BPC load (x_9)	-5E-07	2E-06	-0.279	0.785	-4E-06	3E-06
Zesa (x_{10})	8E-06	5E-06	1.723	0.111	-2E-06	2E-05
Wind (x_{11})	6E-06	2E-06	3.135	0.009	2E-06	1E-05
PV (x_{12})	5E-06	1E-06	3.471	0.005	2E-06	7E-06

The first order RoCoF model for the overall Eskom IPS is estimated by model (a):

$$System\ RoCoF = 0.4914 + [-110.43x_1 + 45.33x_2 - 2.42x_3 - 0.2326x_4 + 0.0085x_5 + 0.01x_6 + 0.0198x_7 - 0.023x_8 - 0.005x_9 + 0.0079x_{10} + 0.057x_{11} + 0.046x_{12}]/(1.0E-5) \quad \text{(a)}$$

6.8 Conclusion

It is clear from the results that the Fast Primary Response factors may be too slow to react to large disturbances during light loading conditions. Therefore, kinetic energy, stiffness of the system and the amount of generator loading prior to tripping determine the RoCoF. All the power stations and area Fast Primary Response models (to be developed in Chapter 7, 8 and 9), can be referenced to the Kendal power station PMU. The bulk of the Eskom generation is in the Northeast area; therefore it is expected that the centre of system inertia is in this area. Furthermore, Kendal power station has more PMU historic data when compared to other PMUs installed in other Eskom network locations

7. THE SYSTEM INERTIA WITHOUT FPR MODEL DEVELOPMENT

7.1 Introduction

The aim of this chapter is to study the large disturbances and propose a possible way of estimating the system inertia without FPR using the MVA. The first part is the choice of dependent and independent variables. The second part evaluates the impact of disturbance location and the factors affecting the system inertia during the first 300 ms following the disturbances in the network and develops a simplified model. Discussion of the results and conclusions are then made at the end of the chapter.

7.2 System inertia dependent variable

The inertia dependent variable is derived by rearranging Equation 2.13 to calculate the Inertia Constant without FPR using the RoCoF (sourced from PMU data), f_{start}, f_{300ms}, t_{start}, t_{300ms}, (sourced from PMU data), power loss ΔP (sourced from EMS data) in system VA base and frequency at the start time of the disturbance. System damping and stiffness are assumed zero. The Inertia Constant (H) is defined as the inertia dependent variable (y_n) given by Equation 7.1.

$$H = \frac{\left(\frac{(P_{start} - P_{300ms})}{P_{start}} (t_{start} - t_{nadir}) \right)}{2\left(\frac{f_{start} - f_{nadir}}{f_{start}} \right)} \tag{7.1}$$

Where:

f_{300ms}, and t_{300ms} apply 300 ms after the start of the disturbance (Hz)

7.3 System inertia independent variables

The first independent variable x_1 is the system load, which is equivalent to generation sent-out.

The second independent variable x_2 is the starting frequency in Hz.

The third independent variable x_3 is the sum of all the synchronous generator moments of inertia (*J*)..

7.4 Results for the system inertia using the MVA method

Table 7-1 shows the Inertia Constant models for the selected Eskom areas (Mpumalanga and North) and Majuba power station (East). The first part of the table comprises the observations, the s_ε, the R^2, the SSE, the *F statistic* and the *significance of F*. The second part of the table shows the independent variables and coefficient values obtained from the MVA.

Table 7-1: Comparison of the Inertia Constant per Eskom area and independent variable coefficients (print in colour. Red=poor; yellow=average; green=good)

	Model	All PS	North-East	North	Majuba	Majuba 123
	Observations	27	10	8	9	6
Model validation	R Square	0.18	0.66	0.69	0.61	0.96
	Standard Error	0.39	0.09	0.09	0.51	0.25
	SSE	3.48	0.04	0.04	1.28	0.12
	F statistic	1.65	3.93	2.99	2.59	15.24
	Significance of F	0.21	0.07	0.16	0.17	0.06
	Intercept	61.51	-57.47	-16.98	294.43	505.82
Independent variables and coefficients	Load (gen sent-out) (x_1)	-0.19229	0.00002	0.01658	0.00018	0.00037
	Starting frequency (x_2)	-1.21	1.13	0.33	-6.02	-10.38
	System total J (x_3)	0.000042	0.309691	0.000063	0.696460	0.940421

The correlation of the combined past disturbances for the entire system was poor. The Coefficient of Determination (R^2) was found to be 0,18. By breaking down the data into North East and Lephalale areas, the R^2 improved to 0,66 and 0,69 respectively. The R^2 of all units in Majuba power station model was 0,61. Since the units at Majuba power station have different sizes and ratings, the station was divided into two stations. The Majuba 123 R^2 improved to 0,96 and good standard

error, small SSE, large *F statistic* and small *significance of F*. This signifies that the model yields better results at a power station level and with units of similar type.

Using Majuba 123 model, the Eskom system Inertia Constant without stiffness, can be estimated by model (b):

$$\begin{aligned} S_n H &= x_1 b_1 + x_2 b_2 + x_3 b_3 + b_0 \\ &= 0.00037 x_1 - 10.38 x_2 + 0.9404 x_3 + 505.82 \end{aligned} \tag{b}$$

Where:

$$S_n = \sum_i^n \frac{J_{0m} \omega_{0m}^2}{2H_i}$$

This method was also extended to other power stations and area models with an increased number of observations and high level of accuracy.

7.5 Conclusion

In this chapter, the estimation of system inertia without FPR considered the contribution of synchronous generators to system inertia. The other factors were excluded and a linear Swing Equation was assumed. Efforts were made to use this method to predict the actual and measured Inertia Constant and frequency nadir and resulted in large errors. The following chapter investigates the impact of disturbance location and the stiffness (inertia with FPR) of the system.

8. ESTIMATION OF THE INERTIA WITH FPR AND PREDICTION OF THE FREQUENCY NADIR FOLLOWING DISTURBANCES USING THE MVA METHOD

8.1 Introduction

This chapter is divided into three sections. The introduction is followed by section 8.2, which analyses how various factors behave during small disturbances. The study was performed to determine the contribution of every factor that is expected to contribute to the Inertia with FPR. This was performed by cumulatively adding each factor in order to determine the contribution and effectiveness during the single frequency disturbances.

The disturbances in the Lephalale area, which includes the Matimba and Medupi power stations, are used as an example in this work. Other models are found in Appendix A. The second reason is that Lephalale is connected to neighbouring countries Botswana and Zimbabwe. The strength of the neighbouring countries during disturbances is also of interest.

The validations of the Lephalale area models are in Section 8.3.4 and 8.3.5. The predicted model Inertia with FPR frequency nadir was validated against the actual calculated H and measured frequency using PMU data. The correlation can then be used to make an estimation of the maximum instantaneous frequency deviation and time it would take to reach the frequency nadir. The summary of other area model results (predicted vs. actual frequency nadir) are presented in section 8.4 and 8.5.

8.2 Cumulative Inertia with FPR factors vs Coefficient of Determination of the Medupi model

Small disturbances can be defined as frequency disturbances where IDR does not operate during an incident. The aim is to validate the use of the Inertia with FPR model using known parameters and measurements. The study was performed to determine the contribution of identified factors that are expected to contribute to

the frequency response. R^2 measures the proportion of the variation in Inertia with FPR that is explained by the variation in the factors that are expected to contribute to the Inertia with FPR. The factors are system total moment of inertia (J), stiffness of the system, spinning reserve, generation load losses, international tie-lines (BPC load and Zesa), Apollo HVDC and renewables (wind and PV).

In this section, techniques that allow the determination of the relationship between Inertia with FPR and multiple variables are presented. Figure 8-1 shows the cumulative factors measured against the Coefficient of Determination (R^2) of the Medupi power station. The positive and negative coefficients are also highlighted.

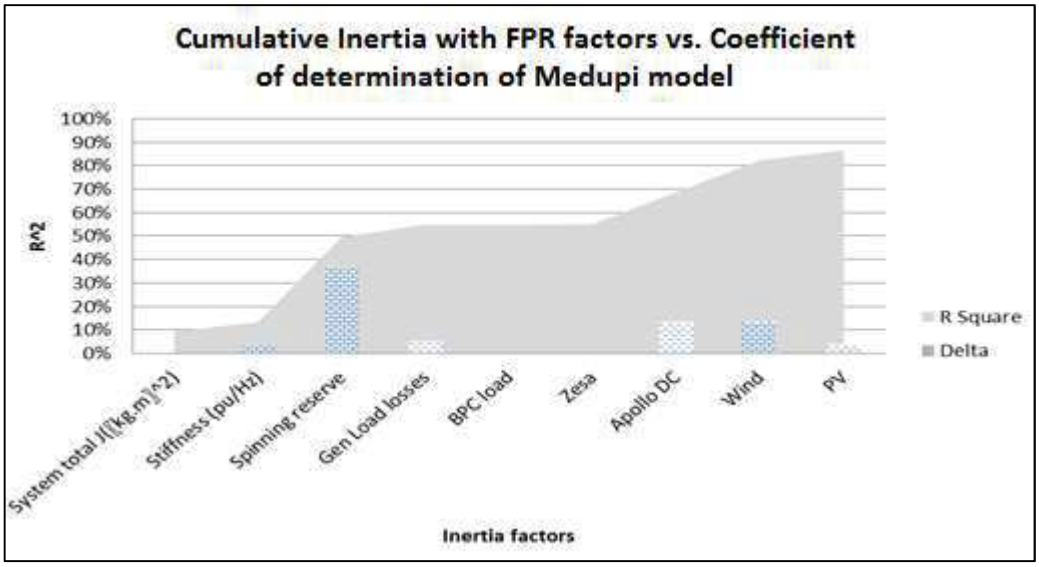

Figure 8-1: Cumulative Inertia with FPR versus Coefficient of Determination of the Medupi PS model.

The correlation between the dependent variable Inertia with FPR and the independent variable (total moment of inertia) is poor (only for the Medupi model). This is explained by the generation dispatch pattern, which is predominately-base-load for Eskom.

Additional stiffness shows a small correlation improvement in this model. The stiffness of the system relies heavily on the instantaneous reserves and the load-damping factor. Following a disturbance, the governors are too slow to react during the Inertial Response.

Spinning reserves increase the correlation, meaning that the instantaneous reserves contribute greatly to the variation in the Inertia with FPR. The higher the spinning reserve the higher the Inertia with FPR.

BPC and ZESA generation was small during the study period and the cumulative delta change was 0%. The two utilities are small compared to the Eskom network and are not expected to assist frequency response following a disturbance in the Eskom network. The electrical impedance connecting Eskom and neighbouring countries was also high. This could also be because of long generation outages and the drought experienced by the SADC region in the past two years where Eskom was exporting power to the north most of the time.

Table 8-1 shows a detailed summary of results and validation of the Medupi model.

Table 8-1: Medupi inertia with FPR model

	Regression Statistics						
	Multiple R	0.930					
	R Square	0.865					
	Adjusted R Square	0.804					
	Standard Error	0.895					
	Observations	30					
	ANOVA						
		df	*SS*	*MS*	F	Significance F	
	Regression	9	102.8	11.4	14.3	0.0	
	Residual	20	16.0	0.8			
	Total	29	118.8				
		Coefficients	*Standard Error*	*t Stat*	*P-value*	*Lower 95%*	*Upper 95%*
	Intercept	9.0444	4.470	2.024	0.057	-0.279	18.368
Eskom AC system	System total MOI (J)	0.0547	0.880	0.062	0.951	-1.780	1.890
	Stiffness	3.9226	0.925	4.239	0.000	1.993	5.853
	Spinning reserve	0.0001	0.000	0.902	0.378	0.000	0.000
	Genix Load losses	-0.0009	0.000	-2.583	0.018	-0.002	0.000
Tielines	BPC load	0.0011	0.001	1.240	0.229	-0.001	0.003
	Zesa	-0.0017	0.002	-1.071	0.297	-0.005	0.002
	Apollo DC	-0.0030	0.001	-4.683	0.000	-0.004	-0.002
RES	Wind	0.0035	0.001	4.476	0.000	0.002	0.005
	PV	-0.0016	0.001	-2.477	0.022	-0.003	0.000

Referring to Table 3-1, the model is good because s_ε is small, R^2 is close to one, the *F statistic* is large and the *significance of F* is zero. This statistic shows that 86.5% of the variation in the power system Inertia with FPR during all 30 transient events is explained by the variation in the number of the Eskom generators on the network, stiffness, spinning reserve, generator load losses, international interconnectors and renewables. The remaining 13.5% is unexplained. This is a relatively good fit compared to other models in Appendix A.

8.3 Medupi Inertia with FPR model coefficients

The first order Inertia with FPR model for Medupi power station is estimated by model (c):

$$y = \{9.04 + 0.054x_1 + 3.92x_2 + [0.071x_3 - 0.87x_4 + 1.05x_5 - 1.67x_6 - 2.96x_7 + 3.53x_8 - 1.55x_9]/1000 + \varepsilon\}/(2*10) \quad (c)$$

8.3.1 Eskom AC system

From the Table 8-1 *Eskom AC system* section, each factor is explained by describing what its coefficient b_n indicates in terms of its weight and influence on the dependent variable Inertia with FPR and whether it is linearly or non-linearly or multicollinearly related.

The intercept for the Medupi Inertia with FPR model is $b_0 = \frac{9.04}{2*10}$. This is the average Eskom power system moment of inertia (*J)* when all of the other independent variables are zero.

The coefficient $b_1 = 0.054$ indicates that for an additional moment of inertia $J_{esk,gen}$ that is added by synchronous generators and turbines to the power system, the Eskom power system Inertia with FPR increases by $\frac{5.4}{2*10}\%$ if the other independent variables in this model are held constant. The values of the test statistics *t* = 0.062 and *P-value* = 0.951 are evidence that the moment of inertia of

the Eskom generators and the Eskom power system Inertia with FPR are non-linearly related.

The coefficient $b_2 = 3.92$ indicates that for an additional stiffness of the system β that is added by governor valves and load composite factor (steady state increase in frequency), the Eskom power system Inertia with FPR increases by $\frac{3.92}{2*10}$ higher if the other independent variables in this model are held constant. The values of the test statistics: t = 4.2 and *P-value* = zero are evidence that the stiffness of the system and Inertia with FPR in this model are linearly related.

The coefficient $b_3 = 7.E\text{-}05$ indicates that for an additional spinning reserve of 1000 MW, the Inertia Constant increases by $\frac{0.07}{2*10}$ %. The values of the test statistics t = 0.9 and *P-value* = 0.378 imply that the Inertia with FPR and spinning reserve for this model are non-linearly related.

The coefficient $b_4 = 9.E\text{-}04$ indicates that for an additional generation load loss of 1000 MW, the Inertia with FPR decreases by $\frac{0.9}{2*10}$%.The values of the test statistics t = -2.58 and *P-value* = 0.01. There is evidence to infer that generation load losses and Inertia with FPR in this model are linearly related. The impact of generator load losses is large for the Eskom network primary response. In most cases, when load losses are high, other generators in the system are picked up to their Maximum Continuous Rating (MCR) to replace the lost planned generation, which impacts negatively on spinning reserve and the stiffness of the system. This is classified as the multicollinearity factor.

The percentage point increase of spinning reserve and stiffness of the system in Medupi, Matimba and Lephalale is small. The load composite factor is expected to be low since the voltage dependent type loads in the Lephalale area are small. Matimba and Medupi power stations are high in the economic dispatch merit order and are normally operated at full output. The units in this area are normally not scheduled for instantaneous reserves. Therefore, the spinning reserves close to

Medupi power station are expected to be low and rely on the assistance of the fast Mpumalanga and Eastern region generators.

8.3.2 International coefficients

From the Table 8-1 *tie-lines* section, each factor is explained by describing what its coefficient b_n indicates in terms of its weight and influence on the independent variable Inertia with FPR and whether it is linearly or non-linearly or multicollinearly related.

The coefficient $b_5 = 0.0011$ indicates that for an additional 1000 MW that is added by BPC load to the power system, the IPS Inertia with FPR increases by $\frac{0.11}{2*10}$ % if the other independent variables in this model are held constant.

The coefficient $b_6 = 0.0017$ indicates that for each additional 1000 MW that is exported to the Zesa network, the Inertia with FPR decreases by $\frac{0.17}{2*10}$ %.

The coefficient $b_6 = -0.0016$ indicates that for an additional 1000 MW that is added by the Apollo HVDC line, the Inertia with FPR decreases by $\frac{0.16}{2*10}$ %. The values of the test statistics for the *t* and *P-value*s, indicate that there is evidence of a linear relationship between the above coefficient and the Inertia with FPR.

The contributions of ZESA and BPC load were too low. Most probably, this was as the result of the draught experienced by the Southern African region in the period of study (years 2014-2016) where there was less hydro generation in the northern parts of the SAPP. This resulted in Eskom exporting energy up north.

8.3.3 RES coefficients

From the Table 8-1 *RES* section, each factor is explained by describing what its coefficient b_n indicates in terms of its weight and influence on the dependent variable Inertia with FPR and whether it is linearly or non-linearly or multicollinearly related.

The relationship between Eskom power system Inertia with FPR (Medupi) and wind energy is described by $b_8 = 0.0035$ From this number in this model, for an additional 1000 MW of wind energy in the Eskom network, the system primary response increases by $\frac{0.35}{2*10}$. % The values of the test statistics t = 4.4 and *P-value* = zero indicate the existence of a linear relationship between the wind energy and the Inertia with FPR. The current wind penetration does not show any negative impact on the Inertia with FPR with respect to the Medupi model. This is due to the stochastic nature of the wind pattern in South Africa. A time series model will have to be applied to get the realistic impact of wind generation.

The relationship between Eskom power system Inertia with FPR (Medupi) and PV is described by $b_9 = -0.0016$ From this number in this model, for an additional 1000 MW of PV in the Eskom network, Inertia with FPR decreases by $\frac{0.16}{2*10}$ %. The values of the test statistics t = -2.4 and *p value* = 0.02 is evidence of the existence of a linear relationship between the PV eand the Eskom power system Inertia with FPR.

PV shows some negative impact on the Inertia with FPR model. Contrary to the wind generation, the PV generation is deterministic. The output of the model is fully determined by the parameter values. However, more PV could force the SO to take some of the synchronous generators off the grid. Currently hydro pump storage generators are affected. These generators are peaking plants and fast to ramp up or down to generate during the day and pump at night. If more PV is installed and all other factors remain the same, the SO will be forced to take off some of the base-load synchronous generators, which will impact negatively on the system inertia. Currently generators in the Lephalale area are inexpensive compared to other generators in the Eskom network, therefore during low load conditions, the SO will take off the next expensive power station, which negatively affects the Inertia with FPR.

8.3.4 Model validation for Medupi normal incidences

Table 8-2 shows the Medupi, Matimba and Lephalale model results following Medupi unit trips. The table compares the measured Inertia with FPR from PMU data and the Medupi, Matimba and Lephalale models.

Table 8-2: Model validation following a Medupi unit trip (single contingency).

Incident Date/time and System response		Actual Inertia Constant (H) vs Medupi model		measured frequency nadir vs Medupi model			Actual frequency nadir vs models %error in the North		
date/time	ΔP (MW)	Swing Eq. (s)	model (s)	t_{start} (Hz)	Actual f_{nadir} (Hz)	Model f_{nadir} (Hz)	Medupi	Matimba	Lephalale
17/02/17 01:41	130.3	0.72	0.701	50.16	50.04	50.05	7.4%	2.2%	2.2%
17/03/12 11:29	98.3	0.47	0.470	49.93	49.80	49.80	-2.6%	16.2%	16.0%
17/03/12 23:50	230	0.75	0.807	49.96	49.77	49.78	7.9%	-5.5%	4.8%
17/03/13 13:38	118.2	0.62	0.461	49.99	49.83	49.83	2.4%	1.8%	11.4%

The above results show that the errors between the actual measurements are below a ±10% error margin. The Medupi model is thus validated for single disturbances. The possible reason for large errors outside ±5% is accuracy of reported or recorded data and measurement errors. The Inertia with FPR model can be improved by further investigating the non-linear independent variables and upgrading a linear model to a polynomial model.

Figure 8-2 shows the overall results of the entire FPR predicted frequency nadir following single disturbances. From 355 disturbances, 225 events were within ±5% error. 51 events resulted in errors between ±10% and ±5%. The errors greater than 10% were largely from Arnot, Duvha units 4, 5 and 6 and HVDC trips. The poor errors account for 8% of the sampled data. The power stations which had no or poor models, were predicted by electrically closer models. Note that the model was developed using previous year disturbances (June 2015- Dec 2016) and the results shown occurred in the period June 2014 to March 2017. Thus, the model is also valid for the period outside the study period.

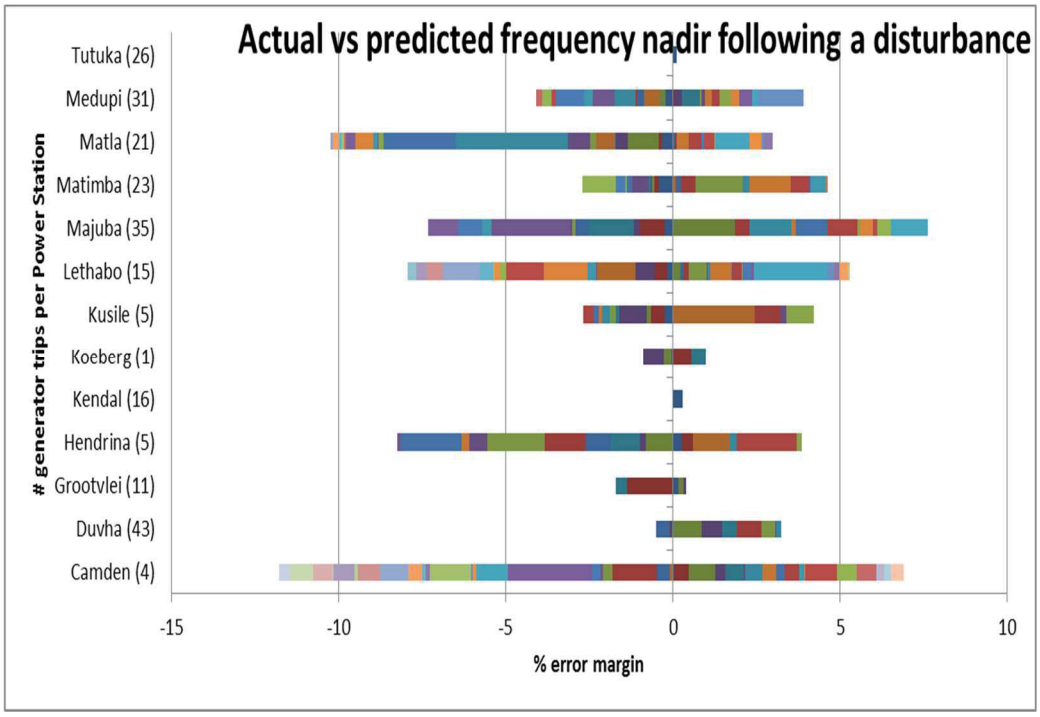

Figure 8-2: Measured vs predicted frequency nadir %errors for all power station models excluding HVDC and particular power stations.

8.3.5 Model validation for IDR events

Instantaneous Demand Response (IDR) is consumer load contracted to respond to a drop in frequency and is included in the Instantaneous Reserve of the power system. The purpose of the Instantaneous Reserve is to arrest the frequency at acceptable limits following a contingency, for example a generator trip.

A sample of past IDR events that were excluded from the Medupi model were studied. The main aim was to establish whether the model can correctly predict the Inertia with FPR and frequency nadir, assuming the unavailability of other primary and demand responses. The three incidents are discussed using data shown in Table 8-3 and Table 8-4.

Table 8-3: Previous IDR events and model estimates of the Inertia with FPR

date/time	change in system (MW)	IDR	Event duration dt(s)	H(pmu) measured (s)	Medupi model H (s)	Medupi H error	fstart (Hz)	f extrem (Hz)	Model f Nadir (Hz)
15/08/19 12:17	714	406	0.4	0.60	0.63	6%	49.88	49.57	49.17
16/02/09 13:13	517	379	0.5	0.53	0.52	-2%	49.94	49.59	49.42
16/04/17 00:16	449	328	0.6	0.68	0.75	10%	50.06	49.62	49.61

Table 8-4: Factors affecting Medupi Inertia with FPR during IDR events

#	Eskom sentout (MW)	Spinning reserve (MW)	Steady state increase in f(Hz)	Genix Load losses (MW)	BPC load (MW)	Wind (MW)	PV (MW)	dfdt
1	26012	3406	0.85	2741	178	77	1466	-0.3688
2	28298	1945	0.67	2232	-513	235	836	-0.3444
3	21355	9146	0.74	1800	123	278	0	-0.3827

(1) From the first incident, Medupi 6 tripped from an output of 714 MW. The Eskom system sent-out was 26012 MW, spinning reserve was 3406 MW, generation load losses were 2741 MW, PV output was 1466 MW. Most of the generators that provide instantaneous reserve were at maximum output. Two OCGTs were on load due to shortage of generation.

Following an incident, IDR operated and arrested the frequency at 49.57 Hz within 800 ms (Δt). The measured Inertia with FPR with reference to the PMU at Kendal power station was 0.595 s. The model error margin was 6%, which is within the ±10% target.

The model shows that if IDR and other under frequency schemes were unavailable, the frequency would have triggered UFLS operation, which was set at 49.20 Hz.

(2) From the second incident, Medupi 6 tripped from an output of 517 MW. The Eskom system sent-out was 28298 MW, spinning reserve was 1945 MW, generation (load) losses were 2232 MW, PV output was 836 MW. Following an incident, IDR operated and arrested the frequency at 49.59 Hz within one second (Δt). The measured Inertia with FPR with reference to the PMU at Kendal power

station was 0.522 s. The model error margin was -2%, which was within the ±10 percentage target.

The model shows that if IDR were unavailable, the frequency would have reached 49.42 Hz. Prior to an incident above, the generation load losses and PV were very high thereby reducing the amount of spinning reserve.

(3) From the third incident, Medupi 6 tripped from an output of 449 MW. The Eskom system sent-out was 21355 MW, spinning reserve was 9146 MW, generation (load) losses were 1800 MW, PV output was 0 MW.
Following an incident, IDR operated and arrested the frequency at 49.62 Hz within 0.6 s. The measured Inertia with FPR with reference to the PMU at Kendal power station was 0.681 s. The model error margin was 10%, which was within the ±10% target. The model shows that if IDR were unavailable, the frequency would have reached 49.61 Hz. Prior to an incident above, the generation load losses and RES were relatively low and the spinning reserve was high.

For all three events, the model correctly estimated the Inertia with FPR within ±10% margin of error. Thus, the model is also valid for IDR events that were excluded from the model.

8.4 Overall Inertia with FPR model and model validation

The purpose of the study was to determine the impact of disturbance location on the inertia with FPR model. A number of selected large power stations were studied and the results are presented in Figure 8-3. The overall system Inertia with FPR yielded a poor correlation of 12%. Breaking down the overall FPR into areas/grids resulted in better correlation averaging 60%. By further breaking down into individual power stations, the correlation became even better. From these results, the location of disturbances affects the Inertia with FPR. System FPR was studied per area/power station and models were developed in order to acquire the best results.

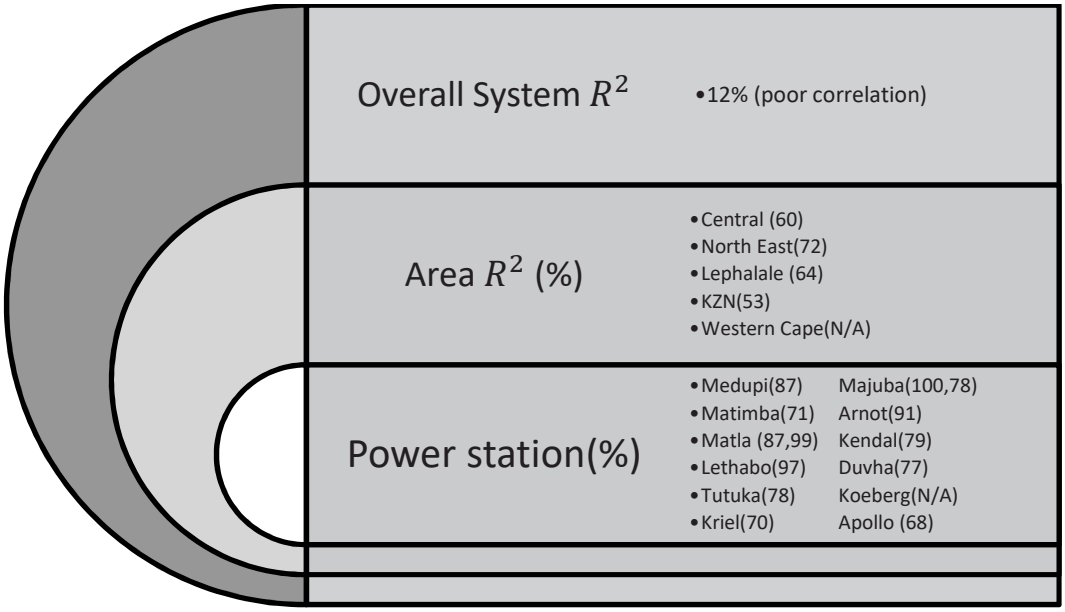

Figure 8-3: Overall system inertia with FPR correlation results.

Note that some power station models had to be split into two due to network connection points, since the combined correlation resulted in large errors, i.e. correlation of Matla (all units) resulted in 48%,. By splitting the model into two, Matla units 1234 (connected to 275 kV) resulted in 87% correlation and Matla units 5 6 (connected to 400 kV) resulted in 99%. Similarly, Arnot, Majuba (different H between units 123 and 456) and Duvha (different droop setting between units 123 and 456).

8.5 Inertia with FPR model validation for normal incidences

In this section, the FPR model was validated against the previous incidents. Table **8-5** shows the overall results of the entire Inertia with FPR predictions following single disturbances. Note that the model was developed using the previous year disturbances (June 2015-December 2016) and the results shown are 2014 and 2017 incidents. The units with no and/or poor/bad R^2 models were best predicted by other developed models.

Table 8-5: All Inertia with FPR model predictions vs measured values from Swing Equation

date/time	unit	H %error	Best predicted by Model
14/07/01 22:34	Grootvlei 6	1.66%	Arnot
14/07/07 12:14	Kendal 3	2.89%	Majuba 123
14/07/23 11:38	Duvha 1	-0.54%	Apollo
14/07/23 15:03	Majuba 5	-2.30%	Apollo
14/07/28 23:13	Duvha 4	4.31%	Kriel
14/07/29 17:54	Kendal 5	3.32%	Apollo
14/07/31 22:54	Kriel 5	4.33%	Lephalale
14/08/03 19:59	Duvha 1	7.97%	Duvha
14/08/06 09:54	Matimba 1	-4.31%	Majuba 123
14/08/07 22:13	Kriel 2	4.40%	Apollo
14/08/22 03:22	Matla 5	-3.20%	Kriel
14/08/25 08:09	Matla 4	-1.24%	Central
14/08/26 02:06	Tutuka 6	1.04%	Kriel
14/08/28 11:06	Matla 6	-0.77%	Majuba 123
14/09/02 15:46	Matimba 4	-7.60%	Majuba 456
14/09/08 15:45	Majuba 5	-3.91%	Majuba 456
14/09/10 17:48	Majuba 4	2.14%	Kriel
14/10/09 19:49	Majuba 4	-5.67%	Apollo
14/10/13 19:08	Tutuka 2	0.28%	Majuba 123
14/10/15 10:38	Matimba 6	-1.77%	Apollo
14/10/22 12:23	Lethabo 4	-1.56%	Lephalale
14/10/22 22:36	Tutuka 1	-1.93%	Tutuka
14/11/06 11:31	Majuba 5	0.42%	Majuba 456
14/11/07 07:09	Majuba 1	-11.60%	Majuba 456
14/11/12 03:16	Majuba 6	0.73%	Kriel
14/11/12 14:05	Grootvlei 4	-0.31%	Apollo
14/11/13 12:16	Majuba 3	1.37%	Central

14/11/14 04:53	Matla 1	-0.20%	Tutuka
14/11/15 16:41	Duvha 2	3.21%	Arnot
14/11/16 04:41	Duvha 5	5.23%	Majuba 123
14/11/19 12:13	Kriel 4	-2.72%	Majuba 123
14/11/19 16:38	Majuba 6	5.51%	Duvha
14/11/19 23:45	Majuba 6	0.30%	Lephalale
14/11/20 06:14	Majuba 6	0.75%	Kriel
14/11/20 11:28	Hendrina 1	-3.28%	Apollo
14/11/22 20:48	Kriel 1	1.34%	Majuba 123
14/11/23 04:36	Matla 2	-0.87%	Majuba 123
14/11/23 08:31	Kriel 1	1.68%	Apollo
14/11/30 09:08	Kriel 6	2.14%	Matimba

The results show that the majority of the 2014 incidences were poorly predicted by the corresponding power station models. This can be attributed to the low PMU sample rate resolution (100 ms). Therefore, it is important for the SO to archive the disturbances at high sample rates (20 ms) for future and further studies. Figure 8-4 shows the 2017 summary results of other power stations models with high PMU sample rate.

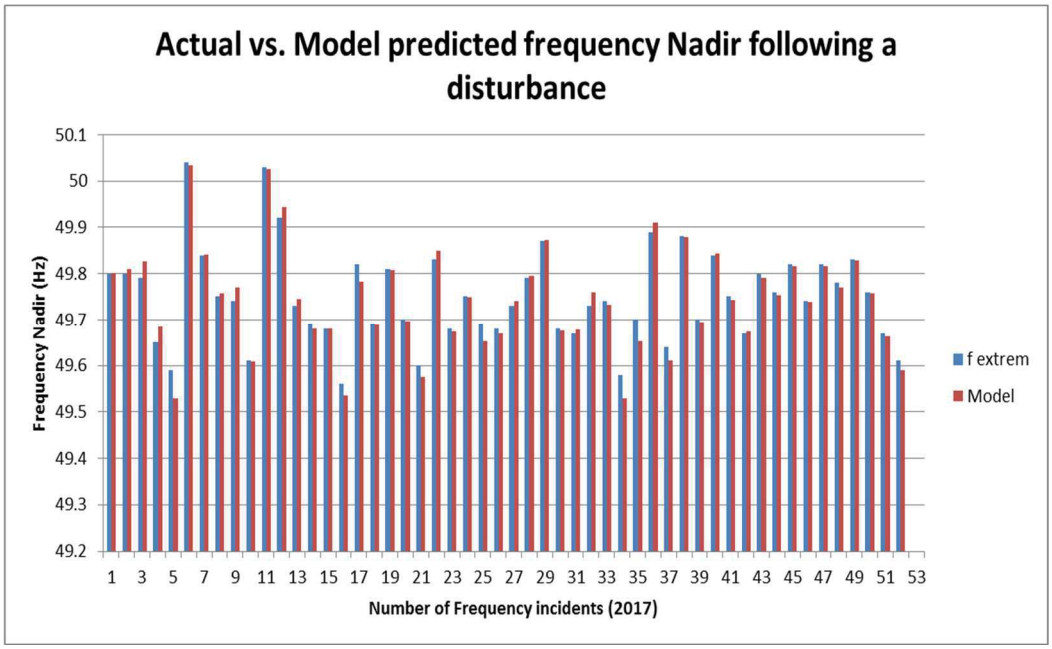

Figure 8-4: Summary of all power station model validations for 2017 disturbances.

The above results show that the comparison between the measured and model frequency nadir are close. The full results of the inertia with FPR models are included in Appendix A.

9. FACTORS AFFECTING ESKOM INERTIA WITH FPR

9.1 Introduction

This chapter focuses on the short-term frequency stability and understanding the relationship between system Inertia with FPR of the Eskom power system including but not limited to RES, location of disturbance, stiffness of the system and the interconnected parts of the Southern African Power Pool (SAPP). By understanding factors affecting the system inertia, an online (real-time) inertia with Fast Primary Response (FPR) model can be developed. There is a significant body of literature available which documents the factors affecting system inertia in utilities worldwide [4], [6], [17], [27]. However, it must be noted that power system networks are different in sizes and characteristics. Figure 9-1 illustrates the relationship between RoCoF changes following the loss of a generator against relatively high, medium and low system Inertia with FPR.

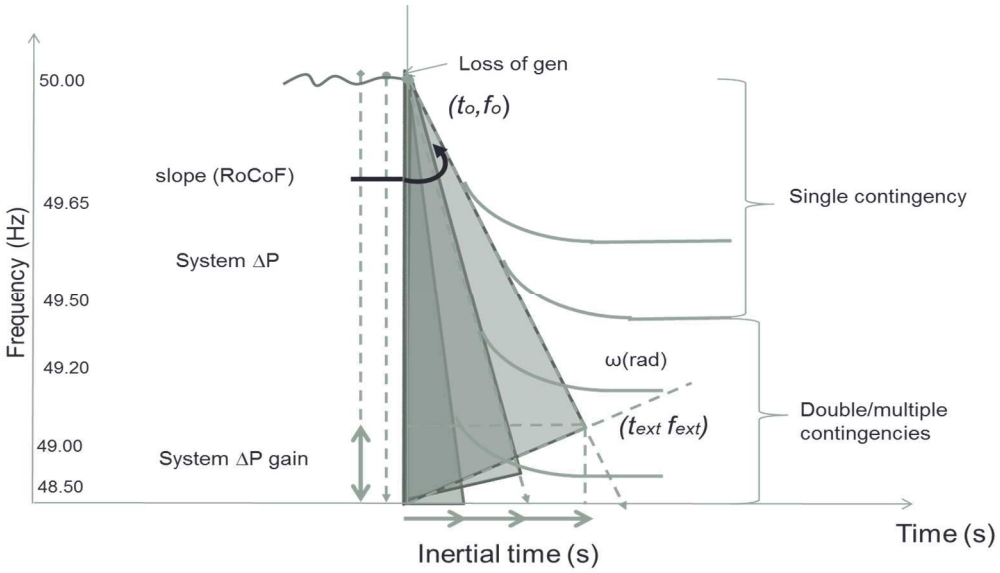

Figure 9-1: RoCoF as a function of system inertia but now with FPR.

This chapter begins by providing a background of the Eskom network, generation, load centres and typical known challenges. Although a Koeberg unit in the Western Cape is the largest unit in the Eskom network, it caused fewer frequency

incidents between the years 2014-2016 than large coal-fired units in the Mpumalanga and Limpopo provinces. For this reason, the incidences in the Western Cape province are not covered in this study. The areas considered in this study are Lephalale (Medupi and Matimba), KwaZulu Natal (Majuba), North East (Kendal, Tutuka, Matla and Kriel) and Central (Duvha, Lethabo and Apollo HVDC). The results of the factors affecting the Eskom system FPR are presented.

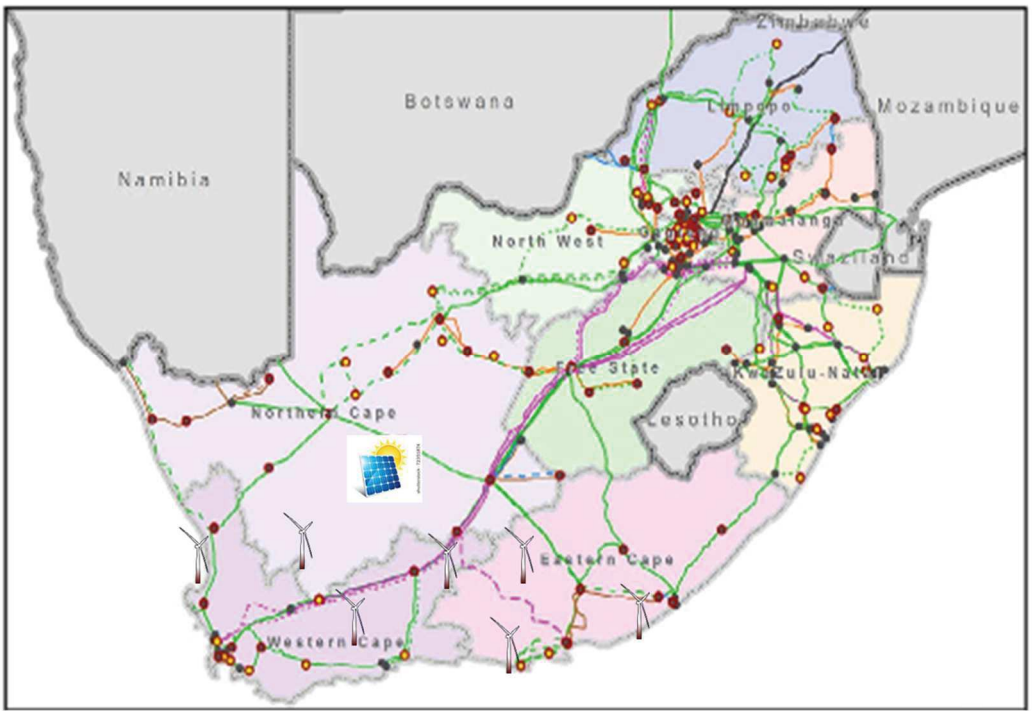

Figure 9-2: South Africa's existing and planned transmission grid, generation and RES. Adopted from [10] (permission obtained for use of data).

9.2 Eskom generation and load centres

This section reviews the Eskom generation and load centres. Topics addressed per centre or province include the average peak load, type of customers, existing and new generation and general challenges affecting the grid stability.

9.2.1 The Limpopo province

Approximately 2.8 GW of Eskom's total load is in the northern part of the country. The major customers are the re-distributors, residential customers, industrial factories, agricultural customers, commercial customers and the international interconnector (Botswana) [10]. The local generation bulk supply is

Matimba power station, the newly built Medupi power station and a few IPPs. These power stations are in the Lephalale area of the Limpopo province. The main grid challenges are transient stability during outages. It must be noted that power generated in this province must be evacuated to other areas over long lines. Lephalale is a developing area with relatively small local load demand compared to other large load centres [10].

9.2.2 The KwaZulu-Natal province

The KwaZulu-Natal province is situated on the eastern seaboard of South Africa. The economic activity in the KwaZulu-Natal province comprises about 7 GW of load and the major customers are the re-distributors, residential customers, agricultural customers, traction customers and commercial customers. The generation bulk supply is mainly from the Mpumalanga province, Drakensberg and Ingula pump storage schemes and diesel fired OCGTs. The closest large source of power is Majuba power station at the northeast border between the KwaZulu-Natal province and Mpumalanga province [10].

9.2.3 The Gauteng province

Geographically, Gauteng is the smallest province in South Africa. Approximately one third of electricity consumption in the country is in this province. The economic activity in the Central grid comprises about 13 GW and the major customers are re-distributors, residential customers and large commercial customers. The generation bulk supply is mainly from Mpumalanga, Free State, Lephalale and HVDC (from Mozambique). There are only two IPPs, both small coal-fired power stations, owned and operated by the municipalities in Gauteng. The current challenges are equipment/lines/cable overloading due to limited servitudes for expansions/strengthening and high residential load during peak hours [10].

9.2.4 The Mpumalanga province

Approximately 4 GW of Eskom's total load is in the north-eastern parts of the country. The Mpumalanga province houses about 12 power stations, 22 GW of installed capacity and the newly constructed Kusile coal-fired power station with

the total capacity of 4.8 GW on completion. Current load characteristics in the province are comprised of mining, commercial, industrial and residential [10].

9.2.5 The Western Cape province

Approximately 4 GW of Eskom's total load is in the Western Cape province. The major customers are re-distributors, residential customers, agricultural customers, industrial customers, mining customers and commercial customers. The generation bulk supply is mainly from the local Palmiet pump storage scheme and Koeberg nuclear power stations. The deficit between Koeberg and the greater Cape load is offset by the generation pool in the Mpumalanga province via the Cape Corridor network. Ankerlig and Gourikwa OCGTs are mainly utilised for general shortage of plant or management of Cape transfer limits [10]. Koeberg and Palmiet units in the Western Cape network, caused fewer frequency incidents in the past three years than large coal-fired units in the Mpumalanga and Limpopo provinces. For this reason the incidences in the Western Cape province are not covered in this work, as there is not enough data from the Eskom EMS and WAMS.

9.2.6 The Eastern Cape

Approximately 1.5 GW of Eskom's total load is in the south-eastern part of the country. The major customers are tourism, residential customers, agricultural customers and industrial customers. The generation bulk supply is mainly from the local renewable wind parks. The deficit is offset by the generation pool in the Mpumalanga province via the Cape Corridor and KwaZulu-Natal. Port Rex gas turbines and a diesel fired (IPP) OCGT are mainly utilised for general shortage of plant, management of local transfer limits and voltage control. Major grid challenges are that adding more embedded renewable generation will require adequate network integration plans [10].

9.2.7 The Northern Cape province

Geographically, The Northern Cape province is the biggest province in South Africa. The economic activity in the Northern grid comprises about 0.7 GW load and the major customers are commercial customers, mining customers and

agricultural customers. The generation bulk supply is mainly from the Mpumalanga province and local PV plants. Van Der Kloof and Gariep hydro power stations are mainly utilised as peaking power stations in conjunction with the Department of Water and Sanitation. The main grid challenges are low fault levels and radial networks impacting reliability and Quality of Supply during outages [10].

9.2.8 The Free State province

Approximately 2.4 GW of Eskom's total load is in the middle part of the country. The major customers are the re-distributers, mining customers, residential customers, agricultural customers, traction customers and industrial types of load. The generation bulk supply is mainly from the Mpumalanga power pool. The local Renewable Energy Sources includes wind and PV parks. Major grid challenges are that adding more embedded renewable generation will require adequate network integration plans and suffer low fault levels [10].

9.2.9 The North West province

Approximately 2.4 GW of Eskom's total load is in the north-western part of the country. The major customers are mining customers, re-distributers, residential customers, agricultural customers and industrial types of load. There are no power stations in this province. The generation bulk supply is mainly from the Limpopo and Mpumalanga power pool [10].

The first four provinces, Limpopo (Lephalale), Central, Mpumalanga and kwaZulu-Natal will be used to study the FPR since there are enough large synchronous generator frequency events from these provinces. Koeberg and Palmiet power stations were excluded from this work because of the small number of frequency incidents. The last four provinces, Eastern Cape, Northern Cape, Free State and North-West were excluded in the next sub-section, because there are only a few or no synchronous generators in these provinces.

9.3 Fast Primary Response (FPR) model coefficients comparison between areas and power stations

This section determines the Inertia with FPR area and power station models. The aim is to compare the performance of all the Inertia with FPR models with Kendal power station as the reference of Eskom's centre of inertia and frequency.

The models were built using normal incidences where the starting frequencies prior to a unit trip were within the normal operating frequency dead-band, i.e. between 49.85-50.15 Hz. It was observed in Chapter 4.5.5 from frequency incident data that the IDR acts like a very fast governor and restricts the system natural frequency nadir (minimum frequency reached after a disturbance). Such incidents in this chapter were excluded.

Comparing the models fairly, the regression analysis for each power station in this section was normalised to zero constant intercept in Excel. Table 9-1 summarises the coefficients of selected power stations models in different areas. It is divided into four sections, namely, model validation, Eskom AC system coefficients, international tielines and RES. Each section will be discussed separately in the following subsections.

Table 9-1: Comparison of areas and power station Inertia with FPR models (print in colour. Red=poor; yellow=average; green=good)

		Area		Lephalale		KZN		North East					Central		
		Model		Medupi	Matimba	Maj 123	Maj 456	Tutuka	Matla 3456	Kendal	Arnot	Kriel	Duvha	Lethabo	Apollo
		Observations		29	23	12	14	25	18	14	15	18	18	16	15
Model validation		R Square	R^2	0.99	0.98	1.00	0.97	0.96	0.97	0.98	0.98	0.99	0.99	0.99	0.91
		Standard Error	S_ε	1.07	1.12	0.33	1.81	2.26	1.89	1.26	1.65	0.93	0.96	0.93	3.61
		F statistic		151	71	508	21	40	33	28	31	74	66	100	7
		Significance of F		0.00	0.00	0.00	0.01	0.00	0.00	0.00	0.00	0.00	0.00	0.00	0.03
	Coef.	Independent variable													
Eskom AC system	b_1	System total MOI(J)	(x_1)	2.3	1.7	2.5	0.3	1.6	0.9	0.6	5.2	0.9	0.8	3.2	-8.9
	b_2	Stiffness (pu/Hz)	(x_2)	9.5	4.5	35.0	61.9	57.4	29.3	6.3	-0.5	19.6	30.7	8.8	56.3
	b_3	Spinning reserve (x1GW)	(x_3)	0.2	0.3	-1.1	1.2	0.6	0.2	-0.1	-0.6	0.1	0.2	1.1	0.4
	b_4	Genix Load losses (x1GW)	(x_4)	-1.2	-0.2	-0.3	2.6	-0.7	1.8	0.6	-0.4	-0.2	-0.5	-2.3	-2.1
Tielines (x1GW)	b_5	BPC load	(x_5)	-0.4	2.5	4.9	-6.8	-0.9	-6.1	1.7	7.2	0.5	-0.2	-5.4	45.8
	b_6	Zesa	(x_6)	0.5	0.9	-13.7	1.4	15.7	5.3	-0.6	6.2	1.2	-0.7	17.6	20.3
	b_7	Apollo DC	(x_7)	-2.4	-1.1	-1.1	-10.1	-8.6	-5.8	0.5	-7.8	-0.5	-1.6	-5.5	-45.7
RES (x1GW)	b_8	Wind	(x_8)	3.9	-3.2	-14.2	-14.9	0.5	2.5	2.8	-2.1	1.2	-0.1	4.1	11.5
	b_9	PV	(x_9)	-1.7	-1.1	-3.1	4.5	4.2	1.0	-1.3	-3.0	-0.1	-1.7	4.2	4.6

9.3.1 Validation of selected power stations inertia with FPR models

Referring to Table 3-1, except for Majuba power station two (units 4, 5 and 6) and Apollo HVDC converter station, all the models in Table 9-1 are good since R^2 is close to 1 the *F statistic* is large and the *significance of F* is zero. This is an indication that most of the variation in Inertia with FPR is explained by the regression model and that the models are good.

The worst performing model is that for the Apollo HVDC converter station. This could be in line with Nordic [17] findings that when a generator or importing HVDC connection trips, the estimated inertia value is always higher than the actual inertia value. The inaccuracy could be due to the voltage dependency of the loads in the Central 275 kV network and the strength of the 275 kV network in the Central grid close to the HVDC infeed.

9.3.2 AC power station Inertia with FPR model coefficients

This part of Table 9-1comprises the total system moment of inertia, stiffness of the system, spinning reserve and generation load losses. The coefficient b_1 of all

the models shows that for an additional moment of inertia $J_{esk,gen}$ that is added by synchronous generators and turbines to the power system, the Inertia with FPR increases (as expected). The Apollo HVDC converter station is asynchronous; therefore, HVDC imports do not contribute to the system Inertia with FPR.

The power stations in the north-east and Eastern areas of the network, which are connected to the 400 kV system, have larger stiffness coefficients, b_2, compared to other power stations in remote areas (Lephalale and Arnot). This can be interpreted as during disturbances around the 400 kV network in the Central and Mpumalanga areas, the generators closer to the disturbance are fast to react to the loss of generation in that particular area.

Lethabo power station in the Central area, is connected to the 275 kV network and connected to other power stations via 275/400 kV step-up transformers which have high impedance, making Lethabo electrically remote to other power stations. This power station has a smaller stiffness coefficient, b_3. This can be interpreted as the power stations in the Mpumalanga area which are connected to the 400 kV system, contribute less FPR during disturbances at Lethabo power station.

Spinning reserve is highly related to the stiffness of the system. The coefficient b_4 shows that for an additional generation load loss of 1000 MW, the Inertia with FPR generally decreases. The negative impact of generator load losses is large for the network's FPR. In most cases, when load losses are high, the output of the other generators in the system is increased close to their Maximum Continuous Rating (MCR) to replace the lost generation, which impacts negatively on spinning reserve and the stiffness of the system. The interdependency between the independent variables is classified as the multicollinearity factor. This means that some of the independent variables such as spinning reserve and stiffness are either non-linearly or highly correlated with one another. This indicates that spinning reserve should be managed locally, i.e. per area by the SO.

9.3.3 Tie-line Inertia with FPR model coefficients

The BPC (b_5) and Zesa (b_6) utilities are relatively small compared to the Eskom network and are not expected to assist significantly with the frequency response following a large disturbance in the Eskom network. The electrical impedance connecting Eskom and neighbouring countries is also high due to the weak tie-lines between these countries. Apollo HVDC (b_7) is consistently negative for all the power station Inertia with FPR models.

9.3.4 RES inertia with FPR model coefficients

This part of a table comprises wind (b_8) and PV (b_9). The large negative impact of wind energy is in the eastern area where no wind generation is installed. When there is an excess of wind energy during low demand, the SO is forced to take off some of the base load synchronous generators. Previously units at Majuba power station in the Eastern area were being regularly taken off the grid over periods of low load to accommodate the wind generation. This weakens the system, the stiffness of the KZN province and the Inertia with FPR. Other areas are not highly impacted.

9.4 Conclusion

In this chapter, the load and generation centres in the Eskom network were discussed. The four areas, Lephalale, Central, KwaZulu-Natal and Mpumalanga were selected for FPR model development. The remaining other provinces were excluded based on the small number of generator frequency events.

The models were developed using normal incidences using Kendal power station as the reference of Eskom's centre inertia and frequency. All the model results, except for Majuba power station (units 4, 5 and 6) and Apollo converter station were good based on the small s_ε , R^2 close to 1 and large *F statistic*.

The strong and weak areas with respect of the stiffness of the system were identified. This can contribute to future grid planning and real-time operations in managing the system inertia and primary response.

9.5 Recommendation for future work

The primary frequency control schemes installed in South Africa's power transmission system were designed for steady state settings with hard limits. Based on the evidence that the frequency dynamics are faster, the schemes should be revised to mitigate fault events before a critical frequency drop can occur and to shed close-to-required load at the time of an incident.

The Inertia with FPR model can be improved by further investigating the non-linear independent variables and upgrading a linear model to a polynomial model.

More PMU installations in different key substations and power stations are required in the SAPP network for better network visibility and awareness.

Network expansion should consider operational challenges in planning stages.

The impact of two-shifting the units due to excess generation must be further studied. This is more likely to reduce generator life in future, as the load profile continues to change.

The models can be used in the control centre to monitor the stability limits and make informed decisions given the rapidly changing demand patterns and generation types.

The worst performing model was that for the Apollo HVDC converter station. This could be that when a generator or importing HVDC connection trips, the inaccuracy was because of the voltage dependency of the loads in the Central 275 kV network and the strength of the 275 kV network in the Central grid close to the HVDC infeed. Possible mitigation is to install an inter-tripping scheme at the Apollo 275 kV capacitors. The HVDC line and convertor station bridge incident data should be separated and studied in isolation. The installation of PMUs at Apollo and Songo will give a better insight into the dynamics of this part of a network.

10. CONCLUSIONS

In this work, an inertia model of the Eskom power system to determine the relationship between factors affecting the power system inertia and the RoCoF using the MVA method is presented. It is based on the use of a Swing Equation Method to estimate the inertia from disturbances and equated with the known and unknown variables related to system inertia at the time of an incident (regression). The response of the entire network (except for the Western Cape area) during these disturbances was studied.

To this end, the conclusions below were reached.

As more zero-inertia generators i.e. asynchronous generators, are added in the Eskom power grid, the traditional synchronous generators, which provide inertia to the system, are starting to be displaced, put into cold reserve or two-shifted and see early retirement. The slow economic growth with high asynchronous penetration translates to less synchronous generation dispatch by the SO. This has a negative impact on system inertia with and without FPR.

The first model, which approximates the Rate of Change of Frequency (RoCoF) occurring within 300 ms following a disturbance, was studied. For the entire sample data studied, disturbance location (with reference to Kendal in the north-eastern area of South Africa) does not introduce significantly large errors in the system RoCoF model following a single disturbance. The relationships between RoCoF and system inertia at different areas, were shown to be linear. The results resulted in 96% correlation for the randomly selected frequency disturbances.

The GCSA does not specify the minimum spinning and instantaneous reserves per area. From the findings in this work, the instantaneous response is most effective when the contracted units have adequate spinning reserve. For effective power system inertia and primary response management, the spinning reserve should be managed per local area by the SO.

Reducing the contribution of conventional synchronous generators to accommodate renewable energy power generation reduces the system inertia. The two inertia models developed showed that reduction of rotational energy provided by synchronous generators negatively impacts the RoCoF and the inertia of the system.

The large negative impact of wind energy is in the eastern area (KZN) where no wind generation is installed. When there is an excess of wind energy during low demand, the SO is forced to take off some of the base-load synchronous generators. Previously units at Majuba power station in the eastern area were being regularly taken off the grid over periods of low load to accommodate the wind generation. This weakens the system, the stiffness of the KZN province and the FPR. Other areas were not highly impacted.

However, the relatively low penetration level of RES does not yet have a significant negative impact on the Eskom system inertia. However, future penetration could have a significant negative impact if not managed in real-time. It is important that the SO develops online inertia monitoring systems and insight to deal with future high penetration levels of RES. This will also help the SO with situational awareness and the required RES based on dynamic inertia limits.

When the tool is fully developed, the SO can use the tool for situational awareness, generation dispatch scheduling, inertia forecasting, incident reporting and assist in improving the offline simulation tool parameter tuning.

The model is expected to improve with time as the accuracy of the statistical approach requires large amounts of data. The model can be used to determine and monitor the maximum level of RES in real-time. The model is still to be developed within the Eskom SCADA system and will be improved by extracting more frequency incidents and using time series algorithms to forecast the system Inertia with FPR.

Spinning reserve and stiffness of the system play a significant role in the model accuracy. However, spinning reserve should be divided and managed locally, especially in weak areas.

The assumption that the (aggregated) Inertia Constant, *H*, is constant for all Swing Equations of a multi-area system is not valid for the Inertia with FPR model.

The primary frequency control schemes installed in South Africa's power transmission system were designed for steady state settings with hard limits. Based on the evidence that the frequency dynamics are faster, the primary frequency schemes should be revised to mitigate fault events before a critical frequency drop can occur and to shed close-to-required load at the time of an incident. The RoCoF model can be explored further and utilised in conjunction with the under-frequency schemes.

The disturbance location is vital for the system Inertia with FPR model, where the stiffness of the system factor is of interest. The correlation of the combined past disturbances for the entire system was poor, the Coefficient of Determination R^2 was found to be 12%. By breaking down the data into regions and power station levels, the inertia with FPR model improved to an average of 65% and 87% respectively.

The major contributions of this research are summarised as follows:

1. To the author's knowledge, Multivariate Analysis has never been used to estimate and predict the power system Inertia without FPR, Inertia with FPR and RoCoF following a disturbance in power systems. The factors affecting the FPR and RoCoF of the Eskom network were identified and analysed. All the models developed were validated using the *Coefficient of Determination*, *standard error, Sum of Squared Errors (SSE)*, *F statistic and* the *significance of F*.

2. A paper titled “Development of a dynamic multivariate power system inertia model” was accepted by the South African Cigre National Committee to be presented at the Cigre International Symposium in Paris 2018 (C2-204). The paper is included in Appendix D. The comments and contributions from Eskom industry experts are included in Appendix E.
3. A paper “A Dynamic Multi-Variate Approach to the Management of Power System Inertia” was published in SAUPEC 2017 and included in Appendix C.
4. The model uses analytics, of which the data was available and sourced directly from the Eskom SO. Neither new equipment nor new software was required to implement the model. The models can be easily incorporated into the system operating control system (SCADA/TEMSE).
5. The study managed to separate the difference between Inertial Response provided by the system inertia and system FPR using the analytics or MVA.
6. This work identified statically the factors contributing to system inertia and the factors that do not for the system RoCoF following the disturbance. Main factors are kinetic energy from synchronous generators and the amount of generation lost. The higher the generation sent-out does not necessarily translate to higher system’s RoCoF. The only factor that can be linked to the generation sent-out is the hydro pump storage power station’s mode of operation. This has shown the contribution of water to the hydro power station unit’s inertia when generating or pumping compared to when operated in SCO mode.
7. The Eskom network weak areas were identified in the study by analysing the stiffness of the system. This can contribute into future grid planning and real-time operations in managing the system inertia.
8. During large disturbances, the coefficients of RES, spinning reserve, HVDC and load losses are very small and distort the *t-test* of the coefficients of the RoCoF. Examples would be during low load and/or excess generation capacity conditions when the SO is forced to take synchronous generation off the grid, which affects the system inertia.

9. The negative impact of Unplanned Capacity Load Factor (UCLF) is large for the Eskom network primary response model. When generation load losses are very high, other generators in the system are picked up to their Maximum Continuous Rating (MCR) to replace the lost planned generation, which impacts negatively on spinning reserve and the stiffness of the system. Contrary to Fast Primary Response, generation load losses have a positive impact on the RoCoF model. This is because when losses are high, the SO dispatches more peaking plants, which adds more inertia to the network.

11. REFERENCES

[1] Department of Energy, "South African Integrated resource plan for electricity 2010-2030 rev 2," *Energy.gov.za*, Mar-2011. [Online]. Available: http://www.energy.gov.za/IRP/irp%20files/IRP2010_2030_Final_Report_20110325.pdf.

[2] National Energy Regulator of South Africa, *South African Grid Code - Requirements for Renewable Power Plants*, vol. Rev 2.9. National Energy Regulator of South Africa.

[3] Republic of South Africa Department of Energy, "Integrated resource plan update assumptions, base case results and observations revision 1," *Energy.gov.za*, Nov-2016. [Online]. Available: http://www.energy.gov.za/IRP/2016/Draft-IRP-2016-Assumptions-Base-Case-and-Observations-Revision1.pdf.

[4] S. Sharma, S.-H. Huang, and N. D. R. Sarma, "System inertial frequency response estimation and impact of renewable resources in ERCOT interconnection," in *Power and Energy Society General Meeting, 2011 IEEE*, 2011, pp. 1–6.

[5] National Energy Regulator of South Africa, *South African Grid Code - Network Guide*, vol. 9. National Energy Regulator of South Africa, 2014.

[6] P. Kundur, N. J. Balu, and M. G. Lauby, *Power system stability and control*. New York: McGraw-Hill, 1994.

[7] P. Kundur *et al.*, "Definition and classification of power system stability IEEE/CIGRE joint task force on stability terms and definitions," *IEEE Trans. Power Syst.*, vol. 19, no. 3, pp. 1387–1401, Aug. 2004.

[8] L. Musaba, "Challenge of capacity growth in the southern african power pool," *RERA Reg. Electr. Regul. Assoc. Comm. Train. Lusaka Zamb.*, 2008.

[9] P. V. Goosen, P. Riedel, and J. W. Strauss, "GMPC Enables Energy Transmission over Interconnected SAPP Grid," *IEEE Trans. Power Deliv.*, vol. 18, no. 3, Jul. 2003.

[10] Eskom, "Eskom Transmission Development Plan 2016 – 2025," *www.eskom.co.za*, Oct-2015. [Online]. Available: http://www.eskom.co.za/Whatweredoing/TransmissionDevelopmentPlan/Documents/2016-2025TDP__Oct2015Rev5.pdf.

[11] A. Ulbig, T. S. Borsche, and G. Andersson, "Impact of Low Rotational Inertia on Power System Stability and Operation," *ArXiv13126435 Math*, Dec. 2013.

[12] M. Prof Jahed, A. Rashaad Amra, G. Gloria Mnguni, and S. Seeraj Mohamed, "Analysis of Eskom's finances position -full Report," Parliament of the Republic of South Africa, Cape Town, South Africa, Mar. 2017.

[13] Republic of South Africa Department of Energy, "Integrated Resource Plan for Electricity." Republic of South Africa Department of Energy, 2013.

[14] Statistics South Africa, "The South African economy shrinks by 0,7%," *Statssa.gov.za*. [Online]. Available: http://www.statssa.gov.za/?p=9989.

[15] G. Lalor, A. Mullane, and M. O'Malley, "Frequency Control and Wind Turbine Technologies," *IEEE Trans. Power Syst.*, vol. 20, no. 4, pp. 1905–1913, Nov. 2005.

[16] F. M. Gonzalez-Longatt, “Effects of the synthetic inertia from wind power on the total system inertia: simulation study,” presented at the 2012 2nd International Symposium On Environment Friendly Energies And Applications, Newcastle upon Tyne, UK, 2012.
[17] E. Ørum *et al.*, “Future system inertia, NORDIC report,” European Network of Transmission System Operators for Electricity, Avenue Cortenbergh, Brussels, Belgium, 2015.
[18] P. Tielens and D. Van Hertem, “Grid inertia and frequency control in power systems with high penetration of renewables,” 2012.
[19] T. Inoue, H. Taniguchi, Y. Ikeguchi, and K. Yoshida, “Estimation of power system inertia constant and capacity of spinning-reserve support generators using measured frequency transients,” *IEEE Trans. Power Syst.*, vol. 12, no. 1, pp. 136–143, Feb. 1997.
[20] “Definition and Classification of Power System Stability IEEE/CIGRE Joint Task Force on Stability Terms and Definitions,” *IEEE Trans. Power Syst.*, vol. 19, pp. 1387–1401.
[21] Electric Power Research Institute, *Power Systems Dynamics Tutorial*. Palo Alto, CA: 1016042, 2009.
[22] S. Guo and J. Bialek, “Synchronous machine inertia constants updating using Wide Area Measurements,” in *Innovative Smart Grid Technologies (ISGT Europe), 2012 3rd IEEE PES International Conference and Exhibition on*, 2012, pp. 1–7.
[23] K. G. S. Darshit S. Patel, “A Low Order System Frequency Response Model for Large Power System and Adaptive Load Shedding,” *Int. J. Adv. Res. Electr. Electron. Instrum. Eng.*, vol. 04, no. 05, pp. 3845–3852, May 2015.
[24] M. Keely, F. McNamara, J. Hope, and Witmarsh-Everiss, M.J, “Modeling of Post Generation Loss Frequency Behavior in Power Systems,” *Cigré 1994 Sess. 38- 307*, Aug. 1994.
[25] P. Wall, F. González-Longatt, and V. Terzija, “Demonstration of an inertia constant estimation method through simulation,” in *Universities Power Engineering Conference (UPEC), 2010 45th International*, 2010, pp. 1–6.
[26] T. Wu, Z. Alaywan, and A. D. Papalexopoulos, “Estimation of WECC System Inertia Using Observed Frequency Transients,” *IEEE Trans. Power Syst.*, vol. 20, no. 2, pp. 1188–1190, 2005.
[27] P. M. Ashton, C. S. Saunders, G. A. Taylor, A. M. Carter, and M. E. Bradley, “Inertia Estimation of the GB Power System Using Synchrophasor Measurements,” *IEEE Trans. Power Syst.*, vol. 30, no. 2, pp. 701–709, Mar. 2015.
[28] D. P. Chassin, Z. Huang, M. K. Donnelly, C. Hassler, E. Ramirez, and C. Ray, “Estimation of WECC system inertia using observed frequency transients,” *IEEE Trans. Power Syst.*, vol. 20, no. 2, pp. 1190–1192, May 2005.
[29] G. Keller, *Statistics For Management And Economics*, 7th ed. Cincinnati: Thomson South-Western, 2005.
[30] P. M. Ashton, C. S. Saunders, G. A. Taylor, A. M. Carter, and M. E. Bradley, “Inertia Estimation of the GB Power System Using Synchrophasor Measurements,” *IEEE Trans. Power Syst.*, vol. 30, no. 2, pp. 701–709, Mar. 2015.

[31] *Digsilent user manual*. Gomaringen, Germany: DIgSILENT GmbH, 2015.
[32] H. D. Piriz, A. R. Cannatella, E. Guerra, and D. A. Porcari, "Inertia of Hydro Generators. Influence on the Dimensioning, Cost, Efficiency and Performance of the Units," *Cigré 2012*, pp. A1-102, 2012.
[33] J. O'Sullivan, "Studying the Maximum Instantaneous Non-Synchronous Generation in an Island System—Frequency Stability Challenges in Ireland," *IEEE Trans. Power Syst.*, vol. 29, no. 6, pp. 2943–2951, 2014.
[34] M. Gumede, M. Ntusi, and M. Rampokanyo, "Optimise demand response for primary frequency control," in *Technology solutions and innovations for developing economies*, Cape Town, South Africa, 2017.
[35] IEEE C37.118.1-2011, "IEEE Standard for Synchrophasor Measurements for Power Systems." IEEE Power Engineering Society.
[36] P. M. Ashton, G. A. Taylor, M. R. Irving, I. Pisica, A. M. Carter, and M. E. Bradley, "Novel application of detrended fluctuation analysis for state estimation using synchrophasor measurements," *IEEE Trans. Power Syst.*, vol. 28, no. 2, pp. 1930–1938, May 2013.

APPENDIX A: Inertia plus Fast Primary Response area and power stations model

Table 1: Lephalale area inertia plus FPR models

	Model		Matimba				Medupi				Lephalale Area			
Regression Statistics	Multiple R		0.842				0.930				0.801			
	R Square		0.708				0.865				0.642			
	Adjusted R Square		0.470				0.805				0.567			
	Standard Error		1.125				0.895				1.249			
	Observations		21.000				30.000				53.000			
ANOVA				*SS*	*F statistic*	*Significance F*		*SS*	*F statistic*	*Significance F*		*SS*	*F statistic*	*Significance F*
	Regression			33.8	3.0	0.0		102.8	14.3	0.0		120.3	8.6	0.0
	Residual			13.9	1.3			16.0	0.8			67.1	1.6	
	Total			47.7				118.8				187.4		
			Coefficients	*Standard Error*	*t Stat*	*P-value*	*Coefficients*	*Standard Error*	*t Stat*	*P-value*	*Coefficients*	*Standard Error*	*t Stat*	*P-value*
	Intercept		8.393	6.997	1.200	0.256	9.114	4.440	2.053	0.053	5.620	3.872	1.452	0.154
Eskom AC system	System Total MOI	(x_1)	-0.252	1.433	-0.176	0.863	0.040	0.867	0.046	0.964	0.690	0.807	0.855	0.397
	Stiffness	(x_2)	2.469	2.469	1.000	0.339	3.924	0.925	4.242	0.000	3.794	0.969	3.916	0.000
	Spinning reserve	(x_3) x1 GW	0.265	0.000	1.568	0.145	0.071	0.000	0.900	0.379	0.089	0.000	1.113	0.272
	Genix Load losses	(x_4) x1 GW	-0.681	0.001	-1.353	0.203	-0.872	0.000	-2.585	0.018	-0.892	0.000	-3.103	0.003
Tie-lines x1 GW	BPC load	(x_5)	1.140	0.001	0.933	0.371	1.055	0.001	1.250	0.226	0.171	0.001	0.236	0.815
	ZESA	(x_6)	-0.186	0.001	-0.124	0.903	-1.685	0.002	-1.083	0.292	1.390	0.001	1.224	0.227
	Apollo HVDC	(x_7)	-0.786	0.001	-0.910	0.382	-2.968	0.001	-4.695	0.000	-1.685	0.001	-2.889	0.006
RES x 1GW	Wind	(x_8)	-2.237	0.002	-1.256	0.235	3.540	0.001	4.475	0.000	1.894	0.001	2.076	0.044
	PV	(x_9)	-1.259	0.001	-1.037	0.322	-1.561	0.001	-2.480	0.022	-1.715	0.001	-2.618	0.012

Table 2: KZN inertia plus FPR area models

	Model		Majuba 123				Majuba 456				KZN (Majuba 123456)			
Regression Statistics	Multiple R		1.000				0.882				0.730			
	R Square		1.000				0.779				0.533			
	Adjusted R Square		0.999				0.281				0.271			
	Standard Error		0.050				1.967				1.696			
	Observations		12.000				14.000				26.000			
ANOVA				*SS*		*F statistic*	*Significance F*		*SS*		*F statistic*	*Significance F*		*SS*		*F statistic*	*Significance F*
	Regression			28.5		1260.9	0.0		54.5		1.6	0.4		52.6		2.0	0.1
	Residual			0.0		0.0			15.5		3.9			46.0		2.9	
	Total			28.5					69.9					98.6			
			Coefficients	*Standard Error*		*t Stat*	*P-value*	*Coefficients*	*Standard Error*		*t Stat*	*P-value*	*Coefficients*	*Standard Error*		*t Stat*	*P-value*
	Intercept		6.514	0.580		11.228	0.008	-20.650	43.809		-0.471	0.662	6.628	11.743		0.564	0.580
Eskom AC system	System Total MOI	(x_1)	1.605	0.195		8.223	0.014	4.796	9.876		0.486	0.653	1.027	2.746		0.374	0.713
	Stiffness	(x_2)	31.173	0.575		54.207	0.000	73.576	34.086		2.159	0.097	16.743	9.286		1.803	0.090
	Spinning reserve	(x_3) x1 GW	-1.084	0.000		-40.988	0.001	1.227	0.001		1.810	0.144	-0.170	0.000		-0.757	0.460
	Genix Load losses	(x_4) x1 GW	-0.453	0.000		-9.871	0.010	2.890	0.002		1.504	0.207	-0.383	0.000		-0.767	0.455
Tie-lines x1 GW	BPC load	(x_5)	4.451	0.000		17.599	0.003	-6.361	0.004		-1.693	0.166	0.203	0.002		0.124	0.903
	ZESA	(x_6)	-12.835	0.001		-21.659	0.002	0.041	0.006		0.007	0.995	-0.039	0.004		-0.010	0.992
	Apollo HVDC	(x_7)	-2.393	0.000		-7.087	0.019	-9.632	0.009		-1.120	0.325	-2.220	0.004		-0.625	0.541
RES x 1GW	Wind	(x_8)	-14.114	0.000		-51.407	0.000	-21.302	0.015		-1.447	0.221	-6.599	0.004		-1.658	0.117
	PV	(x_9)	-3.329	0.000		-11.392	0.008	4.673	0.004		1.123	0.324	-2.339	0.002		-1.377	0.187

Table 3: North area inertia plus FPR models

Model	Arnot				Kendal				Kriel			
Multiple R	0.952				0.892				0.837			
R Square	0.907				0.796				0.700			
Adjusted R Square	0.740				0.336				0.363			
Standard Error	1.553				1.387				0.988			
Observations	15.000				14.000				18.000			
		SS	*F statistic*	*Significance F*		*SS*	*F statistic*	*Significance F*		*SS*	*F statistic*	*Significance F*
Regression		117.5	5.4	0.0		30.0	1.7	0.3		18.3	2.1	0.2
Residual		12.1	2.4			7.7	1.9			7.8	1.0	
Total		129.6				37.7				26.1		
	Coefficients	*Standard Error*	*t Stat*	*P-value*	*Coefficients*	*Standard Error*	*t Stat*	*P-value*	*Coefficients*	*Standard Error*	*t Stat*	*P-value*
Intercept	-20.293	15.236	-1.332	0.240	4.283	10.847	0.395	0.713	-0.249	12.299	-0.020	0.984
System Total MOI (x_1)	8.754	2.925	2.993	0.030	-0.166	2.246	-0.074	0.945	0.907	2.743	0.331	0.749
Stiffness (x_2)	16.740	21.603	0.775	0.473	7.055	4.967	1.420	0.229	19.728	7.385	2.671	0.028
Spinning reserve (x_3) x1 GW	-0.274	0.000	-0.730	0.498	-0.080	0.000	-0.265	0.804	0.069	0.000	0.408	0.694
Genix Load losses (x_4) x1 GW	-0.157	0.001	-0.260	0.805	0.738	0.001	1.038	0.358	-0.227	0.000	-0.743	0.479
BPC load (x_5)	8.825	0.004	2.108	0.089	1.600	0.002	1.016	0.367	0.513	0.001	0.554	0.595
ZESA (x_6)	9.379	0.005	1.841	0.125	-1.583	0.004	-0.402	0.708	1.175	0.002	0.676	0.518
Apollo HVDC (x_7)	-6.700	0.002	-2.752	0.040	0.214	0.004	0.055	0.959	-0.503	0.001	-0.522	0.616
Wind (x_8)	-1.177	0.004	-0.287	0.786	2.985	0.003	1.141	0.317	1.205	0.002	0.667	0.523
PV (x_9)	-2.376	0.002	-1.253	0.266	-1.509	0.002	-0.867	0.435	-0.073	0.001	-0.092	0.929

Table 4: Matla inertia plus FPR model

Model	Matla 1234				Matla 56				Matla all			
Multiple R	0.941				0.995				0.693			
R Square	0.886				0.990				0.481			
Adjusted R Square	0.628				0.904				0.169			
Standard Error	1.679				0.564				2.270			
Observations	14.000				11.000				25.000			
		SS	*F statistic*	*Significance F*		*SS*	*F statistic*	*Significance F*		*SS*	*F statistic*	*Significance F*
Regression		87.3	3.4	0.1		32.7	11.4	0.2		71.5	1.5	0.2
Residual		11.3	2.8			0.3	0.3			77.3	5.2	
Total		98.6				33.0				148.8		
	Coefficients	*Standard Error*	*t Stat*	*P-value*	*Coefficients*	*Standard Error*	*t Stat*	*P-value*	*Coefficients*	*Standard Error*	*t Stat*	*P-value*
Intercept	39.432	21.008	1.877	0.134	59.999	65.187	0.920	0.526	-3.536	15.213	-0.232	0.819
System Total MOI (x_1)	-8.872	5.360	-1.655	0.173	-11.465	13.411	-0.855	0.550	1.509	3.222	0.468	0.646
Stiffness (x_2)	-77.066	32.602	-2.364	0.077	-6.085	29.091	-0.209	0.869	21.684	13.405	1.618	0.127
Spinning reserve (x_3) x1 GW	0.418	0.000	0.948	0.397	0.633	0.000	3.713	0.167	-0.041	0.000	-0.146	0.886
Genix Load losses (x_4) x1 GW	2.035	0.001	1.929	0.126	-0.993	0.001	-0.869	0.545	1.279	0.001	1.412	0.178
BPC load (x_5)	-4.583	0.003	-1.528	0.201	-1.870	0.002	-0.818	0.564	-4.016	0.002	-2.026	0.061
ZESA (x_6)	0.112	0.004	0.029	0.978	7.319	0.009	0.825	0.561	4.053	0.003	1.535	0.146
Apollo HVDC (x_7)	3.554	0.004	0.945	0.398	-1.642	0.002	-0.903	0.532	-2.545	0.003	-0.990	0.338
Wind (x_8)	5.834	0.003	2.132	0.100	-6.125	0.006	-0.957	0.514	3.654	0.003	1.323	0.206
PV (x_9)	8.987	0.004	2.367	0.077	-1.330	0.001	-0.990	0.503	0.424	0.002	0.259	0.799

Table 5: Central area inertia plus FPR models

Model		Apollo				Lethabo				Duvha			
Multiple R		0.822				0.982				0.879			
R Square		0.676				0.965				0.772			
Adjusted R Square		0.092				0.912				0.516			
Standard Error		3.737				0.658				0.928			
Observations		15.000				16.000				18.000			
			SS	*F statistic*	*Significance F*		*SS*	*F statistic*	*Significance F*		*SS*	*F statistic*	*Significance F*
Regression			145.5	1.2	0.5		71.1	18.2	0.0		23.4	3.0	0.1
Residual			69.8	14.0			2.6	0.4			6.9	0.9	
Total			215.4				73.7				30.2		
		Coefficients	*Standard Error*	*t Stat*	*P-value*	*Coefficients*	*Standard Error*	*t Stat*	*P-value*	*Coefficients*	*Standard Error*	*t Stat*	*P-value*
Intercept		43.095	55.169	0.781	0.470	21.289	7.592	2.804	0.031	-15.944	12.473	-1.278	0.237
System Total MOI	(x_1)	-19.370	14.193	-1.365	0.231	-1.521	1.949	-0.780	0.465	4.458	2.848	1.565	0.156
Stiffness	(x_2)	61.221	38.105	1.607	0.169	2.538	5.714	0.444	0.673	37.215	9.276	4.012	0.004
Spinning reserve	(x_3) x1 GW	1.029	0.001	1.048	0.343	0.815	0.000	2.665	0.037	0.141	0.000	1.517	0.168
Genix Load losses	(x_4) x1 GW	-2.237	0.001	-1.825	0.128	-2.151	0.000	-4.411	0.005	-0.413	0.000	-1.543	0.162
BPC load	(x_5)	47.549	0.023	2.048	0.096	-2.974	0.002	-1.447	0.198	-0.441	0.001	-0.498	0.632
ZESA	(x_6)	17.126	0.010	1.698	0.150	13.999	0.003	4.211	0.006	1.609	0.003	0.519	0.618
Apollo HVDC	(x_7)	-48.670	0.026	-1.887	0.118	-5.640	0.002	-2.268	0.064	-1.930	0.001	-1.990	0.082
Wind	(x_8)	10.510	0.008	1.267	0.261	4.039	0.002	1.781	0.125	0.986	0.003	0.387	0.709
PV	(x_9)	7.123	0.005	1.414	0.216	3.870	0.001	5.134	0.002	-1.794	0.001	-2.333	0.048

Table 6: Tutuka inertia plus FPR model

	Model		Tutuka			
Regression Statistics	Multiple R		0.882			
	R Square		0.777			
	Adjusted R Square		0.644			
	Standard Error		2.329			
	Observations		25.000			
ANOVA				*SS*	*F statistic*	*Significance F*
	Regression			284.0	5.8	0.0
	Residual			81.4	5.4	
	Total			365.4		
			Coefficients	*Standard Error*	*t Stat*	*P-value*
	Intercept		2.421	13.287	0.182	0.858
Eskom AC system	System Total MOI	(x_1)	1.090	2.827	0.386	0.705
	Stiffness	(x_2)	57.281	12.213	4.690	0.000
	Spinning reserve	(x_3) x1 GW	0.556	0.000	3.157	0.007
	Genix Load losses	(x_4) x1 GW	-0.752	0.001	-1.362	0.193
Tie-lines x1 GW	BPC load	(x_5)	-1.116	0.002	-0.476	0.641
	ZESA	(x_6)	15.565	0.003	4.608	0.000
	Apollo HVDC	(x_7)	-8.742	0.003	-2.851	0.012
RES x 1GW	Wind	(x_8)	0.427	0.005	0.082	0.936
	PV	(x_9)	4.111	0.001	2.745	0.015

APPENDIX B: Inertia plus FPR model validation results - 2014-2017

System Frequency nadir error		date/time	Generator incident	Change in power	Calculated H from swing eq.	fstart	fnadir predicted	Best Predicted by
EMS	PMU	Yy/mm/dd hh:mm		MW	s	Hz	Hz	model
0.24%	0.00%	2015/07/27 14:11	Duvha 5	135.2	1.14730	50.0167	49.7996	Kendal
0.60%	0.01%	2016/05/17 04:06	Grootvlei 2	112.1	0.59914	49.9035	49.8033	Duvha
0.36%	0.03%	2016/09/23 15:32	Kriel 6	310.1	0.34877	50.0335	49.7254	Majuba
0.26%	0.05%	2016/01/24 02:00	Kriel 3	187.3	0.57199	49.9645	49.7883	Medupi
0.28%	0.05%	2017/02/22 03:26	Matla 3	304.8	0.47549	49.9308	49.6992	Matimba
1.15%	0.08%	2015/02/21 01:56	Majuba 5	383	0.46834	49.9660	49.6807	Kriel
0.02%	0.12%	2015/08/30 04:28	Medupi 6	310	0.81061	50.1126	49.7721	Kriel
0.96%	0.13%	2016/05/25 21:53	Lethabo 2	268.4	0.35232	49.9102	49.7347	Kriel
0.51%	0.14%	2016/04/23 15:22	Camden 6	143.4	0.41336	50.0230	49.7977	Matimba
0.67%	0.14%	2015/09/19 00:07	Duvha 2	425	0.72382	50.0063	49.6963	Tutuka
0.26%	0.15%	2015/03/07 05:42	Matimba 5	216.5	0.56729	49.8823	49.7079	Kriel
0.68%	0.16%	2015/10/01 18:17	Duvha 2	80.9	0.18467	49.9409	49.9039	Apollo
2.81%	0.16%	2015/01/26 21:03	Majuba 6	124.2	0.34014	49.8388	49.6460	Lephalale
0.78%	0.18%	2015/10/18 02:03	Kriel 3	276.3	0.46777	50.0606	49.7790	Matimba
1.76%	0.18%	2016/06/10 13:15	Majuba 1	271.2	0.28400	49.9360	49.7538	Medupi
2.05%	0.19%	2016/08/24 11:00	Tutuka 5	460.4	0.41660	49.9978	49.6789	Medupi
1.79%	0.20%	2014/11/14 04:53	Matla 1	321.3	0.73710	50.0434	49.7533	Kendal
1.73%	0.23%	2016/07/12 12:53	Duvha 6	464.5	0.36850	50.0651	49.7476	Kriel
2.98%	0.24%	2016/07/18 08:59	Matla 4	351	0.23616	49.9707	49.6684	Matimba
0.37%	0.25%	2016/09/03 17:51	Grootvlei 3	116.9	0.23699	49.8987	49.7873	Arnot
3.63%	0.28%	2014/10/13 19:08	Tutuka 2	492.7	0.85904	50.0791	49.6985	Tutuka
2.10%	0.28%	2016/09/30 13:12	Medupi 5	429.2	0.87239	50.1343	49.7458	Tutuka
2.46%	0.28%	2015/10/09 09:27	Camden 5	139.9	0.48275	49.8778	49.7793	Kriel
1.65%	0.29%	2016/12/07 04:44	Matla 5	238.9	0.45252	49.8757	49.6599	Matimba
1.14%	0.30%	2014/11/19 23:45	Majuba 6	387.3	0.84386	50.0496	49.7240	Matimba
0.01%	0.30%	2015/08/28 23:47	Majuba 4	346.7	0.92813	50. 22	49.7859	N/A
0.01%	0.30%	2015/08/28 23:47	Majuba 4	346.7	0.92813	50. 22	49.7859	N/A
7.76%	0.31%	2015/12/22 02:22	Kriel 1	267.9	0.44446	49.9671	49.6825	Matimba
0.66%	0.31%	2014/11/12 14:05	Grootvlei 4	140.4	0.59547	49.8592	49.7410	Kriel
1.47%	0.31%	2016/07/06 15:32	Duvha 6	393.6	0.30589	50.0153	49.6713	Kriel
1.47%	0.31%	2016/07/06 15:33	Duvha 6	393.6	0.30589	50.0153	49.6713	Kriel
2.22%	0.37%	2016/04/19 21:46	Medupi 6	722.9	1.00037	50.1649	49.6719	Lephalale
2.37%	0.37%	2015/08/12 11:12	Medupi 6	472	0.52341	50.0079	49.6579	Lethabo
0.89%	0.42%	2014/11/06 11:31	Majuba 5	151.4	0.52273	49.9622	49.8098	Majuba
2.46%	0.44%	2015/10/09 09:27	Camden 5	139.9	0.48275	49.8778	49.7793	Kriel
0.83%	0.47%	2015/06/27 12:22	Duvha 6	333.7	0.55268	49.9116	49.6881	Lethabo
1.17%	0.47%	2015/07/05 23:00	Tutuka 1	135.6	0.69288	49.9769	49.8151	Duvha
0.69%	0.49%	2015/12/10 06:40	Koeberg 2	353.4	0.56636	50.0633	49.7798	Kriel
2.95%	0.51%	2015/12/02 05:35	Duvha 1	357.4	0.61165	49.8076	49.6265	Apollo
0.91%	0.54%	2016/07/18 08:59	Matla 4	397.6	0.26752	49.9707	49.6684	Kriel

0.71%	0.54%	2015/08/30 01:09	Medupi 6	401	1.84385	50.2510	50.0418	Matla
2.00%	0.54%	2014/07/23 11:38	Duvha 1	184.9	0.18139	49.8985	49.7964	Kriel
1.32%	0.55%	2015/02/22 23:29	Kriel 1	201.3	1.23737	50.0923	49.8329	Kendal
1.02%	0.56%	2017/02/17 01:41	Medupi 5	130.3	1.43671	50.1633	50.0356	Matimba
2.44%	0.58%	2015/10/18 21:40	Matla 5	149.9	0.45705	50.1209	49.9607	Kriel
1.58%	0.59%	2015/10/28 15:00	Duvha 6	468	0.44352	49.9510	49.6501	Apollo
1.48%	0.60%	2017/03/13 13:38	Medupi 5	118.2	0.62124	49.9938	49.8273	Matimba
4.47%	0.62%	2015/08/30 01:09	Medupi 6	401	1.84385	50.2510	50.0418	Tutuka
3.20%	0.63%	2015/10/24 00:26	Lethabo 6	289.7	0.29448	49.9868	49.7064	Apollo
2.44%	0.63%	2016/05/20 05:37	Medupi 6	241.4	0.50306	49.8125	49.6715	Duvha
0.17%	0.65%	2016/09/30 11:50	Majuba 6	310.5	0.43713	50.1041	49.8000	Medupi
0.81%	0.65%	2016/05/25 07:11	Kriel 4	401	0.37822	50.0251	49.7143	Lephalale
0.95%	0.66%	2017/03/12 11:29	Medupi 6	98.3	0.47435	49.9332	49.8041	Medupi
1.24%	0.69%	2015/11/14 14:00	Camden 3	89.6	0.26164	49.9134	49.8061	Kriel
3.44%	0.70%	2016/02/17 13:24	Matimba 6	251.6	0.27786	49.8586	49.7446	Apollo
1.77%	0.71%	2015/07/09 15:46	Tutuka 4	336.8	0.49118	49.8806	49.6680	Apollo
15.56%	0.73%	2015/12/02 18:49	Kriel 6	141.9	0.20669	49.9854	49.6995	Medupi
0.71%	0.73%	2014/11/12 03:16	Majuba 6	240.4	0.66848	50.0441	49.7828	Lephalale
1.30%	0.75%	2014/11/20 06:14	Majuba 6	112.3	0.76138	49.9568	49.8240	Lephalale
0.12%	0.77%	2017/02/23 13:34	Medupi 5	385.4	1.39007	50.0331	49.7082	Kendal
3.96%	0.77%	2014/08/28 11:06	Matla 6	366	0.66828	50.0035	49.7465	Tutuka
1.86%	0.77%	2016/12/15 11:45	Hendrina 6	121	0.41814	50.0550	49.8796	Kriel
0.75%	0.83%	2016/10/13 15:43	Kriel 2	207.9	0.47950	50.0032	49.8237	Kriel
5.37%	0.85%	2016/07/22 19:05	Lethabo 2	522.7	0.37459	50.1187	49.7059	Tutuka
0.69%	0.85%	2016/12/16 14:23	Medupi 6	228.6	0.67252	49.8970	49.6677	Kriel
5.32%	0.86%	2015/07/20 14:13	Tutuka 4	226.1	1.95431	49.8972	49.7406	Matla
1.49%	0.87%	2016/01/03 01:58	Duvha 1	109.3	0.56213	50.0377	49.9407	Matimba
3.78%	0.87%	2014/11/23 04:36	Matla 2	364.8	0.94370	50.0136	49.7474	Tutuka
2.83%	0.88%	2015/12/04 00:40	Kriel 3	378.4	0.40370	49.8671	49.6775	Majuba
3.40%	0.88%	2015/11/04 06:53	Duvha 1	131.6	0.32552	49.9673	49.7912	Duvha
0.19%	0.89%	2016/05/10 00:20	Kriel 4	294.1	0.62221	49.9496	49.7090	Matimba
0.13%	0.92%	2016/01/26 03:50	Majuba 2	516.4	0.70636	50.0896	49.6904	Tutuka
0.66%	0.92%	2015/09/02 01:25	Medupi 6	459	1.42635	50.0986	49.7328	Matimba
4.21%	0.93%	2016/02/23 18:17	Duvha 4	260	0.47376	49.9842	49.7979	Lethabo
2.44%	0.93%	2016/08/25 15:14	Matla 6	230.3	0.21110	49.9642	49.7107	Matimba
6.00%	0.94%	2015/08/21 16:07	Matimba 2	276.3	1.10808	49.9809	49.7332	Matla
1.20%	0.95%	2016/07/09 09:25	Majuba 3	385.4	0.28091	50.0160	49.6701	Matimba
0.52%	0.95%	2015/09/28 21:19	Kendal 1	605.8	0.57175	50.0990	49.6983	Apollo
0.90%	0.96%	2015/09/29 14:48	Duvha 5	140.2	0.13358	49.9542	49.7382	Duvha
0.01%	0.97%	2015/01/24 16:41	Duvha 2	133.4	0.78947	50.1792	50.0087	Tutuka
1.18%	0.98%	2015/12/03 09:36	Kriel 4	214.9	0.67274	49.8027	49.6668	Majuba
0.70%	0.99%	2015/10/07 07:14	Lethabo 3	205.1	0.40084	50.1051	49.8788	Lethabo
5.61%	1.01%	2015/01/01 19:34	Matla 5	186.8	0.53282	50.0366	49.7796	Matla
8.26%	1.03%	2017/03/17 16:54	Kendal 3	210.5	0.23182	49.8967	49.7558	Tutuka
0.18%	1.04%	2014/08/26 02:06	Tutuka 6	264.4	0.98486	50.0539	49.8382	Lephalale

1.96%	1.11%	2015/12/05 16:12	Kriel 2	251	0.41987	50.0665	49.7836	Tutuka
1.62%	1.14%	2015/06/10 13:57	Medupi 6	296.4	0.39503	49.9465	49.7327	Majuba
0.75%	1.14%	2015/06/11 01:46	Kriel 4	394	0.53322	49.9681	49.7000	Kriel
1.51%	1.18%	2015/10/24 00:26	Lethabo 6	289.7	0.29448	49.9868	49.7064	Lephalale
0.12%	1.19%	2016/08/16 09:49	Lethabo 5	444.7	0.38991	50.0831	49.7166	Lephalale
1.41%	1.19%	2016/04/22 00:39	Medupi 6	444	1.02540	50.1227	49.7115	Matla
0.65%	1.20%	2015/11/14 14:00	Camden 3	89.6	0.26164	49.9134	49.8061	Kriel
0.97%	1.24%	2016/10/25 03:49	Kriel 3	208.9	0.29040	49.9119	49.7006	Lephalale
0.90%	1.24%	2014/08/25 08:09	Matla 4	246.7	0.79713	49.9996	49.8013	Duvha
4.43%	1.25%	2016/01/02 05:15	Duvha 6	222.9	0.54552	49.9679	49.7986	Matimba
4.86%	1.28%	2016/10/14 04:40	Matimba 4	283	0.54842	49.9884	49.7121	Matimba
3.44%	1.32%	2015/01/16 10:30	Matla 4	389.3	1.34297	49.8906	49.6701	Apollo
0.79%	1.34%	2014/11/22 20:48	Kriel 1	95.2	0.54392	50.0246	49.8704	Tutuka
2.30%	1.36%	2016/07/16 08:44	Majuba 3	436.9	0.36894	50.0068	49.6678	Lethabo
0.57%	1.37%	2016/02/09 15:13	Tutuka 1	112.5	0.33041	49.9673	49.8276	Lethabo
1.98%	1.37%	2014/11/13 12:16	Majuba 3	243.6	1.01889	49.9167	49.7247	Duvha
2.08%	1.38%	2015/06/11 01:01	Kriel 1	170.8	0.92473	50.0384	49.8529	Matimba
1.78%	1.42%	2016/04/18 03:29	Medupi 6	229.1	1.06754	49.8729	49.6952	Matimba
0.55%	1.43%	2015/10/20 01:52	Duvha 1	294.8	0.45608	50.0208	49.7827	Matla
2.30%	1.45%	2016/07/16 08:44	Majuba 3	436.9	0.36894	50.0068	49.6678	Lethabo
5.53%	1.46%	2016/07/22 19:18	Lethabo 4	557.2	0.32606	50.0498	49.6741	Matimba
0.24%	1.46%	2017/02/22 08:00	Duvha 2	134.7	0.42935	49.8658	49.7659	Tutuka
1.56%	1.46%	2015/08/30 04:28	Medupi 6	310	0.81061	50.1126	49.7721	Kriel
4.40%	1.47%	2015/12/29 18:01	Matimba 4	432.2	0.54040	50.1075	49.7168	Medupi
5.49%	1.47%	2016/12/03 21:37	Hendrina 8	120.5	0.46227	50.0744	49.9147	Matimba
1.22%	1.48%	2016/05/18 11:37	Kriel 3	374.4	0.29000	49.9825	49.6929	Lephalale
0.43%	1.48%	2016/11/23 05:16	Kendal 3	254.7	0.20126	49.9289	49.6756	Lephalale
2.98%	1.48%	2016/07/12 12:53	Duvha 6	464.5	0.36850	50.0651	49.7476	Kriel
0.34%	1.51%	2016/07/09 09:25	Majuba 3	385.4	0.28091	50.0160	49.6701	Lethabo
0.57%	1.55%	2016/12/07 02:08	Lethabo 6	211.9	0.62717	49.7946	49.6629	Tutuka
0.87%	1.56%	2014/10/22 12:23	Lethabo 4	476.7	0.88616	50.1375	49.7150	Matimba
0.67%	1.58%	2015/09/19 00:07	Duvha 2	425	0.72382	50.0063	49.6963	Medupi
2.44%	1.58%	2017/03/02 10:12	Tutuka 3	285.9	1.53453	49.8049	49.6790	Apollo
4.39%	1.59%	2016/05/23 22:57	Matla 4	395.3	0.46072	50.1228	49.7587	Kendal
2.46%	1.61%	2016/07/24 18:35	Tutuka 2	410.8	0.37829	50.0055	49.6713	Tutuka
2.47%	1.62%	2016/07/24 18:35	Tutuka 2	410.8	0.37829	50.0055	49.6713	Tutuka
0.05%	1.63%	2015/12/23 22:38	Kriel 5	202	0.52474	49.9844	49.8236	Majuba
1.95%	1.66%	2017/03/21 07:04	Grootvlei 5	129.6	-0.00210	49.9805	49.8288	Kendal
0.16%	1.66%	2014/07/01 22:34	Grootvlei 6	130.1	0.87086	49.8629	49.7917	Lethabo
1.56%	1.67%	2015/10/18 02:03	Kriel 3	276.3	0.46777	50.0606	49.7790	Matimba
0.66%	1.68%	2014/11/23 08:31	Kriel 1	122.6	0.85435	49.8526	49.7643	Kriel
5.49%	1.72%	2015/10/15 20:49	Kendal 5	240.8	0.27108	50.1110	49.7451	Matimba
2.76%	1.77%	2014/10/15 10:38	Matimba 6	358.4	0.45051	49.9006	49.6855	Kriel
2.84%	1.78%	2016/08/25 15:14	Matla 6	310.9	0.28587	49.9642	49.7107	Kendal
1.58%	1.83%	2015/01/29 21:24	Kendal 6	409.8	0.48310	50.1630	49.7900	Lethabo

3.25%	1.84%	2016/05/06 07:12	Camden 6	155.7	0.33987	50.0101	49.8031	Lethabo
1.53%	1.85%	2016/02/22 16:09	Majuba 1	118.5	0.17202	49.8331	49.7480	Lethabo
2.83%	1.88%	2016/01/24 22:22	Majuba 1	227.7	0.49129	49.9620	49.7222	Lephalale
3.19%	1.89%	2015/10/14 17:02	Kriel 6	240.8	0.56691	50.0932	49.9486	Duvha
1.80%	1.90%	2015/07/19 02:02	Kriel 2	222.1	0.56506	49.8745	49.7689	Matla
0.69%	1.90%	2017/03/12 23:50	Medupi 6	230	0.74520	49.9633	49.7672	Lephalale
3.66%	1.91%	2016/02/27 23:13	Majuba 6	249.5	0.51148	49.8723	49.7667	Apollo
1.02%	1.93%	2014/10/22 22:36	Tutuka 1	204.2	0.49922	50.0481	49.8229	Kendal
6.35%	2.09%	2017/03/01 14:51	Kusile 1	185.8	0.63399	50.0400	49.7998	Matimba
1.04%	2.12%	2015/03/18 14:55	Medupi 6	263	0.38701	49.8727	49.6673	Kriel
1.06%	2.14%	2014/11/30 09:08	Kriel 6	435.3	0.72167	50.0374	49.7320	Medupi
0.78%	2.14%	2014/09/10 17:48	Majuba 4	503.5	0.96593	50.1365	49.7732	Lephalale
6.98%	2.16%	2016/08/23 09:42	Kendal 6	237.9	0.31352	50.1715	49.9443	Matimba
5.28%	2.19%	2016/08/12 18:42	Lethabo 3	496.1	0.63571	50.0222	49.6547	Tutuka
1.77%	2.21%	2015/02/07 00:04	Kriel 1	176.9	0.81636	50.0224	49.7884	Kendal
1.74%	2.23%	2015/03/08 00:07	Tutuka 4	364.6	0.43736	50.0273	49.6715	Matimba
3.93%	2.25%	2017/02/28 13:49	Duvha 2	379.9	1.21799	49.8657	49.6789	Tutuka
4.76%	2.26%	2015/10/25 04:33	Matimba 6	301.4	1.01869	50.1181	49.7799	Kendal
2.71%	2.30%	2014/07/23 15:03	Majuba 5	327.8	0.80903	49.8613	49.6770	Kriel
2.43%	2.31%	2015/06/17 02:41	Kriel 3	307.9	0.61292	50.0704	49.7909	Kendal
0.87%	2.37%	2015/09/29 14:48	Duvha 5	385.1	0.37847	49.9542	49.7382	Majuba
1.09%	2.40%	2017/02/03 13:53	Kusile 1	480.5	1.07208	49.8604	49.6531	Apollo
2.66%	2.45%	2016/10/11 17:00	Kendal 1	639.4	0.47908	50.1607	49.7052	Lephalale
2.16%	2.45%	2016/08/11 09:43	Majuba 6	462.3	1.71114	50.1434	49.7035	Kendal
2.19%	2.46%	2017/02/25 10:00	Medupi 5	725.6	##########	50.2701	49.8314	Lephalale
7.10%	2.50%	2015/01/07 09:48	Tutuka 3	223.9	0.61030	50.0316	49.7364	Matimba
7.64%	2.50%	2015/10/06 08:58	Tutuka 6	420.4	0.32929	49.9265	49.7073	Apollo
1.33%	2.53%	2017/02/18 00:10	Majuba 2	199.4	1.35797	50.1302	49.9242	Arnot
0.01%	2.56%	2015/12/05 02:16	Majuba 6	124.9	0.47099	49.9357	49.7955	Tutuka
1.49%	2.62%	2016/06/17 12:30	Tutuka 4	442.2	6.36446	50.0020	49.7253	Kriel
2.35%	2.65%	2015/07/10 10:38	Duvha 4	203.7	0.79481	50.0137	49.8095	Tutuka
0.30%	2.66%	2015/10/12 10:06	Tutuka 1	412.5	0.47122	50.1775	49.7957	Kendal
5.11%	2.72%	2014/11/19 12:13	Kriel 4	259.1	1.47129	50.1131	49.8186	Tutuka
2.70%	2.73%	2016/10/05 08:02	Medupi 5	279.2	0.68107	50.0005	49.7003	Arnot
1.99%	2.76%	2015/12/09 16:47	Tutuka 5	440.8	0.53301	50.0974	49.8046	Arnot
5.69%	2.76%	2016/02/27 14:14	Matimba 4	295.7	0.67374	49.8686	49.7256	Duvha
4.62%	2.77%	2017/03/10 15:46	Kriel 5	250.1	0.71679	49.9826	49.7518	Lephalale
3.97%	2.78%	2015/01/02 08:57	Hendrina 1	151.1	0.80496	49.8792	49.7291	Tutuka
0.21%	2.78%	2017/02/17 06:06	Matla 5	328.5	0.57057	49.9709	49.7458	Medupi
13.10%	2.84%	2015/10/11 18:19	Tutuka 1	147.4	0.19306	50.1016	49.8130	Lethabo
0.43%	2.85%	2015/02/10 19:15	Majuba 6	446.6	0.66348	50.1345	49.7081	Kendal
14.75%	2.85%	2015/06/19 06:03	Duvha 6	394.9	1.18878	50.1889	49.8505	Kriel
10.00%	2.89%	2014/07/07 12:14	Kendal 3	533.5	0.44762	50.1593	49.7698	Tutuka
7.14%	2.91%	2016/12/20 20:34	Lethabo 3	454.7	0.43918	50.0782	49.7068	Tutuka
2.40%	2.95%	2015/12/12 05:39	Tutuka 3	427.6	0.67759	50.0058	49.7431	Majuba

1.34%	3.12%	2016/10/13 07:30	Majuba 2	429.1	0.44548	50.1756	49.8084	Matimba
0.81%	3.16%	2015/10/07 07:14	Lethabo 3	205.1	0.40084	50.1051	49.8788	Matimba
1.80%	3.18%	2016/06/17 02:37	Medupi 6	342.2	0.75591	50.0577	49.6908	Matla
4.35%	3.20%	2014/08/22 03:22	Matla 5	297.8	0.91590	50.0410	49.7568	Lephalale
0.89%	3.21%	2017/03/23 15:57	Duvha 1	264.9	0.38013	49.9429	49.7645	Medupi
2.19%	3.21%	2014/11/15 16:41	Duvha 2	266.7	0.53853	49.9567	49.7507	Lethabo
3.61%	3.28%	2017/03/17 09:30	Kriel 3	97.2	0.54000	49.9745	49.8207	Matimba
2.06%	3.28%	2014/11/20 11:28	Hendrina 10	154.4	0.97662	49.9042	49.7981	Kriel
3.86%	3.32%	2014/07/29 17:54	Kendal 5	234	0.64082	49.8257	49.6835	Kriel
1.64%	3.38%	2015/10/25 04:33	Matimba 6	301.4	0.50934	50.1181	49.7799	Lephalale
2.24%	3.41%	2016/12/15 17:33	Medupi 5	468.6	0.47077	50.1148	49.7338	Kendal
6.53%	3.42%	2016/01/29 03:39	Medupi 6	165.3	0.59649	49.9693	49.8205	Matimba
1.07%	3.48%	2015/10/18 21:40	Matla 5	149.9	0.45705	50.1209	49.9607	Kriel
9.31%	3.60%	2016/05/19 18:53	Kriel 6	357.3	0.33346	50.0022	49.7009	Lephalale
6.71%	3.64%	2015/08/11 07:46	Medupi 6	472	0.86748	49.8647	49.6305	Apollo
2.30%	3.68%	2015/02/07 15:28	Duvha 6	351.8	0.40667	50.0361	49.7412	Kendal
6.54%	3.70%	2017/03/03 04:29	Duvha 2	379	0.72630	50.1050	49.7533	Matimba
0.32%	3.74%	2015/10/20 01:52	Duvha 1	294.8	0.45608	50.0208	49.7827	Matla
8.22%	3.90%	2015/11/16 15:59	Kriel 4	355.4	0.65242	49.8986	49.7059	Majuba
0.45%	3.91%	2014/09/08 15:45	Majuba 5	279.5	0.30848	49.9110	49.7025	Majuba
5.33%	3.92%	2015/06/14 23:11	Matimba 2	462.5	0.82554	50.1792	49.7662	Kriel
1.43%	3.96%	2016/07/24 00:46	Tutuka 1	390.1	0.59599	50.1342	49.7985	Matla
3.57%	3.96%	2016/04/09 15:00	Matimba 5	464.9	0.00000	50.0967	49.6684	Kriel
4.22%	3.98%	2016/02/19 21:46	Medupi 6	412.2	0.47954	50.1248	49.7160	Matla
3.81%	4.08%	2016/05/18 22:32	Grootvlei 2	139.6	0.45952	50.1891	50.0079	Tutuka
0.68%	4.09%	2016/01/04 14:16	Duvha 1	452.6	0.61276	49.9121	49.6813	Apollo
0.84%	4.09%	2016/07/19 08:06	Majuba 2	184.9	0.36623	49.8462	49.7618	Apollo
4.34%	4.11%	2015/10/07 09:53	Matla 2	481.8	0.44900	49.9958	49.6890	Kriel
5.53%	4.16%	2015/10/12 10:06	Tutuka 1	412.5	0.47122	50.1775	49.7957	Lethabo
5.81%	4.18%	2016/10/16 15:23	Matimba 5	110.8	0.34290	50.0643	49.8462	Kriel
0.41%	4.19%	2015/07/12 23:08	Duvha 4	260.8	0.60985	50.1978	50.0008	Kriel
0.73%	4.20%	2016/08/20 09:13	Grootvlei 4	132.6	0.09304	49.9312	49.9110	Apollo
1.52%	4.23%	2015/07/05 17:56	Duvha 5	434.2	0.60491	50.0658	49.6528	Medupi
4.78%	4.25%	2015/01/28 01:02	Lethabo 2	452.6	0.90314	50.0675	49.6848	Medupi
2.11%	4.26%	2016/05/11 18:18	Grootvlei 3	111.4	0.30595	49.8271	49.7377	Kriel
5.64%	4.26%	2017/03/11 22:43	Kusile 1	291.4	1.17712	49.8375	49.6701	Tutuka
3.13%	4.27%	2015/08/21 11:55	Matimba 2	329	1.09543	49.8367	49.5710	Matimba
1.51%	4.31%	2014/07/28 23:13	Duvha 4	254.9	0.58035	50.0269	49.7682	Lephalale
0.08%	4.31%	2014/08/06 09:54	Matimba 1	490.9	0.48519	50.1657	49.7873	Tutuka
2.40%	4.33%	2014/07/31 22:54	Kriel 5	209.8	0.81158	49.9093	49.7547	Matimba
1.82%	4.40%	2014/08/07 22:13	Kriel 2	365.4	0.73408	49.9823	49.7652	Kriel
3.90%	4.43%	2016/07/22 19:05	Lethabo 2	522.7	0.37459	50.1187	49.7059	Matimba
2.97%	4.43%	2015/06/09 23:31	Matla 3	364.9	0.47289	50.0066	49.7439	Arnot
4.90%	4.45%	2015/03/05 14:09	Tutuka 6	353.7	0.57776	49.9652	49.6874	Lethabo
2.99%	4.50%	2015/09/02 01:25	Medupi 6	459	1.42635	50.0986	49.7328	Matla

2.20%	4.51%	2016/12/04 01:44	Matla 2	327.8	0.26569	49.9320	49.6589	Matimba
1.23%	4.73%	2015/11/03 21:07	Duvha 1	383.3	0.62539	50.0717	49.8049	Majuba
3.51%	4.80%	2015/10/19 16:53	Kriel 2	348.8	0.54300	49.8033	49.6595	Duvha
2.76%	4.83%	2016/08/30 04:33	Majuba 4	246.8	0.27608	49.9042	49.7047	Matimba
8.33%	4.88%	2015/10/21 13:56	Lethabo 3	458.5	0.51396	49.9158	49.6530	Majuba
20.14%	4.94%	2015/11/10 03:49	Medupi 6	495.5	0.64570	49.9330	49.6886	Majuba
2.05%	5.12%	2015/07/04 12:32	Duvha 6	336.8	1.27910	49.9787	49.7133	Matla
0.62%	5.23%	2014/11/16 04:41	Duvha 5	457.9	0.83123	50.0919	49.7335	Tutuka
15.99%	5.24%	2015/01/21 15:04	Tutuka 6	360	0.21212	49.7255	49.5144	Kriel
1.16%	5.28%	2016/02/18 04:46	Kendal 4	335.3	0.34266	49.9855	49.7258	Majuba
5.53%	5.35%	2016/07/22 19:18	Lethabo 4	557.2	0.32606	50.0498	49.6741	Matimba
10.83%	5.44%	2016/07/07 14:28	Matla 3	447.4	0.31047	49.9506	49.6031	Matimba
1.68%	5.51%	2014/11/19 16:38	Majuba 6	430.6	0.80766	50.0552	49.6561	Matla
1.45%	5.52%	2016/04/26 16:03	Medupi 6	528.7	0.76280	50.1395	49.6699	Medupi
4.34%	5.56%	2015/10/07 09:53	Matla 2	481.8	0.44900	49.9958	49.6890	Kriel
5.64%	5.63%	2015/08/16 11:59	Medupi 6	440.1	0.91818	49.9601	49.6701	Lethabo
6.35%	5.63%	2017/03/01 01:00	Kusile 1	420.5	0.52261	49.9143	49.6861	Apollo
3.35%	5.67%	2014/10/09 19:49	Majuba 4	167.7	0.44498	49.9127	49.7581	Kriel
0.11%	5.68%	2015/12/07 20:47	Duvha 2	103.4	0.14180	50.0358	49.7278	Medupi
1.62%	5.93%	2015/12/04 19:02	Kriel 6	186.9	0.46638	49.9478	49.7766	Duvha
4.41%	6.06%	2017/02/27 03:25	Kriel 5	204.2	0.63612	49.9598	49.7583	Kriel
5.32%	6.07%	2015/11/16 15:59	Kriel 4	355.4	0.65242	49.8986	49.7059	Majuba
2.96%	6.08%	2016/04/09 09:24	Duvha 6	284.7	0.27484	49.8581	49.6530	Medupi
2.87%	6.09%	2015/08/16 13:33	Tutuka 1	314.3	0.99720	50.1598	49.8193	Kendal
4.76%	6.11%	2015/10/19 16:53	Kriel 2	348.8	0.54300	49.8033	49.6595	Apollo
7.40%	6.26%	2016/05/06 10:02	Grootvlei 6	131.2	0.32267	50.1104	49.8961	Duvha
4.25%	6.28%	2017/03/02 06:38	Kusile 1	188.1	1.16850	50.0720	49.8472	Matimba
7.10%	6.29%	2015/11/30 09:20	Tutuka 1	433.5	0.56039	50.0294	49.6975	Kriel
3.46%	6.47%	2015/01/07 08:48	Majuba 2	331.8	0.82885	50.0964	49.7501	Kendal
3.92%	6.76%	2015/10/11 11:48	Tutuka 1	226.7	0.32227	50.0357	49.7164	Matimba
1.49%	6.80%	2016/02/17 06:25	Duvha 4	185.6	0.34530	50.1261	49.9357	Majuba
5.42%	6.92%	2016/10/13 00:58	Duvha 1	344.7	0.46865	50.0434	49.7465	Matimba
1.53%	6.93%	2015/10/31 01:17	Kendal 1	421.2	0.55613	49.9995	49.6605	Apollo
9.25%	6.94%	2015/10/06 08:58	Tutuka 6	420.4	0.32929	49.9265	49.7073	Kriel
2.82%	7.09%	2015/10/11 18:19	Tutuka 1	127.5	0.16687	50.1016	49.8130	Tutuka
5.25%	7.09%	2016/06/26 12:17	Matimba 4	301.4	0.81701	50.1340	49.8071	Matimba
2.56%	7.21%	2015/10/22 14:00	Majuba 6	215.5	0.33642	49.8468	49.7644	Apollo
3.26%	7.28%	2015/10/11 11:48	Tutuka 1	226.7	0.32227	50.0357	49.7164	Kendal
3.50%	7.31%	2016/05/21 22:31	Grootvlei 2	140.3	0.06028	50.0207	50.0110	Lethabo
6.97%	7.47%	2015/10/22 07:41	Duvha 1	350	0.32674	49.8754	49.6863	Duvha
6.79%	7.57%	2016/05/26 14:23	Lethabo 2	362.1	0.36982	49.8518	49.6923	Duvha
2.48%	7.60%	2014/09/02 15:46	Matimba 4	457.8	0.67789	50.1109	49.7553	Majuba
0.68%	7.93%	2015/12/12 05:39	Tutuka 3	427.6	0.67759	50.0058	49.7431	Majuba
5.80%	7.97%	2014/08/03 19:59	Duvha 1	168.1	0.46466	50.0110	49.8047	Matla
3.15%	7.99%	2017/03/06 01:08	Lethabo 5	229.9	1.24406	50.1119	49.8937	Medupi

1.66%	8.00%	2015/01/29 05:49	Kendal 6	153.6	0.59737	50.0704	49.8977	Kendal
15.61%	8.41%	2016/01/02 01:15	Tutuka 2	176.2	0.50022	49.9447	49.7252	Tutuka
20.76%	8.47%	2015/11/10 03:49	Medupi 6	495.5	0.64570	49.9330	49.6886	Majuba
1.70%	8.55%	2016/02/16 16:04	Duvha 4	273.5	0.33216	50.1229	49.8430	Medupi
18.00%	8.59%	2015/01/12 00:42	Grootvlei 6	94.3	0.61011	50.0346	49.8415	Medupi
8.34%	8.79%	2015/02/18 13:31	Kendal 6	472.1	0.67447	50.1600	49.7077	Lethabo
8.85%	9.00%	2016/02/16 21:17	Matimba 6	317.6	0.40403	49.8956	49.7048	Duvha
5.66%	9.03%	2017/02/15 01:49	Matimba 6	373.6	1.81045	50.0816	49.7416	Matimba
0.46%	9.03%	2015/07/17 05:42	Medupi 6	341.6	0.75940	50.0865	49.8066	Medupi
3.04%	9.08%	2016/07/24 19:20	Duvha 6	206.9	0.28813	50.1545	49.7526	Kendal
7.02%	9.29%	2016/02/10 09:52	Matimba 3	294.6	0.51261	49.8688	49.6632	Lethabo
9.33%	9.97%	2017/03/24 22:24	Matla 6	370.2	0.86862	50.0132	49.6768	Apollo
5.04%	10.31%	2016/12/14 13:18	Medupi 5	426.4	0.43721	50.1098	49.7144	Tutuka
5.90%	10.86%	2017/02/26 15:01	Matimba 1	413.3	0.21252	49.9579	49.7234	Tutuka
4.88%	10.92%	2016/10/07 10:01	Kriel 5	434.9	0.40875	49.9994	49.7077	Medupi
0.23%	10.93%	2016/08/18 15:58	Majuba 6	388	0.41315	49.9612	49.7346	Medupi
3.56%	11.19%	2015/12/22 00:53	Majuba 6	303.7	0.44485	49.8841	49.6817	Majuba
0.39%	11.31%	2015/11/17 21:58	Kendal 3	519.5	0.63378	50.1205	49.7182	Medupi
5.29%	11.47%	2015/10/22 07:41	Duvha 1	350	0.32674	49.8754	49.6863	Majuba
3.72%	11.53%	2015/10/28 15:00	Duvha 6	468	0.44352	49.9510	49.6501	Majuba
0.44%	11.60%	2014/11/07 07:09	Majuba 1	474.6	0.95045	50.1847	49.8054	Majuba
3.33%	11.73%	2015/10/21 13:56	Lethabo 3	458.5	0.51396	49.9158	49.6530	Majuba
7.63%	12.19%	2015/11/04 01:07	Matimba 2	297.9	0.60201	49.9167	49.7371	Tutuka
19.92%	12.28%	2016/02/09 10:59	Matla 5	462	0.77947	49.9562	49.7478	Duvha
6.78%	12.33%	2015/10/22 14:00	Majuba 6	215.5	0.33642	49.8468	49.7644	Duvha
0.47%	12.40%	2015/12/12 23:16	Duvha 1	432.5	0.47837	49.9220	49.6670	Medupi
7.63%	12.70%	2015/11/04 01:07	Matimba 2	297.9	0.60201	49.9167	49.7371	Duvha
3.58%	13.00%	2015/12/04 20:26	Majuba 4	420.3	0.50373	50.1176	49.7545	Kendal
2.28%	13.13%	2015/10/15 20:49	Kendal 5	523.2	0.61676	50.1110	49.7451	Majuba
5.59%	13.35%	2015/02/25 14:34	Duvha 6	364.5	0.62359	50.1550	49.8033	Lethabo
9.84%	13.45%	2015/01/17 07:42	Matimba 3	418.9	1.18218	49.9860	49.6822	Kendal
7.38%	13.83%	2016/10/08 21:56	Tutuka 2	239.4	0.55408	50.1616	49.7728	Tutuka
1.31%	13.83%	2016/11/01 17:08	Hendrina 3	174.3	0.51648	50.0746	49.8421	Lephalale
6.43%	14.23%	2015/07/24 19:54	Matla 6	419.2	0.68363	50.0400	49.7334	Lephalale
0.78%	14.54%	2015/11/03 21:07	Duvha 1	383.3	0.62539	50.0717	49.8049	Majuba
2.93%	16.96%	2015/11/04 02:16	Kriel 6	294	0.58732	49.9075	49.7241	Tutuka
1.28%	17.52%	2015/10/31 01:17	Kendal 1	421.2	0.55613	49.9995	49.6605	Medupi
21.22%	17.95%	2016/11/06 21:05	Kendal 3	145	0.22260	50.0840	49.7301	Kendal
2.40%	17.99%	2016/11/05 10:31	Kendal 6	196.4	0.35851	50.1814	49.7658	Matimba
6.10%	18.56%	2014/09/15 21:37	Matimba 1	514.6	1.08207	50.1875	49.8012	Matimba
17.53%	20.09%	2015/07/17 00:32	Apollo Cs	356.2	0.28513	50.0529	49.9524	Kendal
8.33%	20.28%	2016/07/24 19:20	Duvha 6	322.4	0.42880	50.1545	49.7526	Kendal
12.34%	21.62%	2016/02/12 20:37	Medupi 6	585.3	0.53644	50.1624	49.6966	Medupi
2.73%	22.14%	2016/02/10 12:58	Majuba 1	528.4	0.53351	50.0196	49.6707	Lethabo
0.52%	22.69%	2015/09/28 21:19	Kendal 1	605.8	0.57175	50.0990	49.6983	Kriel

22.10%	22.78%	2014/10/08 04:40	Apollo Cs	282	0.17760	50.0537	49.9396	Kendal
0.39%	23.24%	2015/11/17 21:58	Kendal 3	519.5	0.63378	50.1205	49.7182	Medupi
9.56%	23.76%	2016/02/26 06:29	Matimba 4	627.2	0.76751	50.0843	49.7350	Medupi
0.84%	24.58%	2016/02/16 11:54	Lethabo 4	520.3	0.51208	49.9442	49.6614	Kriel
5.14%	24.99%	2015/10/31 19:08	Duvha 1	473.1	0.65501	50.1496	49.8316	Majuba
31.11%	25.52%	2015/07/21 16:13	Apollo Cs	282.7	4.46537	49.9925	49.8649	Kendal
20.10%	26.24%	2016/10/07 12:28	Apollo Cs	239.4	0.06204	49.7946	49.6639	Kendal
25.42%	26.43%	2015/03/20 10:33	Arnot 5	217	0.87712	49.8854	49.7535	N/A
28.15%	27.42%	2015/10/10 02:21	Arnot 6	207.3	0.55034	49.8692	49.7325	N/A
28.15%	27.42%	2015/10/10 02:21	Arnot 6	207.3	0.55034	49.8692	49.7325	N/A
30.78%	28.69%	2015/10/12 11:09	Arnot 6	127.1	0.25421	49.9100	49.7668	N/A
30.78%	28.69%	2015/10/12 11:09	Arnot 6	127.1	0.25421	49.9100	49.7668	N/A
25.40%	29.02%	2016/11/17 18:26	Arnot 1	335.1	0.52619	49.8284	49.6838	N/A
28.48%	29.30%	2014/07/09 07:33	Arnot 3	306.3	0.56879	49.8845	49.7383	N/A
32.20%	29.67%	2015/10/23 21:24	Arnot 6	173.2	0.44136	50.0279	49.8794	N/A
32.20%	29.67%	2015/10/23 21:24	Arnot 6	173.2	0.44136	50.0279	49.8794	N/A
32.09%	32.54%	2015/10/17 23:18	Arnot 1	169.2	0.55218	50.0118	49.8490	N/A
34.30%	32.54%	2015/10/17 23:18	Arnot 1	169.2	0.55218	50.0118	49.8490	N/A
34.10%	32.58%	2014/10/03 12:30	Arnot 2	142.1	0.86757	50.0166	49.8537	N/A
32.59%	33.25%	2015/11/23 02:06	Arnot 3	234.2	0.83477	50.2038	50.0369	N/A
36.66%	33.37%	2015/06/18 00:00	Apollo Cs	198.5	0.48049	50.0242	49.8572	Kendal
21.49%	33.44%	2015/12/01 18:42	Medupi 6	603.7	0.75843	50.1100	49.6720	Kendal
35.65%	36.14%	2015/06/16 18:29	Apollo Cs	191.6	0.14009	50.0932	49.9121	Matla
38.83%	40.24%	2014/08/03 08:41	Arnot 4	205.2	1.28395	50.0379	49.8365	N/A
32.10%	40.85%	2014/10/24 11:21	Arnot 6	250	0.63171	50.0182	49.8139	N/A
46.59%	42.30%	2015/10/13 09:28	Arnot 4	204.4	0.42076	50.0795	49.8677	N/A
46.59%	42.30%	2015/10/13 09:28	Arnot 4	204.4	0.42076	50.0795	49.8677	N/A
62.34%	42.76%	2017/03/07 16:07	Apollo Cs	274.3	1.78265	50.0234	49.8095	Kendal
42.53%	43.03%	2015/02/15 04:30	Apollo Cs	208.4	0.80481	49.9734	49.7584	Matla
42.13%	43.03%	2015/07/06 14:29	Apollo Cs	236.3	0.66112	50.0521	49.8368	Kendal
43.85%	43.95%	2015/08/27 12:39	APOLLO CS	121.9	0.12622	49.9915	49.7718	Kendal
44.20%	44.17%	2015/07/08 21:44	Apollo Cs	245.2	0.67089	50.1409	49.9193	Kendal
20.91%	46.57%	2016/09/10 09:58	Arnot 2	136.1	1.37308	49.9988	49.7660	N/A
54.77%	54.59%	2014/10/23 21:41	Apollo Cs	268.6	0.49995	50.0406	49.7674	Kendal
53.76%	55.17%	2016/04/11 12:56	Arnot 4	223.8	0.39475	50.1485	49.8719	N/A
40.24%	56.10%	2015/06/20 00:00	Apollo Cs	471.4	0.46873	49.8994	49.6194	Kendal
58.32%	60.11%	2016/11/06 03:40	Apollo Cs	145	0.21404	49.9607	49.6604	Matla
50.22%	66.61%	2015/01/12 16:43	Apollo Cs	215.8	0.98434	50.1340	49.7999	Matla
74.28%	68.46%	2016/11/03 10:56	Apollo Cs	210.6	0.34123	50.1421	49.7988	Kendal
69.14%	69.59%	2015/08/02 07:44	Apollo Cs	214.4	0.65447	50.0347	49.6865	Kendal
69.14%	69.59%	2015/08/02 07:44	Apollo Cs	203.8	0.62187	50.0347	49.6865	Kendal
78.18%	78.75%	2015/01/07 13:57	Apollo Cs	195.1	0.34099	50.1059	49.7113	Medupi
68.26%	85.15%	2015/06/11 12:11	Apollo Cs	268.1	0.20317	50.0097	49.5838	Kendal
85.42%	86.29%	2017/03/03 14:15	Apollo Cs	255.6	0.93035	50.1381	49.7054	Kendal
88.52%	87.45%	2015/01/20 18:06	Apollo Cs	346.2	0.64831	50.1486	49.7099	Matla

Appendix C: SAUPEC 2017

ESKOM POWER SYSTEM INERTIA MODEL - A DYNAMIC MULTI-FACTOR APPROACH TO THE MANAGEMENT OF POWER SYSTEM INERTIA

Bonginkosi J. Sibeko* and Dr John M. Van Coller**

** Cnr. Power and Refinery Rd, Simmerpan, 1400, Eskom System Operator, PR. Eng. E-mail: sibekobj@eskom.co.za*
***School of Electrical and Information, Private Bag 3, Wits 2050, E-mail: john.vancoller@wits.ac.za*

Abstract: This research is focused on the behaviour of the power system inertia immediately following a disturbance. The aim is to develop an online (real-time) inertia model. The available historical data is extracted from the Eskom Energy Management System (EMS), Data Energy Centre (DEC) and Wide Area Monitoring System (WAMS). The model includes measured and estimated data from Eskom generators, Independent Power Producers (IPPs) and the interconnected Southern African Power Pool (SAPP). The composite frequency response characteristic of the system (sometimes referred to as the stiffness of the system) is also included. The results will be used to design an inertia model of the Eskom Power System using a Multivariate analysis method to determine the relationship between factors affecting Eskom inertia and estimate other missing and/or unmeasurable variables contributing to the inertial response. If successful, the model can be used for System Operator (SO) Situational Awareness (SA), real time inertia monitoring and to possibly be used in future to optimise the use of IDR (Instantaneous Demand Response), Under Frequency Load Shedding (UFLS) and automated load shedding.

Key words – Inertia, Power system, System Operator (SO), Multivariate analysis, Detrended Fluctuation Analysis, Regression, Swing equation, Situational awareness (SA), Renewables, Spinning reserve, Frequency Stability.

1. INTRODUCTION

In recent years, large-scale deployment of Renewable Energy Sources (RES) generation, mostly in the form of wind turbines, concentrated solar power (CSP) and Photovoltaic (PV) units, has led to substantial generation shares of variable RES power injection in power systems worldwide. The National Development Plan (NDP) of South Africa has a long-term vision of 5 million Solar Water Heaters (SWH) installations, 8.4GW wind turbines, 1GW CSP and 8.4GW Solar PV by 2030 [1]. Currently, wind IPPs are delivering 1440 MW to the grid followed by solar photovoltaic, 960 MW and lastly CSP 200 MW.

It was shown in [3] that the traditional assumption that grid inertia is sufficiently high with only small variations over time is thus not valid for power systems with high RES shares. This has implications for frequency dynamics and power system stability and operation. Frequency dynamics are faster in power systems with low rotational inertia, making frequency control and power system operation more challenging. The developments anticipated in power systems will have far reaching consequences. High shares of inverter connected power generation can have a significant impact on power system stability and power system operation [4].

Energy is stored in the rotating masses of the power system. This energy is often called inertial, stored, or rotational energy [2]. Inertia is defined as the property of an object that resists a change to the object's current speed and direction. The power system has many sources of inertia. Any rotating equipment that is connected to the system is a source of stored rotational energy or inertial energy. The natural resistance of a generator to a change in speed helps to keep the power system frequency constant. In general, the larger the generator, the larger the inertia and the more rotational energy that must be added or removed from the generator to change its speed of rotation [2,3].

Inertia estimation using the Precise Method takes advantage of precise models of a specific generation technology and uses parameter estimation techniques to find the value of inertia (and other parameters) for a specific generation unit as was used by [8] and [4].

The post-mortem analysis of frequency measurements from a single location during a known disturbance to the system is classified as inertia estimation using the Swing Equation method. In [7] estimation of the power system inertia constant and the capacity of spinning-reserve generators using measured frequency transients were used.

This paper presents a power system estimated inertia model by equating the swing equation and precise methods from historic power system frequency disturbance events. Multivariable analysis is used to determine the behaviour, contribution and relationship between independent and dependant parameters. The multiple regression model, is determined and will be used to design an online inertia model.

2. RESEARCH QUESTIONS

The following research questions will be considered:

- By reducing the contribution of conventional synchronous generators to accommodate renewable energy power generation, what would be the resultant impact on network resilience (frequency stability)?
- Are the primary frequency control schemes installed in South Africa's power system

SibekoBJ@eskom.co.za.

adequately calibrated for mitigating fault events before a critical frequency drop can occur?

- Can the use of Instantaneous Demand Response (IDR) and Under Frequency Load Shedding (UFLS) be linked to the online variable system inertia model to shed the required load at the time of an incident?
- In what way does disturbance location, spinning reserve and load types affect the inertial response of the power system?

3. AIM

The aim is to investigate the factors contributing to the system inertia in South Africa's power system using the multivariate analysis method and to develop a power system inertia model.

4. SIGNIFICANCE OF THE STUDY

- Eskom does not have a power system inertia model. This investigation will include IPPs (visibility) and power system damping (stiffness).
- Model development for the Eskom On-line power system inertia will assist System Operator with Situational Awareness (SA), Incident Investigation Inertia forecast and research.
- Possibly be used in future to optimise the use of IDR, UFLS and Automated Load Shedding.

5. BACKGROUND THEORY

Frequency Response can be classified into three different categories; Inertial Frequency Response, Primary Frequency Response and Secondary Frequency Response. Figure 1 below depicts three stages of Frequency deviation following an unbalance in active power.

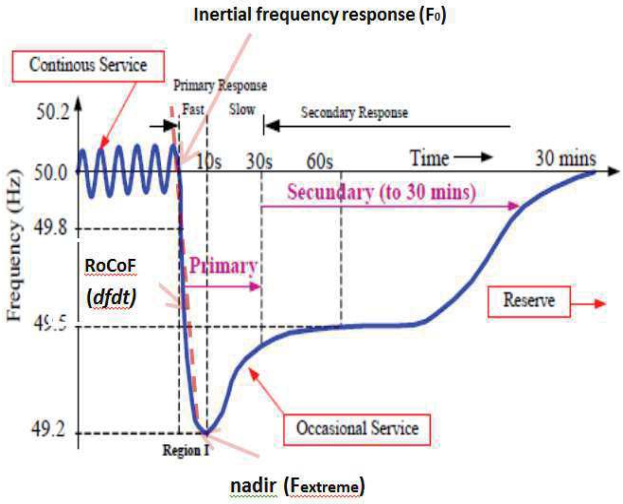

Figure 1: Frequency Response following a large disturbance and controller involvement

This paper focuses on the Inertial Frequency Response also known as Fast Primary Response indicated in figure 1 above.

5.1. Demand Response

Instantaneous Reserve from Demand Response (DR) is consumer load contracted to respond to a drop in frequency. The purpose of the Instantaneous Reserve is to arrest the frequency at acceptable limits following a contingency, i.e. generator trip.

5.2. Inertia of a single machine

The inertia constant H describes the normalised inertia of an individual turbine-generator. It is the ratio between the kinetic energy and its rated apparent power, given by:

$$H = \frac{E_{kin}}{S_{sm}} = \frac{1}{2}\frac{J\omega_{sm}^2}{S_{sm}} = \frac{1}{2}\frac{J(2pf_m)^2}{S_{sm}}[s] \qquad (1)$$

Where

J = moment of inertia of generator and turbine in $kg.m^2$

ω_{sm}= rated mechanical angular velocity of the rotor in rad(mech)/s

S_{sm}= rated apparent power of the generator [VA]

SibekoBJ@eskom.co.za.

f_m = rotational frequency of the synchronous machine

5.3. Inertia of a power system

The inertia constants and rated apparent powers of individual synchronous machines (turbine-generators) can be used to calculate the total inertia of a power system:

$$H_{sys} = \frac{\sum_{i=1}^{N}(S_{smi} \text{ x } H_i)}{S_{sm,sys}} [s] \quad (2)$$

Where $S_{sm,sys}$=$\sum_{i=1}^{N} S_{smi}$

$S_{sm,i}$ = rated apparent power of generator i [VA]

H_i= inertia constant of turbine-generator i [s]

5.4. Estimation of the inertia constant using transients

The behaviour of the frequency deviation following a loss of a large generator or load is approximately represented using equation 5.3 [2, 5]. In the equation, the idea of average system frequency is used, where inter-machine oscillations due to synchronising power and transmission performance are not considered and equivalent system inertia, generator and load are assumed.

$$-\Delta P = M\frac{d\left(\frac{\Delta f}{f_0}\right)}{dt} + K\Delta f \quad (3)$$

Where:

Δf is the change of the frequency (Hz),

ΔP is the amount of generation loss (pu in system load base),

M (2H) is the inertia constant of the system (s),

f_0 is the rated system frequency (Hz),

and K is the power/frequency characteristic of the system (pu/Hz). The value of the power/frequency characteristic becomes large when the spinning reserve of the system is large.

5.5. Composite regulating characteristics of the power system

The composite frequency response characteristic of the system, β, is sometimes referred to as the stiffness of the system [2], is expressed by:

$$\beta = \frac{\Delta P_L}{\Delta f_{ss}} = \frac{1}{R_{eq}} + D \quad MW/Hz \quad (4)$$

Where:

D = composite load-damping constant

$\Delta f_{ss} = \frac{-\Delta P_L}{(1/R_{eq})+D}$ = steady-state frequency deviation

ΔP_L = load change

The composite regulating characteristic of the system is equal to $1/\beta$. Motor loads are dependent on the power system frequency; if the frequency declines, the connected motor load magnitude will also decline and vice versa. A rule of thumb in [10], states that a 1% change in frequency will typically lead to a 2% change in the total system load.

5.6. Multivariate Analysis (MVA)

Multivariate analysis (MVA) is based on the statistical principle of multivariate statistics, which involves observation and analysis of more than one statistical outcome variable at a time [6]. The least squares method aims to produce a straight line that minimizes the sum of the squared differences between the points and the line. That is the coefficients b_0 and $b_1$are calculated so that the sum of the squared deviations $\sum_{i=1}^{n}(y_i - \hat{y}_i)^2$ is minimized. The coefficients $b_{1\ldots,b_k}$describe the relationship between each of the independent variables and the dependent variable in the sample.

SibekoBJ@eskom.co.za.

5.6.1. Assessing the model

The least squares method produces the best straight line. However, there may in fact be no relationship or perhaps a nonlinear relationship between the two variables. If so the straight line model is likely to be inaccurate. To evaluate the model, two statistics and one test model procedure are presented. All these methods are based on the sum of squares of the error.

The deviation between the actual data points and the line are called residuals, given by

$$e_i = y_i + \bar{y}_i \quad (5)$$

The residuals are observations of the error variable. Consequently, the minimized sum of squared deviations is called the sum of squares for error (SSE).

$$SSE = \sum(y_i - \bar{y}_i)^2 = (n-1)\left(s_y^2 - \frac{s_{xy}^2}{s_x^2}\right) \quad (6)$$

Where:

s_y^2 is the sample variance of the dependent variable.

The standard deviation of the error variable, σ_ε, can be used to measure the suitability of using a linear model. Unfortunately, σ_ε is a population parameter and, like most parameters, is unknown. However, σ_ε can be estimated from the data, which is based on SSE. The unbiased estimator of the variance of the error variable σ_ε^2 is

$$s_\varepsilon^2 = \frac{SSE}{n-2} \quad (7)$$

The square root of s_ε^2 is called the standard error of estimate given by

$$s_\varepsilon = \sqrt{\frac{SSE}{n-2}} \quad (8)$$

The value of s_ε is judged by comparing it to the values of the dependent variable y or more specifically the sample mean $\bar{y}$. However, because there is no predefined upper limit on s_ε, it is often too difficult to assess the model in this way. In general, the standard error of estimate cannot be used as an absolute measure of the model's validity.

5.6.2. Coefficient of Determination

The test of β_1 addresses only the question of whether there is enough evidence to infer that a linear relationship exists. In many cases, however, it is useful to measure the strength of that linear relationship, particularly in this paper/project when we want to compare several different models. The statistic that performs such function is called the coefficient of determination, denoted by

$$R^2 = \frac{s_{xy}^2}{s_x^2 s_y^2} \quad (9)$$

$$R^2 = 1 - \frac{SSE}{\sum(y_i - \bar{y})^2} \quad (10)$$

The coefficient of determination is the square of the coefficient of correlation.

$$\sum(y_i - \bar{y})^2 = \sum(y_i - \hat{y}_i)^2 + \sum(\hat{y}_i - \bar{y})^2 \quad (11)$$

Variation in y = SSE + SSR

SSE measures the amount of variation in y that remains unexplained, and SSR measures the amount of variation in y that is explained by the variation in the independent variable x. by incorporating this analysis into the definition of R^2

$$R^2 = 1 - \frac{SSE}{\sum(y_i - \bar{y})^2} = \frac{\sum(y_i - \bar{y})^2 - SSE}{\sum(y_i - \bar{y})^2} = \frac{\text{Explained variation}}{\text{Variation in y}}$$

It follows that R^2 measures the proportion of the variation in y that is explained by the variation in x. A large value of *F* indicates that most of the variation in *y* is explained by the regression equation and that the model is valid. A small value of *F* indicates that most of the variation in *y* is unexplained.

SibekoBJ@eskom.co.za.

The relationships among s_ε, R^2 and F are summarised in Table 1 below.

Table 7: Relationships among $\mathbf{s_\varepsilon}$, $\mathbf{R^2}$ and F

SSE	s_ε	R^2	F	Assessment of Model
0	0	1	∞	Perfect
Small	Small	Close to 1	Large	Good
Large	Large	Close to 0	Small	Poor
$\sum(y_i - \bar{y})$	$\sqrt{\frac{\sum(y_i - \bar{y})^2}{n-k-2}}$	0	0	Useless

6. MODEL DEVELOPMENT

The Southern African Power Pool (SAPP) is made up of South Africa, Botswana, Lesotho, Mozambique, Namibia, Swaziland, Zambia and Zimbabwe, connected through an integrated grid. Approximately 90% of SAPP electricity generation is produced in South Africa. Figure 2 below depicts the overview of SAPP integrated network.

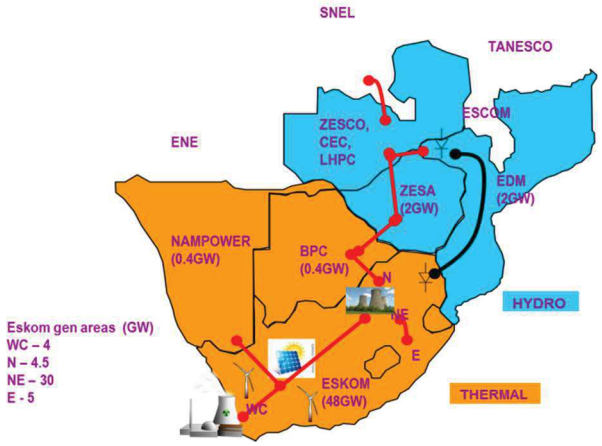

Figure 2: Integrated SAPP network

Cahora Bassa hydro power station in Mozambique dispatches power through parallel ac and dc interconnections and is controlled by the Grid Master Power Controller (GMPC) controls the generation [11]. The bulk dc power flows directly to South Africa while ac power is delivered to Zimbabwe that is also interconnected with the South African ac grid.

It is believed that the following factors depicted in Figure 3 below contribute to the inertial response of the power system [2, 3, 5].

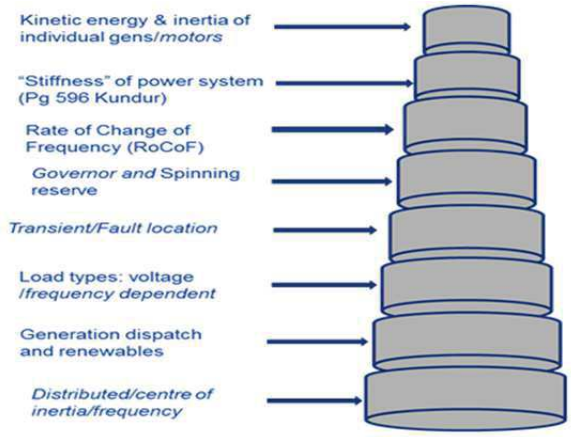

Figure 3: Factors affecting Power System Inertia

From eq. (3)

We define $y = J_{Ave} = \frac{2*2*H*S_{sm}}{\omega_{sm}^2} = \frac{-((\Delta P)*dt)}{d\left(\frac{\Delta f}{f_0}\right)}$

From eq. (1), $H = \frac{E_{kin}}{S_{sm}} = \frac{1}{2}\frac{J\omega_{sm}^2}{S_{sm}}$

we define variable

$$x_1 = J_{esk,gen} = \sum_i^n \frac{2*H_i*S_{sm}}{\omega_{sm}^2}$$

Unknown generator inertia constant (H) will be estimated from reference [9]. The rest of the parameters are summarised in Figure 4 below.

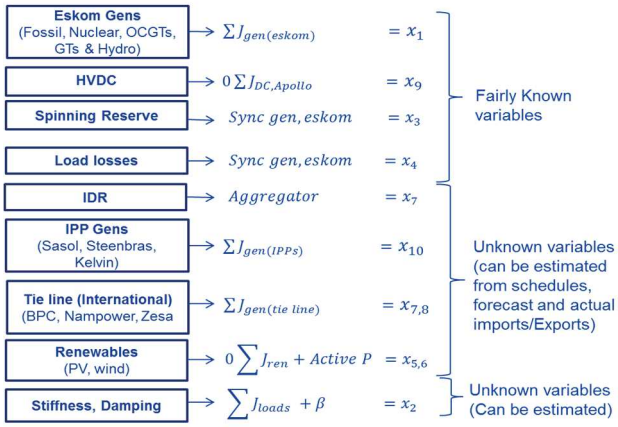

Figure 4: Model development showing known and unknown variables

SibekoBJ@eskom.co.za.

Frequency incident data was collected from Eskom EMS/DEC and WAMS/PMU over the period November 2015-August 2016. The method of extracting data, storing and calculation of required parameters (power system inertia, stiffness, etc.) was developed and it is fully automated. The data is correlated with system snapshots at the time of incidents, correlating the Eskom generator sentouts, load losses, spinning reserve, renewables, tieline, IPP outputs, contracted governor units output and IDR data. The Detrended Fluctuation Analysis (DFA) and Exponential Smoothing methods(7), were used to filter out noise and determine the start and end times of the frequency disturbances.

7. RESULTS AND VALIDATION OF INERTIA MODEL

7.1. Impact of IDR and RoCoF

It was observed from frequency incident data that the IDR acts like a very fast governor response and restricts the system frequency nadir (minimum frequency reached after a disturbance). It was also observed that all the 314 incidents with very small Rate of Change of Frequency (RoCoF) and/or high incident duration (*dt)*, lead to errors. It was found that R^2 is equal to 0.1729 with a standard error of 1.9. This is a poor fit.

7.2. Effects of Transient location and Centre of Inertia

Table 2 below, depicts a summary of regression results of one of the unit trips in central area.

Table 8: Disturbance in Central area

SUMMARY OUTPUT					
Regression Statistics					
Multiple R	0.9999				
R Square	0.9999				
Adjusted R Square	0.9999				
Standard Error	0.0014				
Observations	750				
ANOVA					
	df	*SS*	*MS*	*F*	*Significance F*
Regression	2	14.59	7.29	3714393.36	0
Residual	747	0.0015	1.9639E-06		
Total	749	14.5907			
	Coefficients	*Standard Error*	*t Stat*	*P-value*	
Intercept	-0.0497	0.0184	-2.6997	0.00710	
W_KOEBG_01_400	0.6437	0.0098	65.5676	0	
N_MATMB_01_400	0.3573	0.0098	36.2777	6.0E-167	

We found out that R^2 is equal to 0.9999 with standard error of 0.0014. This statistics tells us that 99.99% of the variation in the Frequency deviation in North Eastern parts of Eskom network during transient is explained by the variation in frequency deviation reading at Koeberg PS (approx. 1500km away from Kendal) and Matimba PS (approx. 500km from Kendal). The value of the test statistics is t = 65.56 for Koeberg, and 36.27 for Matimba with p = 0. There is overwhelming evidence to infer that a linear relationship exists.

In Table 3 below, column 1, 2, and 3 excludes IDR operated and small RoCoF incidents. In column (1), the statistic shows that 72.11% of the variation in the Central area of power system inertia during all the 37 transient events is explained by the variation in Eskom synchronous generators, Stiffness, Spinning reserve, Load losses, Wind, PV, Zesa, BPC load and Apollo DC. The remaining 27.99% is unexplained. Similarly in column (2), the statistic shows that 89.92% of the variation in the Northern area of power system inertia during all the 13 transient events is explained by the same factors. Column (3), all incidents, the statistic shows that 69.13% of the variation in the Total area of power system inertia during all the 50 transient events.

SibekoBJ@eskom.co.za.

Table 3 below, depicts a summary of the Eskom inertia model factors regression results.

Table 9: Summary of regression results

		(1)	(2)	(3)	(4)	(5)
Regression statistics		NE area	N area	All areas excl IDR & sfd		
	Multiple R	0.8492	0.9483	0.8314		
	R Square	0.7211	0.8992	0.6913		
	Adjusted R Square	0.6282	0.5967	0.6218		
	Standard Error	1.2409	1.3574	1.2574		
	Observations	37	13	50		
					t Stat	P-value
	Intercept	-20.110	-22.886	-17.538	-2.8725	0.0065
Eskom AC System	Esk Sync. Gens	5.6729	6.4345	5.1262	3.6812	0.0007
	Stiffness	4.8827	1.7144	3.0903	3.5731	0.0009
	Spinning reserve	0.0004	0.0004	0.0004	5.1350	0.0000
	Load losses	-0.0002	-0.0008	-0.0003	-1.1926	0.2401
RES	Wind	-0.0032	-0.0007	-0.0016	-1.4915	0.1437
	PV	-0.0006	0.0007	-0.0002	-0.3851	0.7022
Int'l	Zesa	0.0005	0.0021	0.0011	0.6853	0.4971
	BPC load	-0.0008	-0.0009	-0.0006	-0.9708	0.3375
	Apollo DC	-0.0006	0.0017	-0.0002	-0.4917	0.6256
Regression	*df*	9	9.0000	9		
	SS	107.5103	49.2997	141.6085		
	MS	11.9456	5.4777	15.7343		
	F	7.7578	2.9729	9.9521		
	Significance F	0.0000	0.200389	0.0000		
Residual	*df*	27.0000	3.0000	40.0000		
	SS	41.5753	5.527655	63.2398		
	MS	1.5398	1.8426	1.5810		
TOTAL	***df***	**36**	**12**	**49**		
	SS	**149.09**	**54.83**	**204.85**		

7.3. Discussion of results

The above results illustrated how transient location affects the behavior of frequency, thus playing an important role in accuracy of the model. As noted in (5), the frequency is not the same throughout the whole system. During a disturbance a measurement location in the system plays a role due to a propagation of frequency wave. The average first order model is estimated by:

$$y = -17.538 + 5.12x_1 + 3.09x_2 + [0.4x_3 - 0.3x_4 - 1.6x_5 + 1.1x_7 - 0.6x_8 - 0.2x_9] * 1000 + \varepsilon$$

7.3.1. *Intercept*

The intercepts for area 1, 2 and 3 are $b_0 = -20.1, -22.89\ and - 17.53,$ respectively. This is the average Eskom power system rotational mass (*J)* when all of the independent variables are 0. In this model, the intercept is meaningless and simply means a total power system blackout. It is misleading to interpret this value, particularly if 0 is outside the range of the values of the independent variables (6).

7.3.2. *Eskom AC System coefficients*

The coefficient $b_1 = 6.31$ specifies that for an additional moment of inertia $J_{esk,gen}$ (pu/$kg.m^2$) that is added by Eskom generators and turbines to the power system, the Eskom power system moment of inertia (J_{ave}) increases by 6.3 percentage points assuming that the other independent variables in this model are held constant.

Value of the test statistics: t = 4.61 p-value = 5.33E-05

There is overwhelming evidence to infer that the Eskom generators and turbines and the Eskom power system moment of inertia are linearly related. Similarly, for an additional Stiffness and Spinning reserve (pu/Hz), there is an increase in Eskom power system moment of inertia (J_{ave}) and the relationship is linearly related.

Notice the Generator load loss coefficient is also negative. In most cases, when load losses are high, other generators in the system are picked up to their Maximum Capability Rating (MCR), which impacts negatively on spinning reserve and the composite frequency response characteristics of the system β.

7.3.3. RES coefficients

The relationship between Eskom power system inertia and wind energy is described by $b_2 = -0.0016$. From this number is found that, in this model, for an additional 1000MW of wind energy in Eskom network, system inertia decreases by 1.6 percentage points.

SibekoBJ@eskom.co.za.

Value of the test statistics: t = -1.7 and p-value = 0.0862

There is no evidence to infer the existence of a linear relationship between the wind energy and the Eskom power system moment of inertia are linearly related.

Similarly, for an additional 1000MW of PV power output, there is a decrease in Eskom power system moment of inertia and the relationship is not linearly related.

The wind and PV coefficients are both negative. This could mean that when the RES output was high during low load (night minimum or during the day), the system operator had to take off synchronous generators, thus reducing the kinetic energy of the system.

7.3.4. *International coefficients*

The coefficient $b_7 = 0.0005$ specifies that for each additional 1000MW that is added by Zesa generators and turbines to the power system, the interconnected power system moment of inertia (J_{ave}) increases by 0.5 percentage points assuming that the other independent variables in this model are held constant.

The coefficient $b_8 = -0.0008$ specifies that for an additional 1000MW that is added by BPC load to the power system, the interconnected power system moment of inertia (J_{ave}) decreases by 0.8 percentage points assuming that the other independent variables in this model are held constant.

The coefficient $b_9 = -0.0006$ specifies that for an additional 1000MW that is added by Songo-Apollo DC line to the power system, the interconnected power system moment of inertia decreases by 0.6 percentage points assuming that the other independent variables in this model are held constant. Values of the test statistics for international t and p-values, indicates that there is no evidence of a linear relationship between the above coefficient and the power system moment of inertia. However, it may also mean that there is a linear relationship between the variables, but because of a condition called multicollinearity.

The relationship among s_ε, R^2 and F proves that the model is good (see table 1). The unmeasurable independent variables, i.e. customer motor loads, contribute to the model error margin.

8. CONCLUSION

In this paper, an inertia model of the Eskom power system using a Multivariate analysis method to determine the relationship between factors affecting the power system inertia is presented. It is based on the use of a swing equation to estimate the inertia from disturbances and equated with the known and unknown variables related to system inertia at the time of an incident using multivariate analysis (regression).

Based on the above findings, the following conclusion may be made.

- Reducing the contribution of conventional synchronous generators to accommodate renewable energy power generation reduces the system inertia. Thus it has a negative impact on frequency stability and predictability.
- The primary frequency control schemes should be revised and calibrated correctly to mitigate fault events before a critical frequency drop can occur and to shed close-to-required load at the time of an incident.
- Transient location affects the behavior of frequency, thus playing an important role in accuracy of the model.
- The unmeasurable independent variables (customer motor loads), contribute to the model error margin.

SibekoBJ@eskom.co.za.

- An additional Stiffness and Spinning reserve (pu/Hz) to the power system, increases in Eskom power system moment of inertia (J_{ave}) and the relationship is linearly related.

9. REFERENCES

[1] *The South African Renewable Energy Independent Power Producers Procurement Programme (REIPPPP) – Lessons Learned 17 March 2016*. [Online]. Available: www.irena.org/EventDocs/RECC/30.%20REIPPPP%20South%20Africa.pdf [Accessed: 01 October 2016].

[2] *P. Kundur, N. J. Balu, and M. G. Lauby, Power System Stability and Control.* New York: McGraw-Hill, 1994.

[3] *System Inertial Frequency Response Estimation and Impact of Renewable Resources in ERCOT Interconnection*, Sandip Sharma, Shun-Hsien Huang and NDR Sarma, Power and Energy Society General Meeting, 2011 IEEE.

[4] *Andreas Ulbig, Theodor S. Borsche, Göran Andersson, "Impact of Low Rotational Inertia on Power System Stability and Operation"*, Capetown, South Africa, IFAC World Congress 2014

[5] *ENTSO-E AISBL, NORDIC report, future system inertia.* [Online]. Available: www.entsoe.eu. [Accessed: 15 July 2016].

[6] Keller, Gerald; Warrack, *Statistics for Management and Economics,* Thomson South-Western, Cincinnati 7th edition. Chapter 16-20, 2005.

[7] T. Inoue, H. Taniguchi, Y. Ikeguchi, and K. Yoshida, "*Estimation of power system inertia constant and capacity of spinning-reserve support generators using measured frequency transients"*, IEEE Trans. PowerSyst., vol. 12, no. 1, pp. 136–143, February, 1997

[8] Song Guo, JanuszBialek, "*Synchronous Machine Inertia Constants Updating Using Wide Area Measurements"*, 3rd IEEE PES Innovative Smart Grid Technologies Europe (ISGT Europe), Berlin, 2012

[9] H. Lee Willis, *Electrical Transmission & Distribution Reference Book*, 5th Edition, ABB, 1997

[10] *EPRI Power Systems Dynamics Tutorial 1016042*, Final Report, July 2009 [Online]. Available: https://www.scribd.com/doc/126840594/EPRI-Power-System-Dynamics-Tutorial [Accessed: 28 October 2016].

[11] P. Riedel, J. W. Strauss, P. V. Goosen, *"Simulation and commissioning of the grid master power controller (GMPC) for the Cahora Bassa HVDC",* Proc. Cigré's Int. Conf. Power Syst., *2001-Sept.-3*

SibekoBJ@eskom.co.za.

Appendix D: A Dynamic Multi-Variate Approach to the Management of Power System Inertia

BJ, SIBEKO **J, Van Coller** **GJ, Hurford**

Eskom SOC Ltd. **Wits University** **Eskom SOC Ltd.**

South Africa **South Africa** **South Africa**

SUMMARY

The slow economic growth and worldwide slump in the commodities markets has led to a reduction in customer demand while at the same time there has been an increase in asynchronous generation penetration. This has resulted in a lower inertia power system supplying the same load levels experience some years ago leading to concerning dynamic behaviour in frequency. The growing concerns on system inertia require more sophisticated and affordable power system real-time tools to manage the challenges of a modern power system. Failure could likely lead to widespread blackouts with significant economic and social impact. As more zero inertia energy sources are added into the Eskom power grid, the traditional synchronous generators, which provide inertia to the system, are starting to be displaced, put into cold reserve or two shifting and see early retirement. The power system inertia immediately following small and large system disturbances was investigated. By understanding factors affecting the system inertia and primary frequency response behaviour, an online inertia model can be developed. Historical data was extracted from the Eskom Energy Management System and Wide Area Monitoring System. The developed model using Multivariate Analysis (MVA) includes measured and estimated data from Eskom generators, Renewable Energy Sources (RESs) and the interconnected Southern African Power Pool. Fast Primary (Frequency) Response (FPR) (as determined by the load behaviour) and system inertia models were developed and validated with past frequency disturbance events (Jan-March 2017). From the comparison between the measured and model results for 30 actual disturbances, 21 disturbances resulted in errors within ±5% and 6 events resulted in errors between ±5% and ±10%. 3 disturbances caused errors greater than ±10%, which were largely from trips at a particular power station and HVDC trips. During a large disturbance, the multivariate coefficients for RESs, HVDC and interconnectors were very small for the pure inertia model (excluding the load frequency behaviour and the generator damping). In contrast, the spinning reserve does contribute significantly to the inertia model, depending on where it is. The location of a disturbance affects the FPR behaviour and the system inertia but not the Rate of Change of Frequency (RoCoF) with reference to the central power station. The strong and weak areas with respect of the stiffness of the system were identified. This can contribute to future grid planning and real-time operations in managing the system inertia and primary frequency response. The model is expected to improve with time as the accuracy of statistical approach requires large amount of data. The model can be used to determine and monitor the maximum level of RESs in real-time.

KEYWORDS

Fast Primary (Frequency) Response (FPR), Inertia, Model, Multivariate Analysis, Rate of Change of Frequency (RoCoF), Spinning reserve, Stiffness, Swing equation, System Operator (SO)

SibekoBJ@eskom.co.za.

1 INTRODUCTION

The South African Grid Code (SAGC) [1] was written prior to the installation of significant amounts of renewable energy generation and hence the Grid Code does not directly cover the system inertia requirements. The SAGC does, however, define the limits of acceptable frequency response and it is therefore important to understand what level of non-synchronous generators can be tolerated before the Grid Code frequency response requirements are breached. Offline inertia studies using simulations are often inaccurate in the operational environment because the network scenarios change rapidly and an extensive set of simulations are required to achieve close to realistic results.

Regulators and System Operators (SOs) want more advanced applications that address system operational matters at near real-time. At any given time, South Africa's System Operator (SO) would like to know how the system will respond to load or generator disturbances. Short-term frequency instability can result in a network with insufficient synchronous generation and insufficient under-frequency load shedding such that the frequency decays rapidly following a loss of generation [2], [3].

The Eskom transmission network is synchronously connected to the neighbouring Southern African Development Community (SADC) utilities [4]. The long single 400 kV AC circuits and asynchronous HVDC interconnectors are relatively weak compared to the Eskom grid. The parts of the country which were considered, include large coal-fired power stations in the North (Lephalale), North-East and East (KwaZulu-Natal). The hydro pump storage stations and the single nuclear power station were excluded due to lack of incident data.
The aim of this paper is to get a better estimate of the power system inertia during changing network conditions. Section 2 describes previous methods of inertia constant estimation. Section 3 is a discussion of multivariate analysis. Section 4 discusses an inertia model that ignores the stiffness of the system. Section 5 discusses the FPR plus inertia model. Section 6 discusses the prediction of the inertia constant and frequency nadir following frequency disturbances. Section 7 is the conclusion.

2 ESTIMATION OF THE SYSTEM INERTIA CONSTANT

Following a generation disturbance, kinetic energy stored in the rotating masses of the generators is released, reducing the Rate of Change of Frequency (RoCoF) [2]. The inertia constant *H* in Equation 1, describes the normalized inertia of an individual generator, measured in seconds (s). It is the ratio between the Kinetic Energy (E_{kin}) in joules at rated speed and rated apparent power (S_{sm}) in VA [2].

$$H = \frac{E_{kin}}{S_{sm}} = \frac{1}{2}\frac{J\omega_{sm}^2}{S_{sm}} \quad (1)$$

Where
J : Moment of inertia ($kg.m^2$)
ω_{sm} : Synchronous speed (rad (mech)/s)

The inertia constant of an individual generator can be estimated from the mechanical data of the generator using the Inertia Constant Method [5] The sum of the inertia constants and the rated apparent powers of individual generators can then be used to calculate the inertia constant of the

SibekoBJ@eskom.co.za.

entire interconnected power system as given by equation 2 [2].

$$H_{sys} = \frac{\sum_{i=1}^{n} S_{ni} H_i}{S_n} \quad (2)$$

Where S_{ni} is the rated apparent power of generator *i* in VA, H_i is the inertia constant of generator i in seconds and S_n is the sum of the rated apparent powers of all the generators. The Inertia Constant Method could be difficult to use for large power systems due to the unavailability of generator data in neighbouring networks[6]. The inertia constant of the power system can also be estimated using the Swing Equation and post-disturbance frequency measurement data from a single location during a known disturbance [6]–[8]. This method is valid for a highly meshed grid, in which all units can be assumed to be connected to the same grid bus, representing the centre of inertia of the given grid [9]. The behaviour of the frequency following a loss of a large generator or load is approximately represented using Equation 3 [2] .

$$\frac{df}{dt} = \frac{\Delta P}{2H} f_{start} + \frac{D}{2H} \Delta f \quad (3)$$

Where
$df\ /\ dt$: is the Rate of Change of Frequency (RoCoF) (Hz/s)
$\Delta P = (P_{start} - P_{nadir})/P_{start}$: Fractional power change (pu)
P_{start}: Generation/Load prior to Generator/Load loss (MW)
P_{nadir}: Generation/Load after Generation/Load loss (MW)
f_{strart} : Frequency at the start of the disturbance (Hz)
H: Inertia constant on system base (s)
D : Power system load damping constant (pu)
Δf: Change in frequency $(f_{start} - f_{nadir})$ (Hz)

The equation does not consider inter-generator oscillations and the stiffness of the system [2]. In [7], [8], the authors ignored the stiffness/damping and validated the models by considering only the standard error. According to [10], the value of the standard error, s_ε, is judged by comparing it to the values of the dependent variable H. However, because there is no predefined upper limit on s_ε, it is often too difficult to assess the model in this way. In general, the standard error of estimate cannot be used as an absolute measure of the model validity [10].This paper evaluates the system RoCoF and inertia constant behaviour following a disturbance by correlating the Swing Equation and the Inertia Constant Methods from historical power system frequency deviation data using Multivariate Analysis (MVA).

3 MULTIVARIATE (MVA) ANALYSIS

Multivariate Analysis (MVA) requires a certain minimum set of data (observations) for the regression to solve and produce accurate results. The approximately 2000 frequency disturbances in the past three years made it possible to perform this study. MVA is based on the statistical principle of multivariate statistics, which involves observation and analysis of more than one statistical outcome variable at a time [10]. MVA requires sets of inputs of *y range* (dependent variable) and *x range* (independent variables) as shown in Table 10. Table 11shows the assessment of a regression model and relationships among_s_ε, R^2 and F [10].

SibekoBJ@eskom.co.za.

Table 10: Dependent (y) and Independent (x) input variables used in the regression analysis tool (similar table is used for the inertia model and the inertia plus FPR model)

Observations	Input y range	Input x range					
1	y_1	x_{11}	x_{12}	x_{13}	x_{14}	...	x_{1n}
2	y_2	x_{21}	x_{22}	x_{23}	x_{24}	...	x_{2n}
3	y_3	x_{31}	x_{32}	x_{33}	x_{34}	...	x_{3n}
⋮	⋮	⋮	⋮	⋮	⋮		⋮
n	y_n	x_{n1}	x_{n2}	x_{n3}	x_{n4}	...	x_{nn}

Table 11**:** Relationships among $\boldsymbol{s_\varepsilon}$, $\boldsymbol{R^2}$ and *F*

SSE	s_ε	R^2	*F statistic*	Assessment of Model
0	0	1	∞	**Perfect**
Small	Small	Close to 1	Large	**Good**
Large	Large	Close to 0	Small	**Poor**

The *Coefficient of Determination* (R^2) measures the proportion of the variation in *y* that is explained by the variation in the independent variable *x*. The *Sum of Squares of Error (SSE)* measures the amount of variation in *y* that remains unexplained and *the Sum of Squared Residuals (SSR)* measures the amount of variation in *y* that is explained by the variation in the independent variable. The *F statistic* is the ratio between the SSR and the SSE. A large value of the F statistic indicates that most of the variation in y is explained by the regression equation and that the model is valid. The *significance of F* indicates that most of the studied variables are jointly significant.

4 SYSTEM INERTIA MODEL IGNORING THE STIFFNESS OF THE SYSTEM

The aim of this section is to study the large disturbances without FPR. This section proposes a possible way of estimating the system inertia using MVA. The first part evaluates the impact of disturbance location and the factors affecting the system inertia during the first 300 ms following the start of a disturbance in the network.

4.1 RoCoF following the start of a disturbance in the network

Figure 5 shows the three stages of the frequency response during a loss of a large generator in the Northern parts of the Eskom network. The measurements were taken from Phasor Measurement Units (PMUs) at Western Cape (Koeberg), Northern (Matimba) and North-East (Kendal) power stations.

SibekoBJ@eskom.co.za.

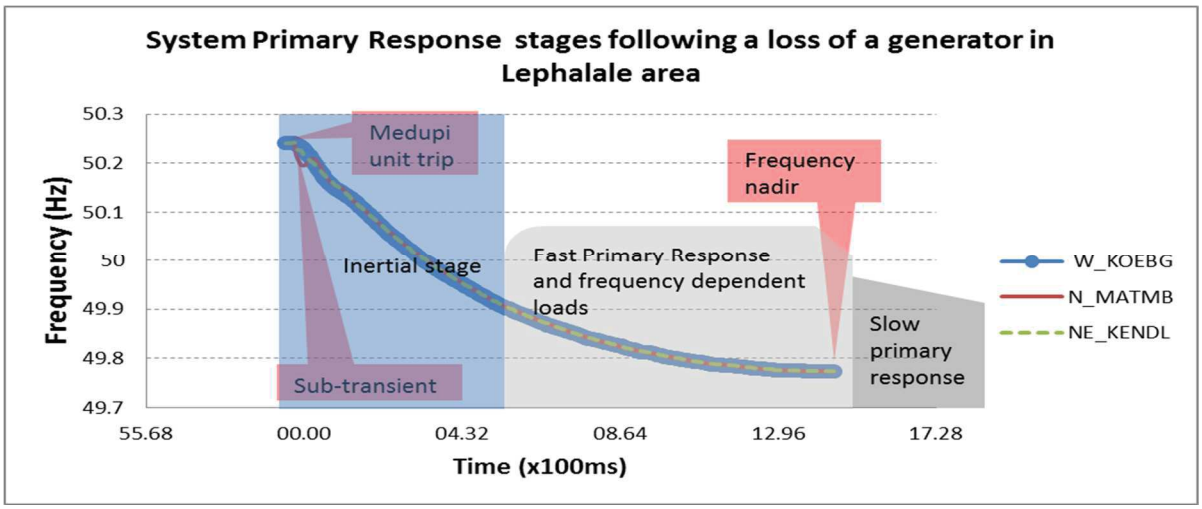

Figure 5: PMU data showing system primary response stages (the time must be multiplied by 100 to get the actual value in ms)

The centre of system inertia and impact of disturbance location were studied using the past frequency disturbances which were randomly selected across the Eskom areas. The moving average [10] and Detrended Fluctuation Analysis (DFA) [11] methods were used to filter out the electromagnetic torque oscillations and PMU measurement noise following large disturbances. The system RoCoF with reference to Kendal power station in the North-East area resulted in an R^2 of 0.96, a standard error of 0.002, a large *F statistic*, a small SSE of 6.3E-05 and the *significance of F* was close to zero. Thus 96% of the variation in the frequency deviation in any part of the Eskom network during the incidences could be explained by the variation in frequency deviation reading at Kendal power station. It follows that Kendal power station could be used as a reference centre of frequency for any disturbance in the network.

4.2 System inertia model development without stiffness factor

- The inertia constant (H) is the **dependent variable** $(\boldsymbol{y_n})$ given by rearranging Equation 2 to calculate the inertia constant (H) using the RoCoF (sourced form PMU data), power change ΔP (sourced from EMS data) in system VA base and frequency at the start time of disturbance f_{start}, System damping and stiffness are assumed to be zero.
- The first independent variable $\boldsymbol{x_{n1}}$ is the sum of all the synchronous generator moment of inertia (J) by rearranging Equation 1.
- The second independent variable $\boldsymbol{x_{n2}}$ is the **system load**, which is equivalent to generation sent-out. The third independent variable $\boldsymbol{x_{n3}}$ is the **system frequency** in Hz.

4.3 Results for the system inertia using the MVA method

Table 12 shows the inertia constant models for the selected Eskom areas (North-East and North) and Majuba power station (East). The first part of the table comprises the observations, the s_ε, the R^2, the SSE, the *F statistic* and the *significance of F*. The second part of the table shows the independent variables and coefficient values obtained from the MVA.

SibekoBJ@eskom.co.za.

Table 12: Comparison of inertia constant per Eskom area and independent variable coefficients

	Model	All PS	North-East	North	Majuba	Majuba 123
	Observations	27	10	8	9	6
Model validation	R Square	0.18	0.66	0.69	0.61	0.96
	Standard Error	0.39	0.09	0.09	0.51	0.25
	SSE	3.48	0.04	0.04	1.28	0.12
	F statistic	1.65	3.93	2.99	2.59	15.24
	Significance of F	0.21	0.07	0.16	0.17	0.06
	Intercept	61.51	-57.47	-16.98	294.43	505.82
Independent variables and coefficients	Load (gen sent-out) (x_1)	-0.19229	0.00002	0.01658	0.00018	0.00037
	Starting frequency (x_2)	-1.21	1.13	0.33	-6.02	-10.38
	System total J (x_3)	0.000042	0.309691	0.000063	0.696460	0.940421

The correlation of the combined past disturbances for the entire system was poor. The Coefficient of Determination (R^2) was found to be 0,18. By breaking down the data into North East and Lephalale areas, the R^2 improved to 0,66 and 0,69 respectively. The R^2 of all units in Majuba power station model was 0,61. Since the units at Majuba power station have different sizes and ratings, the station was divided into two stations. The Majuba 123 R^2 improved to 0,96 and good standard error, small SSE, large *F statistic* and small *significance of F*. This signifies that the model yields better results at a power station level and with units of similar type. Using Majuba the 123 model, the Eskom system inertia constant H (without stiffness), can be estimated by model (a):

$$S_n H = (x_1 b_1 + x_2 b_2 + x_3 b_3)\ in\ MW.s. \quad \text{(a)}$$

Where $S_n = \sum_i^n \frac{J_{sm} * \omega_{sm}^2}{2 * H_i}\ (in\ VA)$ and x_i are the values of the independent variables (MW).

5 FPR PLUS INERTIA MODEL DEVELOPMENT

This section investigates the overall factors that contribute to the system FPR plus inertia model. It starts by defining the FPR plus inertia model dependent and independent variables. The factors influencing the FPR plus inertia model are then determined and analysed. Equation 3 is rearranged to calculate the inertia constant using the power change ΔP (sourced from EMS data) and frequency at the start time of the disturbance (sourced from Eskom PMU data). The inertia constant (H) is defined as the **dependent variable (y_n)** given by Equation 4.

$$H = \frac{\left(\left(\frac{Pstart - Pnadir}{Pstart}\right) * (tnadir - tstart)\right)}{2 * \left(\frac{fstart - fnadir}{f_{start}}\right)} \quad (4)$$

Where :
P_{start}: System generation prior to power change (MW)
P_{nadir}: System generation after power change (MW)

- The first independent variable $\boldsymbol{x_{n1}}$ is the sum of all the **synchronous generator moment of inertia (*J*)** by rearranging Equation 1.
- The second independent variable is the **stiffness of the system $\boldsymbol{x_{n2}}$** and is the steady-state change in frequency for a particular change in generation/load [2]. The stiffness of the system depends on the load damping, spinning reserve and governor droop response (as this can be used to restore the

frequency to its nominal value) [2]. The coherent response of all generators to changes in system load R_{eq} (in *pu*) is assumed and represented by an equivalent generator with an equivalent governor droop. For a system with *n* generators and a composite load-damping constant of *D*, the steady-state fractional frequency deviation Δf_{ss} following a generation/load fractional change ΔP_L is the composite frequency response characteristic β in *pu* as given by Equation 5 [2].

$$\beta = \frac{\Delta P_L}{\Delta f_{ss}} = \frac{1}{R_{eq}} + D \tag{5}$$

- $$\frac{1}{R_{eq}} = \frac{generation\ contributing\ \ to\ regulation\ (MW)}{\frac{regulation\ \%}{100}\ x\ P_{start}(MW)} = \frac{\Delta P_G}{\Delta f_{ss}} \tag{6}$$
- $$D = \Delta P_D / \Delta f_{ss} \tag{7}$$

The units which were committed for instantaneous reserves were used to calculate the spinning reserves per generator at the times of the actual frequency disturbances. In the time scale considered, governors do not have time to respond so that the damping present is due to the load response (FPR).

- The third independent variable was chosen to be the total spinning reserve (x_{n3}) on its own and is the unloaded generation which is synchronised and ready to be used (with or without governor action).
- The fourth independent variable is the **generation load losses** ($\boldsymbol{x_{n3}}$) and was chosen to be the units that are synchronised on the grid but unable to output Maximum Continuous Rating (MCR) (limited ability to provide spinning reserves).
- The simplified models to estimate the contribution from two international interconnectors, Botswana Power Corporation **(BPC)** load ($\boldsymbol{x_{n5}}$) and Zimbabwe Electricity Supply Authority **(ZESA) load** ($\boldsymbol{x_{n6}}$) were developed from the line flows and tie-line schedules.
- Power generated at the Cahora Bassa hydro power station in Mozambique and which is imported into the Eskom network via long HVDC lines was measured at the injection substation, Apollo. **HVDC** ($\boldsymbol{x_{n7}}$) is asynchronous, thus it does not contribute to the inertia constant.
- The Renewable Energy Sources (RESs) are Wind ($\boldsymbol{x_{n8}}$) (may or may not contribute to the moment of inertia depending on the technology) and PhotoVoltaic (PV) ($\boldsymbol{x_{n9}}$) (does not contribute to the moment of inertia).

5.1 Factors influencing the FPR and inertia model

Small disturbances in this study were defined as disturbances where the frequency does not drop below 49.65 Hz (e.g. Instantaneous Demand Response (IDR) does not operate). The study was performed to determine the contribution of identified factors that are expected to contribute to the FPR plus inertia model. The correlation results of the combined past disturbances for the entire system were found to be poor as the $R^2$was found to be only 0,12. The disturbance location is, therefore, important for the FPR plus inertia model, where the stiffness of the system has an effect. By breaking down the data into regions and power station levels, the FPR plus inertia models improved so that the R^2 values were increased to an average of 0,65 to 0,87 respectively. All the power stations and area models were referenced to a centralised power station PMU in the North Eastern parts of South Africa. Table 13shows the FPR plus inertia model validations for the selected

SibekoBJ@eskom.co.za.

power stations. The table comprises the area, power stations, observations, s_ε, R^2, the *F statistic* and the *significance of F*.

Table 13: Comparison of areas and power station inertia plus FPR models

		Area		Lephalale		KZN		North East					Central		
		Model		Medupi	Matimba	Maj 123	Maj 456	Tutuka	Matla 3456	Kendal	Arnot	Kriel	Duvha	Lethabo	Apollo
		Observations		29	23	12	14	25	18	14	15	18	18	16	15
Model validation		R Square	R^2	0.99	0.98	1.00	0.97	0.96	0.97	0.98	0.98	0.99	0.99	0.99	0.91
		Standard Error	S_ε	1.07	1.12	0.33	1.81	2.26	1.89	1.26	1.65	0.93	0.96	0.93	3.61
		F statistic		151	71	508	21	40	33	28	31	74	66	100	7
		Significance of F		0.00	0.00	0.00	0.01	0.00	0.00	0.00	0.00	0.00	0.00	0.00	0.03
	Coef.	Independent variable													
Eskom AC system	b_1	System total MOI(J)	(x_1)	2.3	1.7	2.5	0.3	1.6	0.9	0.6	5.2	0.9	0.8	3.2	-8.9
	b_2	Stiffness (pu/Hz)	(x_2)	9.5	4.5	35.0	61.9	57.4	29.3	6.3	-0.5	19.6	30.7	8.8	56.3
	b_3	Spinning reserve (x1GW)	(x_3)	0.2	0.3	-1.1	1.2	0.6	0.2	-0.1	-0.6	0.1	0.2	1.1	0.4
	b_4	Genix Load losses (x1GW)	(x_4)	-1.2	-0.2	-0.3	2.6	-0.7	1.8	0.6	-0.4	-0.2	-0.5	-2.3	-2.1
Tielines (x1GW)	b_5	BPC load	(x_5)	-0.4	2.5	4.9	-6.8	-0.9	-6.1	1.7	7.2	0.5	-0.2	-5.4	45.8
	b_6	Zesa	(x_6)	0.5	0.9	-13.7	1.4	15.7	5.3	-0.6	6.2	1.2	-0.7	17.6	20.3
	b_7	Apollo DC	(x_7)	-2.4	-1.1	-1.1	-10.1	-8.6	-5.8	0.5	-7.8	-0.5	-1.6	-5.5	-45.7
RES (x1GW)	b_8	Wind	(x_8)	3.9	-3.2	-14.2	-14.9	0.5	2.5	2.8	-2.1	1.2	-0.1	4.1	11.5
	b_9	PV	(x_9)	-1.7	-1.1	-3.1	4.5	4.2	1.0	-1.3	-3.0	-0.1	-1.7	4.2	4.6

5.1.1 Validation of selected power stations FPR plus inertia models

Referring to Table 11, except for Majuba power station 2 (units 4, 5 and 6) and Apollo HVDC converter station, all the models in Table 13 are good. Since R^2 is close to 1 the *F statistic* is large and the *significance of F* is zero. This is an indication that most of the variation in FPR plus inertia is explained by the regression equation and that the models are good. The worst performing model is that for the Apollo HVDC converter station. This could be in line with Nordic [12] findings that when a generator or importing HVDC connection trips, the estimated inertia value is always higher than the actual inertia value. The inaccuracy could be due to the voltage dependency of the loads in the Central 275 kV network and the strength of the 275 kV network in the Central grid close to the HVDC infeed.

5.1.2 AC power station FPR plus inertia model coefficients

This part of table 4 comprises the system moment of inertia, stiffness of the system, spinning reserve and generation load losses. The coefficient b_1 of all the models shows that for an additional moment of inertia $J_{esk,gen}$ that is added by synchronous generators and turbines to the power system, the power system inertia constant H increases (as expected). The Apollo HVDC converter station is asynchronous; therefore, HVDC imports do not contribute to the system inertia constant.

The power stations in the North East and Eastern areas of the network, which are connected to the 400 kV system, have larger stiffness coefficients compared to other power stations in remote areas (Lephalale and Arnot). This can be interpreted as during disturbances around the 400 kV network in the central and North-East areas, the generators closer to the disturbance are fast to react to the

SibekoBJ@eskom.co.za.

loss of generation in that particular area. Lethabo power station in the central area, is connected to the 275 kV network and connected to other power stations via 275/400 kV step-up transformers which have high impedance, making Lethabo electrically remote to other power stations. This power station has a smaller stiffness coefficient. This can be interpreted as the power stations in the North-East area which are connected to the 400 kV system, contribute less inertia during disturbances at Lethabo power station.

Spinning reserve is highly related to the stiffness of the system. The coefficient b_4 shows that for an additional generation load loss of 1000 MW, the inertia constant generally decreases. The negative impact of generator load losses is large for the network's primary frequency response. In most cases, when load losses are high, the output of the other generators in the system is increased close to their Maximum Continuous Rating (MCR) to replace the lost generation, which impacts negatively on spinning reserve and the stiffness of the system. The interdependency between the independent variables is classified as the multicollinearity factor. This means that some of the independent variables such as spinning reserve and stiffness are either non-linear or highly correlated with one another. This indicates that spinning reserve should be managed locally, i.e. per area by the SO.

5.1.3 Tie-line FPR plus inertia model coefficients

The BPC (b_5) and Zesa (b_6) utilities are relatively small compared to the Eskom network and are not expected to assist significantly with the frequency response following a large disturbance in the Eskom network. The electrical impedance connecting Eskom and neighbouring countries is also high due to the weak tielines between countries. Apollo HVDC (b_7) is consistently negative for all the power station PFR plus inertia models.

5.1.4 RESs FPR plus inertia model coefficients

This part of a table comprises wind (b_8) and PV (b_9). The large negative impact of wind energy is in the Eastern area where no wind generation is installed. When there an excess of wind energy during low demand, the SO is forced to take off some of the base load synchronous generators. Previously one or more units at Majuba power station in the Eastern area were being regularly taken off the grid over periods of low load to accommodate the wind generation. This weakens the system, the stiffness of the KZN province and the FPR. Other areas were not highly impacted.

6 PREDICTION OF INERTIA CONSTANT AND FREQUENCY NADIR FOLLOWING FREQUENCY DISTURBANCES

The disturbances in the Lephalale area, which includes two large coal fired power stations with units larger than 700MW each, is used as an example in this paper. The strength of the neighbouring countries of Botswana and Zimbabwe during disturbances is also of interest and both countries are directly connected to the Lephalale area. Table 14 shows a detailed summary of results and validation of the Medupi inertia constant model.

SibekoBJ@eskom.co.za.

Table 14: Medupi inertia constant model regression summary output

	Regression Statistics								
	Multiple R	0.930							
	R Square	0.865							
	Adjusted R Square	0.805							
	Standard Error	0.895							
	Observations	30							
	ANOVA								
		df	*SS*	*MS*	*F*	*Significance F*			
	Regression	9	102.8	11.4	14.3	0.0			
	Residual	20	16.0	0.8					
	Total	29	118.8						
		Coefficients	*Standard Error*	*t Stat*	*P-value*	*Lower 95%*	*Upper 95%*	*Lower 95.0%*	*Upper 95.0%*
	Intercept	9.114	4.440	2.053	0.053	-0.148	18.376	-0.148	18.376
Eskom AC system	System Total MOI (x_1)	0.040	0.867	0.046	0.964	-1.768	1.848	-1.768	1.848
	Stiffness (x_2)	3.924	0.925	4.242	0.000	1.995	5.854	1.995	5.854
	Spinning reserve (x_3) x1 GW	0.071	0.000	0.900	0.379	0.000	0.000	0.000	0.000
	Genix Load losses (x_4) x1 GW	-0.872	0.000	-2.585	0.018	-0.002	0.000	-0.002	0.000
Tie-lines x1 GW	BPC load (x_5)	1.055	0.001	1.250	0.226	-0.001	0.003	-0.001	0.003
	ZESA (x_6)	-1.685	0.002	-1.083	0.292	-0.005	0.002	-0.005	0.002
	Apollo HVDC (x_7)	-2.968	0.001	-4.695	0.000	-0.004	-0.002	-0.004	-0.002
RES x 1GW	Wind (x_8)	3.540	0.001	4.475	0.000	0.002	0.005	0.002	0.005
	PV (x_9)	-1.561	0.001	-2.480	0.022	-0.003	0.000	-0.003	0.000

The inertia constant model is good because s_ε is small, R^2 is close to 1, the *F statistic* is large, and the significance of *F* is zero. The first order inertia constant model for Medupi power station is estimated by model (b):

$$y = H = \{9.04 + 0.04x_1 + 3.92x_2 + [0.071x_3 - 0.87x_4 + 1.05x_5 - 1.67x_6 - 2.96x_7 + 3.53x_8 - 1.55x_9]/1000\}/(10*2) \quad \text{(b)}$$

Each factor is explained by describing what its coefficient b_n specifies in terms of its weight and influence on the dependent variable inertia constant and whether it is linearly or non-linearly or multicollinearly related (*t*-stat and *P*-value). R^2 shows that 86.5% of the variation in the power system inertia constant during all 30 incidents used to develop the model is explained by the variation in the number of Eskom generators on the network, stiffness, spinning reserve, generator load losses, international interconnectors and renewables. The remaining 13.5% is unexplained. This is a good fit.

Table 15 shows the Northern area models following Medupi unit trips. The table compares the calculated inertia constant using Equation 4 and the Medupi, Matimba and Lephalale models.

Table 15: Model validation following a Medupi unit trip (single contingency)

Incident Date/time and System response		Actual inertia constant (H) vs Medupi model		measured frequency nadir vs Medupi model			Actual frequency nadir vs models in the North		
date/time	ΔP (MW)	Swing Eq. (s)	model (s)	fstart (Hz)	Actual f Nadir (Hz)	Model f nadir (Hz)	Medupi error	Matimba error	Lephalale error
17/02/17 01:41	130.3	0.72	0.701	50.16	50.04	50.05	7.4%	2.2%	2.2%

SibekoBJ@eskom.co.za.

17/02/23 13:34	385.4	0.70	0.880	50.03	49.71	49.76	14.5%	-15.4%	10.0%
17/03/12 11:29	98.3	0.47	0.470	49.93	49.80	49.80	-2.6%	-16.2%	-16.0%
17/03/12 23:50	230	0.75	0.807	49.96	49.77	49.78	7.9%	-5.5%	4.8%
17/03/13 13:38	118.2	0.62	0.461	49.99	49.83	49.83	2.4%	1.8%	11.4%

The above results show that the errors between the actual measurements are below a 5% margin. The Medupi model is thus validated for single disturbances. The possible reason for large errors above 5% is accuracy of reported or recorded data. The FPR plus inertia model can be improved by further investigating the non-linear independent variables and upgrading a linear model to a polynomial model.

Figure 6 shows the overall results of the entire FPR plus inertia model predicted frequency nadir following single disturbances. From 30 disturbances, 21 events were within an ±5% error. 6 events resulted in errors between ±10% and ±5%. The errors greater than 10% were largely from Arnot, Duvha units 4,5 and 6, and HVDC trips. The large errors accounted for 17% of the sampled data. The power stations which had no or poor models, were predicted by electrically closer models. Note that the model was developed using the previous year's disturbances (2015-2016) and the model results shown occurred in early 2017 incidences. Thus the model is valid for the period outside the study period.

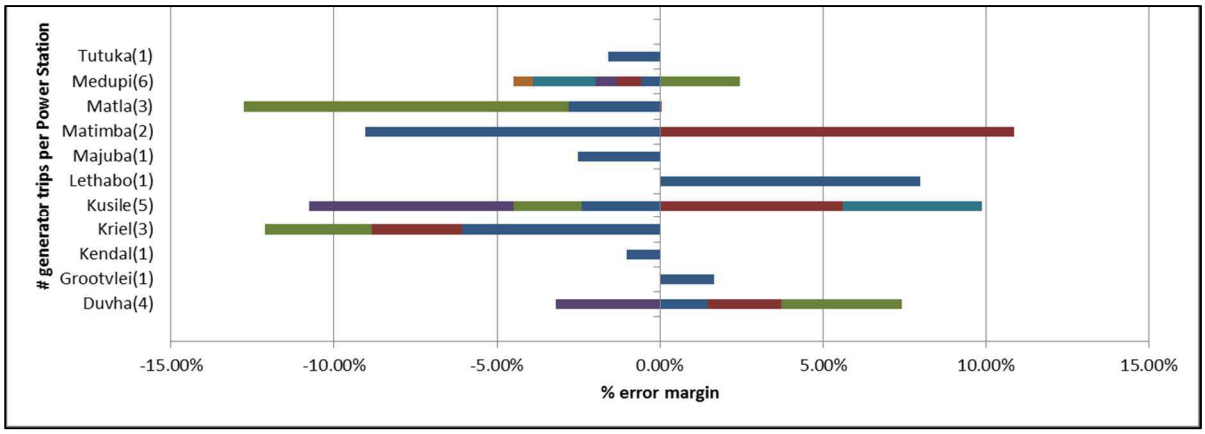

Figure 6: Measured versus predicted inertia constant (H) %errors for all power station models excluding HVDC, Arnot and Duvha unit 4, 5 & 6 trips

7 CONCLUSION

In this work, an inertia constant model of the Eskom power system using Multivariate Analysis was developed to determine the relationship between factors affecting the power system inertia constant. It is based on the use of the swing equation to estimate the inertia constant from disturbances and equated with the known and unknown variables related to system inertia constant at the time of an incident. The location of a disturbance that causes the frequency disturbance

SibekoBJ@eskom.co.za.

affects the FPR behaviour and the system inertia constant but not the RoCoF with reference to the central power station. Therefore, the assumption that the aggregated inertia constant H is constant for all swing equations of a multi-area system is not valid for the Eskom system. The strong and weak areas with respect of the stiffness of the system were identified in the study (related to the magnitude of the frequency nadir). This can contribute to future grid planning and real-time operations in managing the system inertia. The model uses data which is sourced directly from the Eskom SO. Neither new equipment nor purchasing of software is required to implement the model. The models can be easily incorporated into the system operating control system (SCADA) to monitor the impact of RES on the system inertia in real-time.

BIBLIOGRAPHY

[1] National Energy Regulator of South Africa, *South African Grid Code - Network Guide*, vol. 9. National Energy Regulator of South Africa, 2014.

[2] P. Kundur, N. J. Balu, and M. G. Lauby, *Power system stability and control*. New York: McGraw-Hill, 1994.

[3] P. Kundur *et al.*, 'Definition and classification of power system stability IEEE/CIGRE joint task force on stability terms and definitions', *IEEE Trans. Power Syst.*, vol. 19, no. 3, pp. 1387–1401, Aug. 2004.

[4] SAPP, 'Interconnectors | Southern African Power Pool', *Sapp.co.zw*. [Online]. Available: http://www.sapp.co.zw/interconnectors. [Accessed: 21-Dec-2017].

[5] P. Wall, F. Gonzalez-Longatt, and V. Terzija, 'Estimation of generator inertia available during a disturbance', in *Power and Energy Society General Meeting, 2012 IEEE*, 2012, pp. 1–8.

[6] T. Inoue, H. Taniguchi, Y. Ikeguchi, and K. Yoshida, 'Estimation of power system inertia constant and capacity of spinning-reserve support generators using measured frequency transients', *IEEE Trans. Power Syst.*, vol. 12, no. 1, pp. 136–143, Feb. 1997.

[7] S. Sharma, S.-H. Huang, and N. D. R. Sarma, 'System inertial frequency response estimation and impact of renewable resources in ERCOT interconnection', in *Power and Energy Society General Meeting, 2011 IEEE*, 2011, pp. 1–6.

[8] P. M. Ashton, C. S. Saunders, G. A. Taylor, A. M. Carter, and M. E. Bradley, 'Inertia Estimation of the GB Power System Using Synchrophasor Measurements', *IEEE Trans. Power Syst.*, vol. 30, no. 2, pp. 701–709, Mar. 2015.

[9] A. Ulbig, T. S. Borsche, and G. Andersson, 'Impact of Low Rotational Inertia on Power System Stability and Operation', *ArXiv13126435 Math*, Dec. 2013.

[10] G. Keller, *Statistics For Management And Economics*, 7th ed. Cincinnati: Thomson South-Western, 2005.

[11] P. M. Ashton, G. A. Taylor, M. R. Irving, I. Pisica, A. M. Carter, and M. E. Bradley, 'Novel application of detrended fluctuation analysis for state estimation using synchrophasor measurements', *IEEE Trans. Power Syst.*, vol. 28, no. 2, pp. 1930–1938, May 2013.

[12] E. Ørum *et al.*, 'Future system inertia, NORDIC report', European Network of Transmission System Operators for Electricity, Avenue Cortenbergh, Brussels, Belgium, 2015.

SibekoBJ@eskom.co.za.

Appendix E: Comments and contribution by industry experts

RE: Cigre 2018 - Developing a realtime system inertia model using multivariate analysis (in word format)

Adam Bartylak

You forwarded this message on 2018/01/05 02:08 PM.

Sent: Fri 2018/01/05 12:56 PM

To: Bonginkosi Sibeko

Message | Developing a realtime system inertia model using multivariate analysis rev1_AB.docx (410 KB)

Hi Bongi
Very interesting subject and right on time but very difficult reading for someone who finished statistics course 40 years ago ☺
In any case, attached are my comments and corrections wherever I felt like it. They may be good or not but this is all that popped to my mind while reading so take it or leave it.
One comment that is not there:
All international papers must be vetted via Bernard and Thava's office and the most common issue is usually publication of Eskom specific data and information. On few occasions I was asked to make my papers "anonymous" i.e. without any real names or diagrams of Eskom substations, power stations, etc. Geographical areas (Cape, Lephalale, etc.) are usually fine. So normally what I do is to call substations and power stations with letters – A, B, C, ... or you can give them fake names.
Enjoy ☺
Kind Regards and well done !

Adam Bartylak
Corporate Consultant (Protection)
System Operator
Transmission
Tel +27 11 871 3467
Cell +27 71 891 5199
Fax +27 86 662 8138
E-mail adam.bartylak@eskom.co.za

Eskom | Powering your world |

From: Rob Stephen Sent: Fri 2018/01/19 11:12 AM
To: Bonginkosi Sibeko
Cc:
Subject: RE: Cigre 2018 - A Dynamic Multi-Variate Approach to the Management of Power System INERTIA.docx

Bonginkosi,

Thanks for this excellent paper. The only comment I have is that an international audience will not know anything about the power stations mentioned. You may want to describe them as 4000MVA coal fired station in North of country for example (for Medupi) or have a map just showing location and approx. size and fuel source. You can also just number the stations instead of naming them.

One point perhaps not covered is how robust is the model developed. Can we use this for each station going forward for all types of fault at various magnitudes? Can this be used for determination of the effect of renewable integration?

Thanks.

Rob Stephen
GM Master Specialist
Technology Group
Eskom
+27 83 326 2534
rob.stephen@eskom.co.za

SibekoBJ@eskom.co.za.

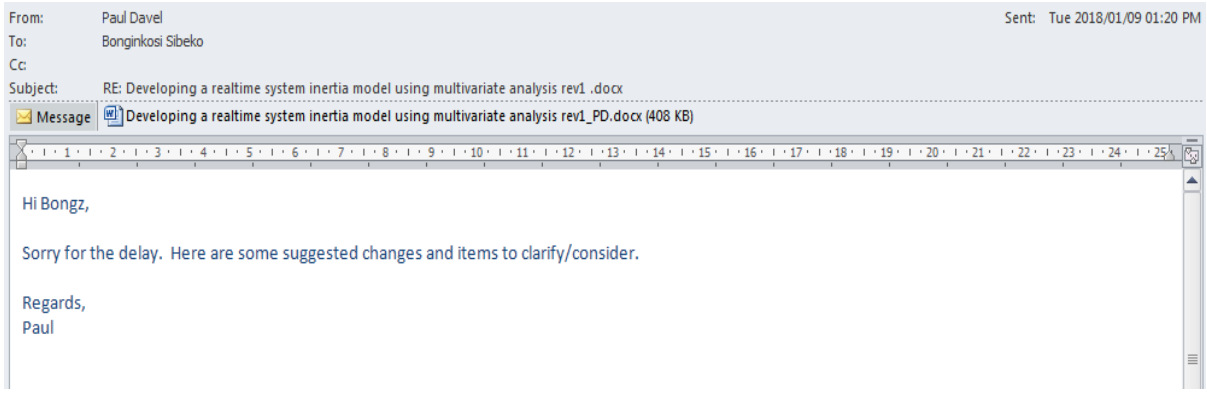

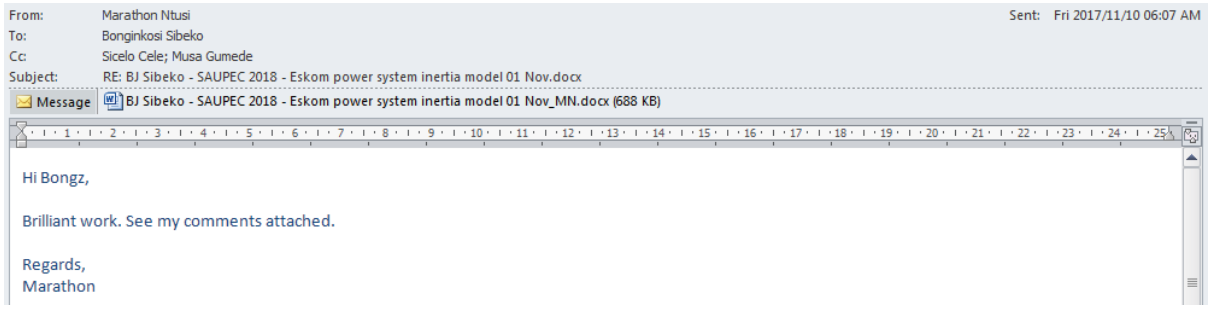

SibekoBJ@eskom.co.za.